AWARD NUMBER: W81XWH-13-1-0220

TITLE: **A Genetically Engineered Mouse Model of Neuroblastoma Driven by Mutated ALK and MYCN**

PRINCIPAL INVESTIGATOR: Rani E. George MD PhD

CONTRACTING ORGANIZATION: Dana-Farber Cancer Institute
Boston, MA 02115

REPORT DATE: September 2015

TYPE OF REPORT: Annual

PREPARED FOR: U.S. Army Medical Research and Materiel Command
Fort Detrick, Maryland 21702-5012

REPORT DOCUMENTATION PAGE

Form Approved
OMB No. 0704-0188

1. REPORT DATE	2. REPORT TYPE	3. DATES COVERED
September 2015	Annual	1 Sept 2014 - 31 Aug 2015

4. TITLE AND SUBTITLE

A Genetically Engineered Mouse Model of Neuroblastoma Driven by Mutated ALK and MYCN

5a. CONTRACT NUMBER

5b. GRANT NUMBER
W81XWH-13-1-0220

5c. PROGRAM ELEMENT NUMBER

6. AUTHOR(S)
Rani E. George MD PhD

E-Mail: rani_george@dfci.harvard.edu

5d. PROJECT NUMBER

5e. TASK NUMBER

5f. WORK UNIT NUMBER

7. PERFORMING ORGANIZATION NAME(S) AND ADDRESS(ES)

Dana-Farber Cancer Institute
Office of Grants and Contracts
450 Brookline Ave, BP3
Boston, MA 02215-5450

8. PERFORMING ORGANIZATION REPORT NUMBER

9. SPONSORING / MONITORING AGENCY NAME(S) AND ADDRESS(ES)

U.S. Army Medical Research and Materiel Command
Fort Detrick, Maryland 21702-5012

10. SPONSOR/MONITOR'S ACRONYM(S)

11. SPONSOR/MONITOR'S REPORT NUMBER(S)

12. DISTRIBUTION / AVAILABILITY STATEMENT

Approved for Public Release; Distribution Unlimited

13. SUPPLEMENTARY NOTES

14. ABSTRACT

During the past year, we have made significant progress towards meeting the goals of the funded grant proposal. We have identified a novel therapeutic strategy for MYCN-amplified neuroblastoma using a novel first-in-class inhibitor of cyclin dependent kinase 7 and have demonstrated selective potent activity against these tumors without general toxicity. Additionally, we have determined that in tumors expressing mutated ALK but without MYCN amplification, the combination of an ALK inhibitor and a transcriptional CDK inhibitor is synergistic. Both these strategies are ripe for clinical development and testing. Finally, our collection of tumors and sympathetic ganglia during different developmental stages will enable us to delineate the genetic and epigenetic changes that occur during tumorigenesis.

15. SUBJECT TERMS
Anaplastic lymphoma kinase, neuroblastoma, ALK, *ALK*^{F1174L}, MYCN, CDK7, transcription, combination therapy.

16. SECURITY CLASSIFICATION OF:			17. LIMITATION OF ABSTRACT	18. NUMBER OF PAGES	19a. NAME OF RESPONSIBLE PERSON
a. REPORT	b. ABSTRACT	c. THIS PAGE			USAMRMC
Unclassified	Unclassified	Unclassified	Unclassified	40	19b. TELEPHONE NUMBER *(include area code)*

Standard Form 298 (Rev. 8-98)
Prescribed by ANSI Std. Z39.18

Table of Contents

Page

1. INTRODUCTION:

This project addresses the FY12 CD PRMRP topic area of **Neuroblastoma.** The overarching goal of our research is to develop effective molecularly targeted therapies for patients with neuroblastoma (NB), a tumor of the peripheral sympathetic nervous system that is responsible for 15% of childhood cancer deaths(Cheung and Dyer, 2013). To this end, we identified somatic activating mutations in the ALK tyrosine kinase receptor in 8-10% of primary NB tumors, which are targetable by small molecule inhibitors (George et al., 2008). We have also developed genetically engineered *ALK*^{F1174L}/MYCN mouse models which develop NB tumors that recapitulate the biology and ALK-inhibitor resistance of this disease (Berry et al., 2012). We have shown that the ALK^{F1174L} potentiates NB formation by MYCN, partly by regulation of MYCN activity (Berry et al., 2012). Specifically, in this project, we will decipher the mechanisms underlying this cooperation and devise novel therapies to target both oncogenic mechanisms through the following aims: 1) Test whether combined inhibition of ALK and downstream oncogenic signaling will be effective in NB cells expressing activated ALK and MYCN, 2) Determine whether direct targeting of MYCN will induce cytotoxicity in NB with ALK-induced upregulation of MYCN and 3) Test whether triple-node targeted therapy directed simultaneously to ALK, MYCN and downstream signaling pathways will improve outcome in *in vivo* models of NB. The findings of this project will provide a clinical trial concept proposal for triple node targeted therapy that blocks ALK, MYCN and intersecting downstream signaling pathways and will provide proof-of-principle that blocking as many nodes as possible at the outset has a better chance than single agent therapy in decimating the tumor cell population.

During the past year, we have made significant progress towards meeting the goals of the funded grant proposal. We have identified a novel therapeutic strategy for MYCN-amplified neuroblastoma using a novel first-in-class inhibitor of cyclin dependent kinase (CDK) 7 and have demonstrated selective potent activity against these tumors without general toxicity. Additionally, we have determined that in tumors expressing mutated ALK but without MYCN amplification, the combination of an ALK inhibitor and a transcriptional CDK inhibitor is synergistic. Both these strategies are ripe for clinical development and testing. Our collection of tumors and sympathetic ganglia during different developmental stages will enable us to delineate the genetic and epigenetic changes that occur during tumorigenesis. We have published this work and have presented these results in several forums.

2. KEYWORDS:

Anaplastic lymphoma kinase, neuroblastoma, ALK, *ALK*^{F1174L}, MYCN, CDK7, transcription, combination therapy.

3. ACCOMPLISHMENTS

What were the major goals of the project?

Aim 1: To test whether combined inhibition of ALK and downstream oncogenic signaling will be effective in NB cells expressing activated ALK and MYCN (months 1-18); 80% completed.

Aim 2: To determine whether direct targeting of MYCN will induce cytotoxicity in NB with activated ALK-induced upregulation of MYCN (months 1-24); 75% completed.

Aim 3: To test whether triple-node targeted therapy (TNT) directed simultaneously to ALK, MYCN and a downstream signaling pathway will improve outcome in *in vivo* models of neuroblastoma (months 18-34) 30% completed.

What was accomplished under these goals?

Key Research Accomplishments

- Completion of a high throughput chemical screen to identify compounds that synergize with ALK inhibitors in ALK-mutated NB
- Identification and validation of transcriptional CDK7 inhibitors as synergizing with ALK inhibitors
- Identification of a novel therapeutic strategy for inhibiting the effects of amplified MYCN in NB.
- Identification of super-enhancers in NBs and their perturbation through CDK7 inhibition.

- Establishment of a repository of tumors and sympathetic ganglia from transgenic MYCN only or MYCN/ALKF1174L animals at different stages of development (E15 to P28).

Task 1: Test whether combined inhibition of ALK and downstream oncogenic signaling will be effective in NB cells expressing activated ALK and MYCN.

1) Major activities: We performed a high-throughput compound screen using ALK^{F1174L}-dependent MYCN non-amplified human NB SH-SY5Y cells and compared viability between cells treated with the screen compound alone and in combination with the ALK inhibitor, crizotinib.

2) Specific Objectives: To identify compounds that would potentiate the effect of crizotinib.

3) Significant results and conclusions: We identified 126 "hits" that were placed into general functional groups. The strongest "hits" among the ~8,000 compounds screened were inhibitors of cyclin dependent kinases (CDKs). The combination of crizotinib and two candidate pan-selective CDK inhibitors, AT7519 and SNS-032 resulted in synergistic activity with significantly increased apoptosis over that of either single agent alone. The most striking combinatorial effect with crizotinib was obtained with SNS-032, a transcriptional CDK inhibitor (CDKi) targeting CDKs 2, 7 and 9 (Conroy et al., 2009), a result that we validated at several different dose combinations (combination index, CI < 1). This effect was associated with a reduction in ALK phosphorylation, downstream signaling, and apoptosis. This effect was observed in NB cells expressing not only ALK^{F1174L}, but also in those expressing ALK^{R1275Q}, the most common NB-associated *ALK* mutation. Synergy was also seen with ceritinib (LDK378), a structurally unrelated ALK inhibitor, in combination with both AT7519 and SNS-032. To begin to decipher the mechanism(s) underlying the synergistic effects of crizotinib/CDKi treatment, and to identify the CDKs whose inhibition led to synergy, we analyzed the gene expression profiles in ALK^{F1174L}-expressing SH-SY5Y cells exposed to synergistic doses of crizotinib and SNS-032, either alone or in combination. Combination treatment led to transcriptional downregulation of a large number of genes compared to single agents alone, with the top-ranked differentially expressed gene sets in the combination-treated cells being those involved in transcription regulation. The primary effect on transcription was corroborated by downregulation of the RNA polymerase II (Pol II) C-terminal domain (CTD) phosphorylation. Together, these findings led us to conclude that the synergistic effect arises primarily from the disruption of transcription mediated by CDKs 7 and 9. These findings were comparable with results obtained using agents that were highly selective for CDK9 (NVP2) or CDK7 (THZ1), CDKs with roles in transcription regulation. Finally, in murine xenograft models of *ALK*-mutated NB, the combination of crizotinib and THZ1 resulted in inhibition of tumor growth and prolongation of survival compared to single agents alone.

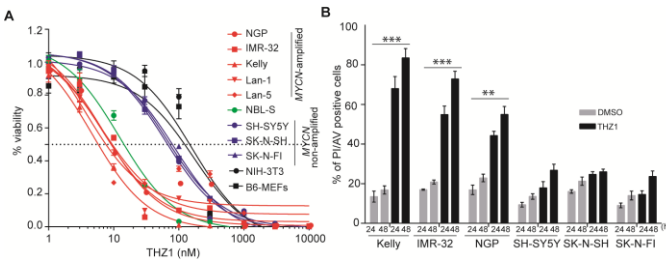

Fig. 1. THZ1 exhibits high potency and selectivity against *MYCN*-amplified NB cells. A. *MYCN*-amplified and nonamplified human NB and murine fibroblast cells after treatment with increasing concentrations of THZ1 for 72hr. Percent cell viability relative to that of DMSO-treated cells is shown. Data represent mean ± SD of 3 replicates. **B.** Apoptosis analyses of NB cells exposed to THZ1 (100nM x 24 and 48hr) by flow cytometry. Data represent mean ± SD of 3 replicates. ***p<0.0001, **p<0.001 (Student's t-test).

Task 2: Determine whether direct targeting of MYCN will induce cytotoxicity in NB with activated ALK-induced upregulation of MYCN.

1) Major activities: We tested a novel inhibitor of cyclin-dependent kinases (CDKs) involved in transcriptional regulation.

2) Specific Objectives: To determine whether the effects of amplified MYCN can be targeted through inhibition of a transcriptional CDK, CDK7.

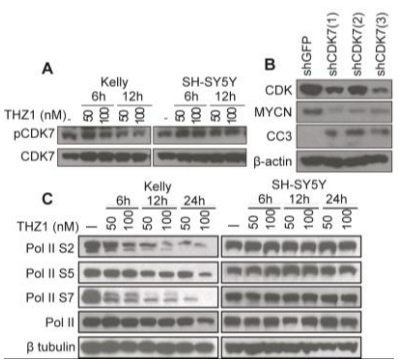

Fig. 2. THZ1 Inhibits General Transcription in *MYCN*-amplified Cells. A, Immunoblot analysis of pCDK7 in *MYCN*-amplified Kelly and nonamplified SH-SY5Y NB cells treated with DMSO or THZ1 at the indicated concentrations for the indicated times. **B,** MYCN expression following shRNA KD of CDK7 in *MYCN*-amplified Kelly NB cells. **C**. phospho-Pol II expression in the same cells as in A, treated as shown.

3) Significant results and conclusions: Using THZ1, a novel covalent CDK7 inhibitor, we demonstrated significant cytotoxicity in MYCN-amplified cells compared to NB cells that expressed mutated ALK as well. MYCN-amplified NB cells were ~10-fold more sensitive to THZ1 than MYCN nonamplified cells, while nontransformed cells were relatively insensitive **(Fig. 1)**. Cell cycle arrest in G2/M (not shown) and apoptosis were seen in *MYCN*-amplified cells treated with THZ1 (**Fig. 2**). CDK7 phosphorylation was also decreased in *MYCN*-amplified cells (**Fig. 2**), consistent with the fact that CDK7 is regulated by phosphorylation within its own activation (T) loop (Larochelle et al., 2012). Depletion of CDK7 through shRNA knockdown (KD) led to increased apoptosis, indicating the on-target effect of THZ1 (**Fig. 2**). Cytotoxicity with THZ1 treatment was associated with downregulation of Pol II CTD phosphorylation in *MYCN*-amplified NB cells (**Fig. 2**), affecting both initiation (pS5, pS7) and elongation (pS2). Decreased activity of CDK1/2, involved in cell cycle regulation, was also seen (not shown)**.** Our results showed that THZ1 inhibits CDK7 potently and selectively in MYCN-amplified NB cells. This response translated to significant tumor regression in a mouse model of high-risk NB, without the introduction of systemic toxicity. THZ1 treatment led to a significant inhibition in tumor growth (**Fig. 3**) that corresponded to decreased proliferation and induction of apoptosis (**Fig. 3**).

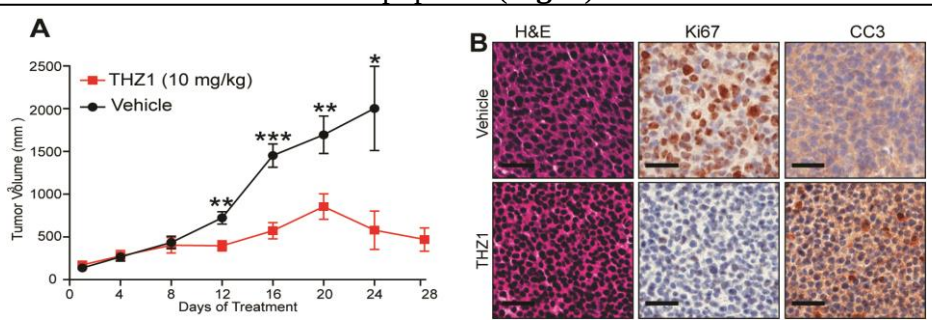

Fig. 3. THZ1 Causes Inhibition of Tumor Growth in Mouse Models of *MYCN*-overexpressing NB. A. Tumor volumes of Kelly *MYCN*-amplified human NB xenografts in NU/NU (*Crl:NU-Foxn1^{nu})* mice treated with THZ1 (10 mg/kg IV twice daily) (n=14) or vehicle (n=9) for 28 days. Mean ± SD values are presented. ***p<0.001; **p<0.01; *p<0.05 (multiple t-test, Holm-Sidak method). **B.** Morphology (H&E), proliferation (Ki67) and apoptosis (cleaved caspase 3, CC3) in the tumors. Scale bar, 25 µM.

To begin to understand the selectivity of THZ1 for MYCN-amplified cells, we first analyzed its effects on MYCN expression, noting decreased RNA and protein levels after treatment **(Fig. 4**) as well as decreased MYCN binding at the promoters of two of its known target genes, MDM2 and MCL1 **(Fig. 4)**. These results indicated that the effects of THZ1 were at least partly through regulation of MYCN levels. Because MYC is known to be a transcriptional amplifier, we next compared the gene expression profiles of cells treated with THZ1, and noted massive transcriptional shutdown limited to *MYCN*-amplified cells (**Fig. 5**). These data suggested that THZ1, by targeting amplified MYCN, affected active transcription within the cell. Indeed, shRNA KD of MYCN in *MYCN*-amplified Kelly NB cells led to significant downregulation of global gene expression (**Fig. 6).** Moreover, ectopic overexpression of MYCN in *MYCN*-nonamplified SH-SY5Y NB cells, led to sensitization of these cells to THZ1 (**Fig. 6**), with significant global transcriptional downregulation (**Fig. 6**). However, the effect was not as striking as in cells expressing endogenously amplified MYCN possibly due to the lack of appreciable MYCN downregulation (**Fig. 6**) in these cells. Together, these data strongly suggest that in *MYCN*-amplified NB cells, MYCN acts as a transcriptional amplifier, and this effect is suppressed by CDK7 inhibition (Chipumuro et al., 2014).

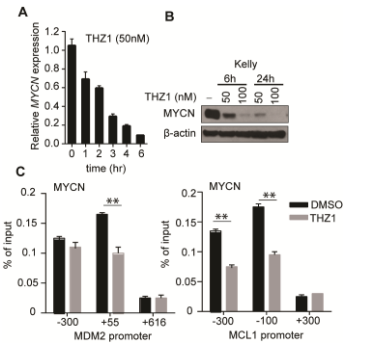

Fig. 4. THZ1 downregulates MYCN expression. A. qRT-PCR analysis of *MYCN* expression in *MYCN*-amplified Kelly cells treated with THZ1. Data normalized to β-actin are presented as mean ± SD of three biological replicates. **B.** Immunoblot analysis of MYCN protein expression in the same cells. **C.** ChIP-qPCR analysis of MYCN binding at the promoters of candidate target genes in *MYCN*-amplified cells following treatment with THZ1, 100 nM x 3 hr. Mean ± SD values for three replicate experiments are shown. **p<0.01 (Student t-test).

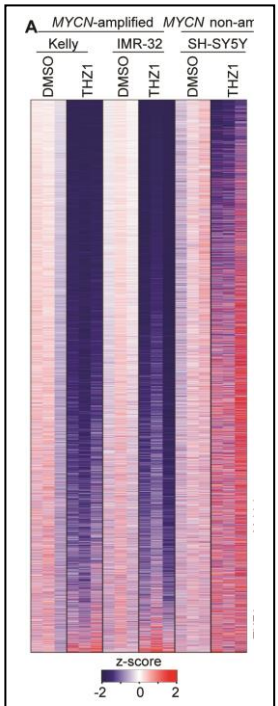

Fig. 5. THZ1 causes downregulation of actively transcribed genes. Heat map of gene expression values in cells treated with THZ1 (100 nM x 6 hr.) vs. DMSO. Rows show z-scores calculated for each cell type.

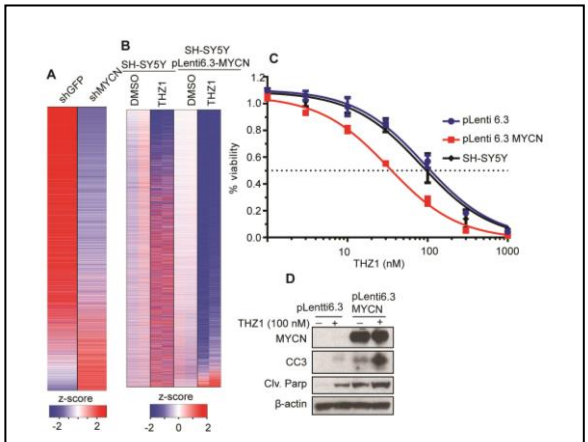

Fig. 6. THZ1 inhibits *MYCN*-driven transcriptional amplification A. Heat map of gene expression values in *MYCN*-amplified NB cells expressing either an shGFP control or a MYCN shRNA **B.** Heat map of differentially expressed genes in *MYCN*-nonamplified SH-SY5Y cells vs. SH-SY5Y cells overexpressing *MYCN* following either THZ1 (100 nM x 6 hr) or DMSO. **C.** Cell viability analysis of untransfected (SH-SY5Y), control vector-expressing (pLenti 6.3) or MYCN-expressing (pLenti 6.3 MYCN) SH-SY5Y cells treated for 72 hr with THZ1. Means ± SD of 3 replicates. **D.** Immunoblot analysis of the indicated proteins in the cells referred to in **C**.

Additionally, we also noted that in MYCN-amplified c ells, oncogenic MYCN is transcriptionally regulated by large enhancer regions or super-enhancers that facilitate its high-level expression and that are especially sensitive to perturbation. The striking treatment selectivity of *MYCN*-overexpressing cells correlated with preferential downregulation of super-enhancer-associated genes, including *MYCN* and other known oncogenic drivers in NB such as ALK **(Fig. 7).** Our results indicate that CDK7 inhibition, by selectively targeting the mechanisms that promote global transcriptional amplification in tumor cells, may be useful therapy for cancers that are driven by MYC family oncoproteins.

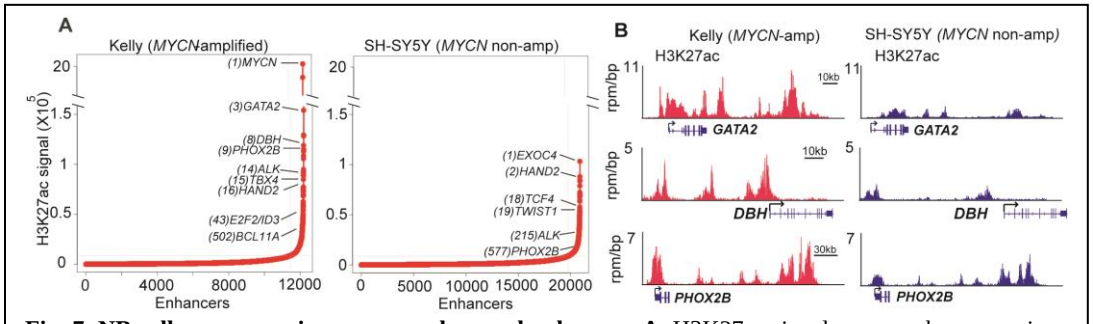

Fig. 7. NB cells possess unique super-enhancer landscapes. A. H3K27ac signal across enhancer regions in NB cells. **B.** ChIP-seq profiles for H3K27ac binding at representative SE-associated gene loci. The x axis shows genomic position and the y axis the signal of histone mark in units of reads per million per base pair (rpm/bp). The gene model is depicted below and scale bars above the binding profiles.

Task 3: Test whether triple node targeted therapy (TNT) directed simultaneously to ALK, MYCN and a downstream signaling pathway will improve outcome in *in vivo* models of neuroblastoma.

1) Major activities: Mouse breeding, collection of transgenic tumors and sympathetic ganglia.

2) Specific Objectives: To generate sufficient in vivo models to conduct therapy trials.

3) Significant results and conclusions: We have now established our transgenic mouse colony and are generating sufficient numbers of ALK/MYCN transgenic mice We have also established a repository of sympathetic ganglia and tumor tissue from transgenic MYCN only or MYCN/ALKF1174L animals at different stages of development (E15 to P28). We have close to 30 samples from MYCN only, ALKF1174L only, MYCN/ALKF1174L and WT animals.

What opportunities for training and professional development has the project provided?

This project has provided training opportunities for my lab manager, a postdoctoral fellow and a technician. These included a) one-on-one training sessions on manuscript writing, b) opportunities to attend conferences (post doc) and seminars (postdoc, lab manager and technician) and c) acquisition of new laboratory skills during the course of the experiments described above.

How were the results disseminated to communities of interest?

Through publications in scientific journals (see Journal publications).

What do you plan to do during the next reporting period to accomplish the goals?

We plan to elucidate the mechanism of action of the synergy between ALK and CDK inhibitors, validate CDK7 inhibition as a tractable therapeutic strategy against MYCN-dependent cancers. We will also assess the genomic and molecular differences between MYCN-only and MYCN/ALK transgenic tumors using high throughput methods (gene expression profiling) and compare these results with publicly available data of human NB tumors. A major effort during the next reporting period will be concentrated on testing whether triple node targeted therapy targeting ALK, MYCN and a downstream signaling pathway such as the PI3K/mTOR or MAPK pathway can cause tumor regression in neuroblastoma models.

4. IMPACT:

What was the impact on the development of the principal discipline(s) of the project?

Our studies have resulted in the identification of two novel therapeutic strategies for high-risk neuroblastoma – single agent treatment in MYCN-amplified NB, and combination treatment in ALK-mutated, MYCN-amplified NB. Our results with the novel CDK7 inhibitor are also applicable to other MYC-driven cancers and hence extend to a larger subset of cancer patients than neuroblastoma.

What was the impact on other disciplines?

Nothing to Report

What was the impact on technology transfer?

Our results with THZ1, the CDK7 inhibitor has provided supporting data for clinical development of this compound by a pharmaceutical company.

What was the impact on society beyond science and technology?

Nothing to Report.

5. CHANGES/PROBLEMS:

Changes in approach and reasons for change

Nothing to Report.

Actual or anticipated problems or delays and actions or plans to resolve them

Nothing to Report

Changes that had a significant impact on expenditures

Nothing to Report

Significant changes in use or care of human subjects, vertebrate animals, biohazards, and/or select agents

Nothing to Report

Significant changes in use or care of human subjects

Nothing to Report

Significant changes in use or care of vertebrate animals.

Nothing to Report

Significant changes in use of biohazards and/or select agents

Nothing to Report

6. PRODUCTS:

Journal publications.

1. Chipumuro E, Marco E, Christensen CL, Kwiatkowski N, Zhang T, Hatheway CM, Abraham BJ, Sharma B, Yeung C, Altabef A, Perez-Atayde A, Wong K-K, Yuan G-C, Gray NS, Young RA, George RE. CDK7 targeting inhibits super-enhancer-associated oncogenic programs in *MYCN*-amplified tumor cells. ***Cell***, 2014, 159 (5):1126–1139. PMID: 25416950. PMCID: 4243043 (yes)
2. Christensen CL, Kwiatkowski N, Abraham BJ, Carretero J, Al-shahrour F, Zhang T, Chipumuro E, Herter-Sprie GS, Akbay EA, Altabef A, Zhang J, Shimamura T, Capelletti M, Reibel JB, Cavanaugh J, Gao P, Liu Y, Michaelsen SR, Poulsen HS, Aref AR, Barbie DA, Bradner JE, George RE, Gray NS, Young RA, Wong K-K. Targeting Transcriptional Addictions In Small Cell Lung Cancer With a Covalent CDK7 Inhibitor. ***Cancer Cell***, 2014, 26(6):909-22. PMID: 25490451. PMCID: 4261156 (yes).
3. George RE. Seek and Ye Shall Find: Subclonal Anaplastic Lymphoma Kinase Mutations. ***Clin Cancer Res.*** Sept. 2015. PMID: 2636299. [Epub ahead of print] (yes).
4. Debruyne DN, Bhatnagar N, Sharma B, Luther W, Moore NF, Cheung N-K, Gray NS, George RE. ALK inhibitor resistance in ALK^{F1174L}-driven neuroblastoma is associated with AXL activation and induction of EMT. ***Oncogene***, in press (yes).

Books or other non-periodical, one-time publications.

Yeung CM and George RE: "The Role of the Anaplastic Lymphoma Kinase Receptor in Neuroblastoma," in Pediatr Adolesc Med, (Eds. Christiansen H, Christiansen NM: Progressive Neuroblastoma: Innovation and Novel Therapeutic Strategies), S. Karger, Basel, 2015, vol 20, pp 107–119 (DOI: 10.1159/000382093) (no)

Other publications, conference papers, and presentations.

Nothing to Report

Website(s) or other Internet site(s)

Nothing to Report

Technologies or techniques

Nothing to Report

Inventions, patent applications, and/or licenses

Nothing to Report

Other Products

Nothing to Report

7. PARTICIPANTS & OTHER COLLABORATING ORGANIZATIONS

What individuals have worked on the project?

Name:	*Bandana Sharma PhD*
Project Role:	*Lab Manager*
Researcher Identifier (e.g. ORCID ID):	
Nearest person month worked:	*5*
Contribution to Project:	*Dr Sharma has performed the mouse breeding, genotyping and tissue collecting experiments.*
Funding Support:	*None*
Name:	*Clarke Hatheway BS*
Project Role:	*Research Technician*
Researcher Identifier (e.g. ORCID ID):	
Nearest person month worked:	*12*
Contribution to Project	*Mr Hatheway assisted with the mouse breeding, genotyping and tissue collecting experiments. He also assisted with the*

	combination studies in Aims 1 and 2.
Funding Support	
Name:	*Hao Huang PhD*
Project Role:	*Postdoctoral fellow*
Researcher Identifier (e.g. ORCID ID):	
Nearest person month worked	*12*
Contribution to Project:	*Performed the experiments in Tasks 1 and 2*
Funding Support:	*None*
Name:	*Rani George*
Project Role:	*PI*
Researcher Identifier (e.g. ORCID ID):	
Nearest person month worked:	*3.36*
Contribution to Project:	*Supervision of all the experiments, mentoring of postdoctoral fellow, technician and lab manager. Ensuring all animal study approvals are in place.*
Funding Support:	*NIH NCI, American Cancer Society Research Scholar Award*

Has there been a change in the active other support of the PD/PI(s) or senior/key personnel since the last reporting period?

Nothing to Report

What other organizations were involved as partners?

Nothing to Report.

8. SPECIAL REPORTING REQUIREMENTS

Nothing to Report.

9. APPENDICES:

Attached.

10. References……..

Berry, T., Luther, W., Bhatnagar, N., Jamin, Y., Poon, E., Sanda, T., Pei, D., Sharma, B., Vetharoy, W. R., Hallsworth, A., *et al.* (2012). The ALK(F1174L) Mutation Potentiates the Oncogenic Activity of MYCN in Neuroblastoma. Cancer Cell *22*, 117-130.
Cheung, N. K., and Dyer, M. A. (2013). Neuroblastoma: developmental biology, cancer genomics and immunotherapy. Nat Rev Cancer *13*, 397-411.

Chipumuro, E., Marco, E., Christensen, C. L., Kwiatkowski, N., Zhang, T., Hatheway, C. M., Abraham, B. J., Sharma, B., Yeung, C., Altabef, A., *et al.* (2014). CDK7 inhibition suppresses super-enhancer-linked oncogenic transcription in MYCN-driven cancer. Cell *159*, 1126-1139.
Conroy, A., Stockett, D. E., Walker, D., Arkin, M. R., Hoch, U., Fox, J. A., and Hawtin, R. E. (2009). SNS-032 is a potent and selective CDK 2, 7 and 9 inhibitor that drives target modulation in patient samples. Cancer Chemother Pharmacol *64*, 723-732.
George, R. E., Sanda, T., Hanna, M., Frohling, S., Luther, W., 2nd, Zhang, J., Ahn, Y., Zhou, W., London, W. B., McGrady, P., *et al.* (2008). Activating mutations in ALK provide a therapeutic target in neuroblastoma. Nature *455*, 975-978.
Larochelle, S., Amat, R., Glover-Cutter, K., Sanso, M., Zhang, C., Allen, J. J., Shokat, K. M., Bentley, D. L., and Fisher, R. P. (2012). Cyclin-dependent kinase control of the initiation-to-elongation switch of RNA polymerase II. Nat Struct Mol Biol *19*, 1108-1115.

Please cite this article in press as: Chipumuro et al., CDK7 Inhibition Suppresses Super-Enhancer-Linked Oncogenic Transcription in MYCN-Driven Cancer, Cell (2014), http://dx.doi.org/10.1016/j.cell.2014.10.024

Cell

CDK7 Inhibition Suppresses Super-Enhancer-Linked Oncogenic Transcription in MYCN-Driven Cancer

Edmond Chipumuro,[1,2] Eugenio Marco,[3,4] Camilla L. Christensen,[5] Nicholas Kwiatkowski,[6] Tinghu Zhang,[7,8] Clark M. Hatheway,[1] Brian J. Abraham,[6] Bandana Sharma,[1] Caleb Yeung,[1,2] Abigail Altabef,[5] Antonio Perez-Atayde,[9] Kwok-Kin Wong,[5] Guo-Cheng Yuan,[3,4] Nathanael S. Gray,[7,8] Richard A. Young,[6] and Rani E. George[1,2,*]

[1]Department of Pediatric Hematology/Oncology, Dana-Farber Cancer Institute and Boston Children's Hospital, Boston, MA 02215, USA
[2]Department of Pediatrics, Harvard Medical School, Boston, MA 02115, USA
[3]Department of Biostatistics and Computational Biology, Dana-Farber Cancer Institute, Boston, MA 02215, USA
[4]Harvard School of Public Health, Boston, MA 02115, USA
[5]Department of Medical Oncology, Dana-Farber Cancer Institute, Boston, MA 02215, USA
[6]Whitehead Institute for Biomedical Research and Department of Biology, Massachusetts Institute of Technology, Cambridge, MA 02139, USA
[7]Department of Cancer Biology, Dana-Farber Cancer Institute, Boston, MA 02215, USA
[8]Department of Biological Chemistry and Molecular Pharmacology, Harvard Medical School, Boston, MA 02115, USA
[9]Department of Pathology, Boston Children's Hospital, MA 02115, USA
*Correspondence: rani_george@dfci.harvard.edu
http://dx.doi.org/10.1016/j.cell.2014.10.024

SUMMARY

The MYC oncoproteins are thought to stimulate tumor cell growth and proliferation through amplification of gene transcription, a mechanism that has thwarted most efforts to inhibit MYC function as potential cancer therapy. Using a covalent inhibitor of cyclin-dependent kinase 7 (CDK7) to disrupt the transcription of amplified *MYCN* in neuroblastoma cells, we demonstrate downregulation of the oncoprotein with consequent massive suppression of MYCN-driven global transcriptional amplification. This response translated to significant tumor regression in a mouse model of high-risk neuroblastoma, without the introduction of systemic toxicity. The striking treatment selectivity of *MYCN*-overexpressing cells correlated with preferential downregulation of super-enhancer-associated genes, including *MYCN* and other known oncogenic drivers in neuroblastoma. These results indicate that CDK7 inhibition, by selectively targeting the mechanisms that promote global transcriptional amplification in tumor cells, may be useful therapy for cancers that are driven by MYC family oncoproteins.

INTRODUCTION

Many human cancers depend on the deregulated expression of *MYC* family members for their aberrant growth and proliferation, with elevated expression of these oncogenes predicting aggressive disease and a poor clinical outcome (Eilers and Eisenman, 2008; Wasylishen and Penn, 2010). Deactivation of MYC in cell lines and MYC-induced transgenic tumors causes proliferative arrest and tumor regression (Arvanitis and Felsher, 2006; Soucek et al., 2008), suggesting that effective targeting of MYC proteins would have broad therapeutic benefit. Recently, several groups reported that oncogenic MYC elicits its plethora of downstream effects in tumor cells through global transcriptional amplification, leading to massively upregulated expression of genes involved in multiple processes (Lin et al., 2012; Lovén et al., 2012; Nie et al., 2012; Schuhmacher and Eick, 2013). When present at physiological levels, MYC binds to the core promoters of actively transcribed genes; however, in tumor cells with *MYC* overexpression, increased MYC levels are observed at both the core promoters and enhancers of the same set of genes, resulting in increased levels of transcripts per cell. This mechanism provides an explanation for the lack of a common *MYC* transcriptional signature and for the diverse effects of deregulated MYC in cancer cells. Another general feature of deregulated MYC is its transcriptional regulation by super-enhancers (SEs), clusters of enhancers that are densely occupied by transcription factors, cofactors, and chromatin regulators (Hnisz et al., 2013). SEs are acquired by cancer cells through gene amplification, translocation or transcription factor overexpression. They facilitate high-level expression of genes, including *MYC,* whose protein products are critical for the control of cell identity, growth, and proliferation, and which are especially sensitive to perturbation (Chapuy et al., 2013; Hnisz et al., 2013; Lovén et al., 2013). These emerging insights into the role of oncogenic MYC as an SE-associated transcriptional amplifier suggest that strategies aimed at disrupting the molecular mechanisms that drive this function might provide useful therapy for different MYC-dependent tumors.

The transcription cycle of RNA polymerase II (Pol II) is regulated by a set of cyclin-dependent kinases (CDKs) that have critical roles in transcription initiation and elongation (Larochelle et al., 2012). In contrast to the cell-cycle CDKs which are largely responsible for cell-cycle transition, these transcriptional CDKs

(especially CDK7, a subunit of TFIIH, and CDK9, a subunit of pTEFb) phosphorylate the carboxy-terminal domain (CTD) of Pol II, facilitating efficient transcriptional initiation, pause release and elongation. Moreover, most CDKs are activated through T-loop phosphorylation by a CDK-activating kinase (CAK), which in metazoans appears to be uniquely controlled by CDK7 (Fisher and Morgan, 1994; Glover-Cutter et al., 2009; Larochelle et al., 2007, 2012; Rossignol et al., 1997; Serizawa et al., 1995). Inhibition of transcriptional CDKs primarily affects the accumulation of transcripts with short half-lives, including antiapoptosis family members and cell-cycle regulators (Garriga and Graña, 2004; Lam et al., 2001), rendering this group of kinases ideal candidates for blocking MYC-dependent transcriptional amplification.

Here, we investigate whether inhibition of transcriptional CDKs can be exploited to disrupt aberrant MYC-driven transcription, using the deregulated expression of *MYCN* as a model. The MYCN protein shares most of the physical properties of MYC (Kohl et al., 1986) and is considered functionally interchangeable, based on the similarity of their transcriptional programs, the cellular phenotypes they induce, and the ability of MYCN to replace MYC during murine development (Boon et al., 2001; Malynn et al., 2000; Toyoshima et al., 2012). In neuroblastoma (NB), a pediatric solid tumor arising in the peripheral sympathetic nervous system, *MYCN* amplification is typically associated with a dismal prognosis, regardless of the treatment used (Brodeur et al., 1984; Seeger et al., 1985).

We demonstrate that THZ1, a newly developed covalent inhibitor of CDK7 (Kwiatkowski et al., 2014), selectively targets *MYCN*-amplified NB cells, leading to global repression of *MYCN*-dependent transcriptional amplification. This response induces sustained growth inhibition of tumors in a mouse model of NB. The remarkable sensitivity of *MYCN*-amplified cells to CDK7 inhibition is associated with preferentially reduced expression of SE-associated oncogenic drivers, especially *MYCN*.

RESULTS

THZ1 Exerts Potent and Selective Effects in *MYC*-Deregulated Cells

To identify CDKs whose depletion might lead to decreased *MYCN* expression and subsequent apoptosis, we performed a short hairpin (shRNA) knockdown screen of CDKs with known transcriptional activities (CDK7, CDK8, CDK9, CDK12, CDK13, and CDK19) in Kelly cells, a human NB line that expresses very high levels of *MYCN* RNA and protein due to genomically amplified *MYCN* (100–120 copies per cell) (Schwab et al., 1983). Genetic depletion of CDK7, CDK8, CDK9, or CDK19 led to marked decreases of *MYCN* RNA and protein with a concomitant increase in cleaved caspase 3 (CC3) expression (Figures S1A and S1B available online). To reproduce these results pharmacologically, we tested a panel of 11 inhibitors with activity against transcriptional CDKs in three *MYCN*-amplified cell lines, observing a range of sensitivities, with the highest potency (IC_{50}, 6–9 nM) shown by a newly developed covalent phenylaminopyrimidine inhibitor of CDK7, THZ1 (Kwiatkowski et al., 2014) (Figure S1C; Table S1). Similar results were obtained when THZ1 was tested against a larger panel of *MYCN*-amplified NB cell lines with varying levels of *MYCN* expression (Figures 1A and S1D). Importantly, NB cells without *MYCN* amplification were far less sensitive to THZ1, with IC_{50} values averaging ten times higher than those of *MYCN*-amplified cells (Figure 1A; Table S1). Notably, the NBL-S cell line, which expresses high levels of *MYCN* without genomic amplification (Cohn et al., 1990) (Figure S1D), was quite sensitive to THZ1, while two nontransformed lines (B6-MEFs and NIH 3T3) were relatively insensitive (Figure 1A). *MYCN*-amplified cells also showed enhanced sensitivity to THZ1R, a reversible analog of THZ1 that lacks the acrylamide moiety required for covalent bond formation, although it was not as potent as the covalent inhibitor (Figure 1B). The strong selectivity of THZ1 for *MYCN*-amplified cells was not restricted to NB, but extended to H262-BT111, a human primitive neuroectodermal tumor cell line expressing amplified *MYCN* (K. Ligon, personal communication) and Raji and Daudi lymphoma cells, both characterized by *MYC* overexpression due to chromosomal translocation (Nishikura et al., 1985; Veronese et al., 1995) (Figure S1E). To probe this preferential effect further, we tested the extent of target engagement in NB cells, using a biotinylated derivative of THZ1 (bio-THZ1) with or without THZ1 pretreatment. Bio-THZ1 consistently bound to CDK7 in both *MYCN*-amplified and nonamplified untreated cells (Figure S1F), but became less efficient after THZ1 treatment, suggesting that target recognition was not a major factor in the enhanced inhibitory effects of THZ1 in *MYCN*-amplified cells.

Next, we studied the growth inhibitory effects of THZ1. *MYCN*-amplified cells treated with THZ1 underwent cell-cycle arrest in G2/M at 24 hr, an effect that was not observed in *MYCN*-nonamplified NB cells, even after 48 hr (Figure 1C). Moreover, THZ1 led to a profound induction of apoptosis in high *MYCN*-expressing cells, but not in cells expressing nonamplified *MYCN* (Figures 1D and S1G). Together, these data indicate that THZ1 induces selective cytotoxicity not only in NB cells with *MYCN* amplification, but also in other cancers overexpressing either the *MYCN* or *MYC* oncogene.

THZ1 Inhibits Tumor Growth in a Mouse Model of Human *MYCN*-Amplified NB

Given the relative lack of target specificity of past CDK inhibitors, leading to adverse effects in normal cells (Lapenna and Giordano, 2009), we assessed the tolerability of THZ1 in non-tumor-bearing mice (n = 6) treated with 10 mg/kg intravenously twice daily. No systemic toxicity was observed even after 4 weeks of continuous administration (data not shown). We next tested the therapeutic effects of THZ1 in xenograft models of *MYCN*-amplified human NB derived from subcutaneous flank injection of Kelly cells. When tumors reached an optimal size (mean volume, ~150 mm^3; range, 75–235 mm^3), the animals were divided into two groups and treated with vehicle (n = 9) or THZ1 as above (n = 14). Treatment was continued for a mean of 20 days (range, 15–24 days) in the control group and 24 days (range, 20–28 days) in the THZ1 group. Mice receiving THZ1 had a statistically significant reduction in tumor growth, again without toxicity (Figure 1E). Two animals remained free of tumor recurrence at 35 and 128 days posttreatment.

Tumors from vehicle-treated mice displayed histological features of human NB with poorly differentiated, small round blue cells displaying high mitotic activity (Figure 1F). By contrast,

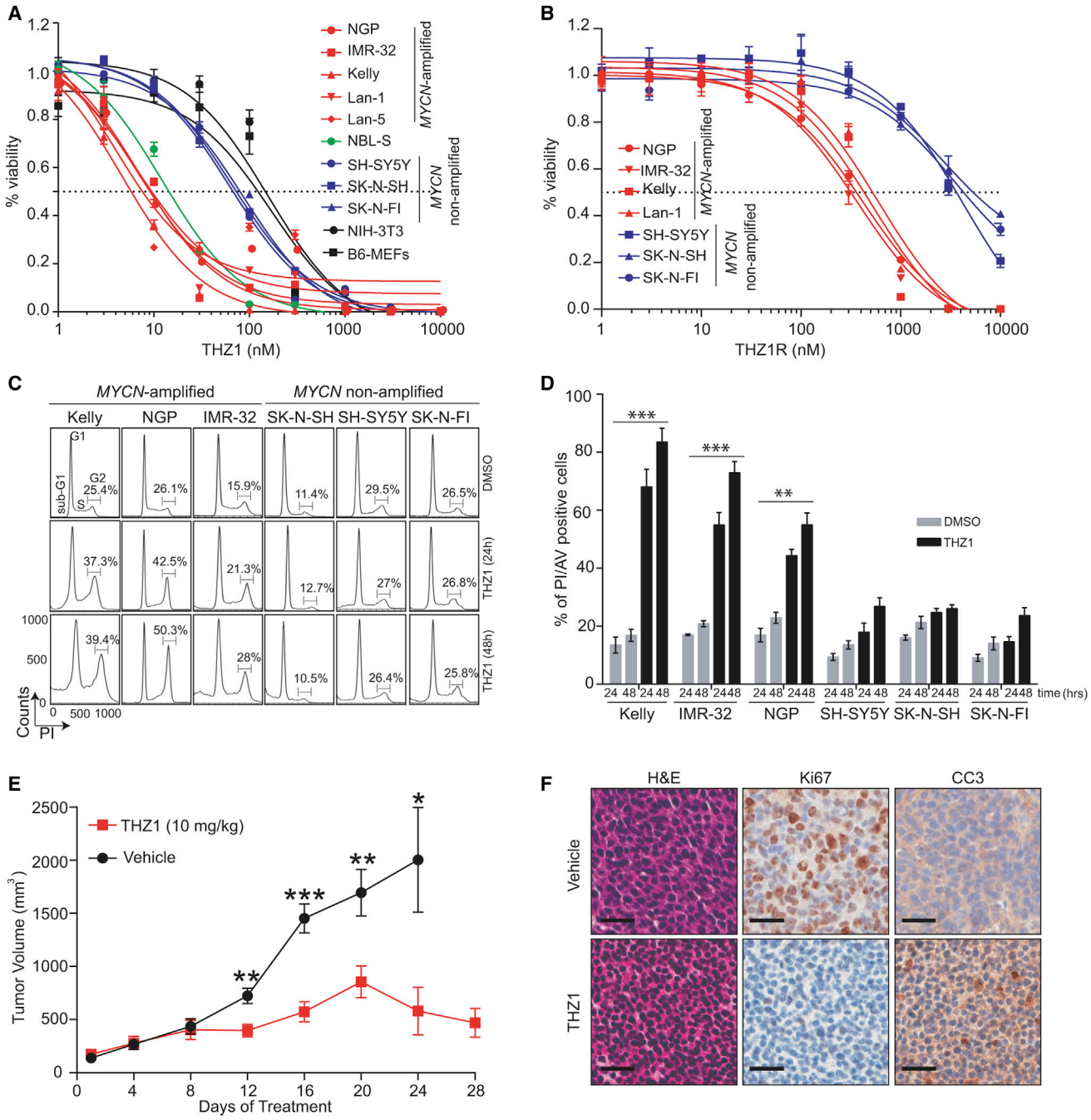

Figure 1. THZ1 Exhibits High Potency and Selectivity against *MYCN*-Amplified Tumor Cells

(A) Dose-response curves of *MYCN*-amplified and nonamplified human NB and murine fibroblast cells after treatment with increasing concentrations of THZ1 for 72 hr. Percent cell viability relative to that of DMSO-treated cells is shown here and in (B). Data represent mean ± SD of three replicates here and in (B).

(B) Dose-response curves of NB cells treated as in (A) with the reversible CDK7 inhibitor THZ1R.

(C) Cell-cycle analysis of *MYCN*-amplified versus nonamplified NB cells exposed to THZ1 (100 nM × 24 and 48 hr) by flow cytometry with propidium iodide (PI) staining. Results are representative of three replicates. The scale and axes are indicated in the lower left corner.

(D) Apoptosis analysis in *MYCN*-amplified and nonamplified NB cells treated with THZ1 as in (C) by flow cytometry with Annexin V staining. Data represent mean ± SD of three replicates. ***$p < 0.0001$, **$p < 0.001$ (Student's t test).

(E) Tumor volumes of *MYCN*-amplified human NB xenografts in NU/NU (*Crl:NU-Foxn1^{nu}*) mice treated with THZ1 (10 mg/kg intravenously [i.v.] twice daily) (n = 14) or vehicle (n = 9) for 28 days. Mean ± SD values are presented. ***$p < 0.001$; **$p < 0.01$; *$p < 0.05$ (multiple t test, Holm-Sidak method).

(F) Immunohistochemical (IHC) analysis of morphology (hematoxylin & eosin [H&E]), proliferation (Ki67) and apoptosis (cleaved caspase 3 [CC3]) in tumors harvested from animals treated with vehicle or THZ1 as in (E) for 12 days. Scale bar represents 25 μM.

See also Figure S1 and Table S1.

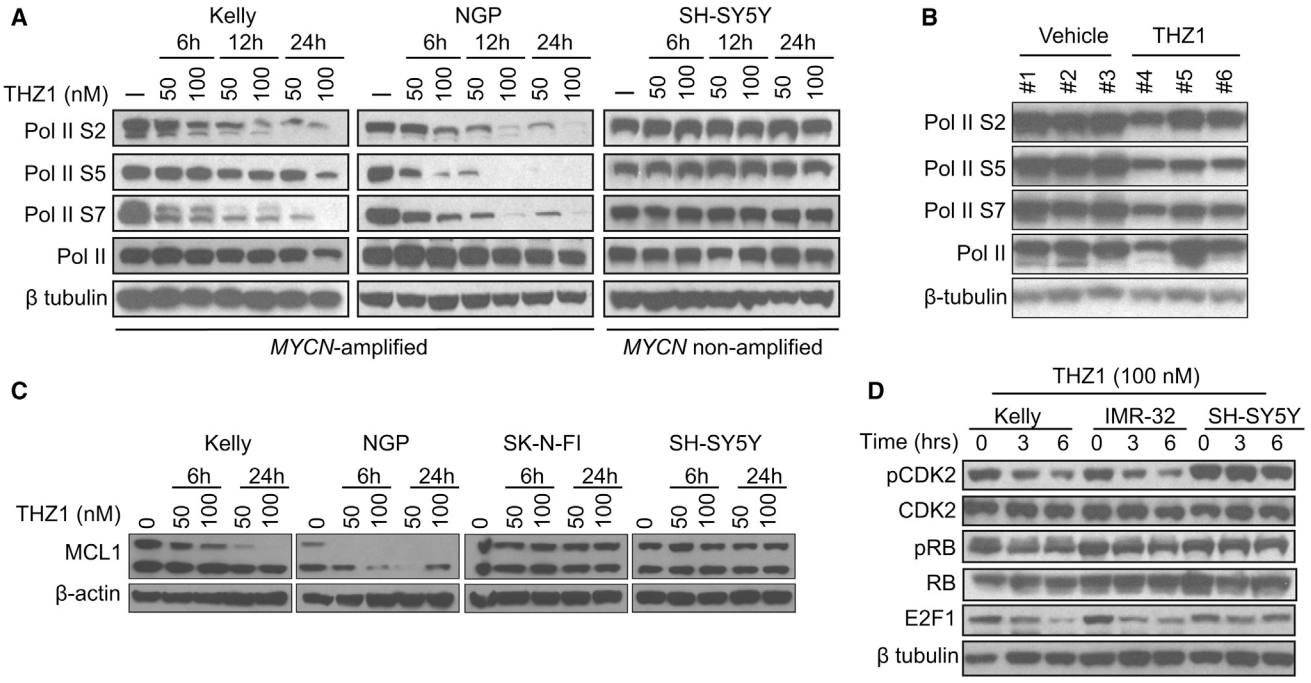

Figure 2. THZ1 Inhibits General Transcription and Cell-Cycle Regulation in *MYCN*-Amplified Tumor Models

(A) Immunoblot analysis of RNA Pol II CTD phosphorylation in *MYCN*-amplified and nonamplified NB cells treated with DMSO or THZ1 at the indicated concentrations for the indicated times.

(B) Immunoblot analysis of RNA Pol II CTD phosphorylation in human NB xenograft tumor cells obtained from mice treated with vehicle or THZ1 (10 mg/kg i.v. twice daily) for 12 days.

(C) Immunoblot analysis of MCL1 in *MYCN*-amplified (Kelly, NGP) versus nonamplified (SK-N-FI, SH-SY5Y) NB cells following treatment with THZ1 at the indicated concentrations and durations.

(D) Immunoblot analysis of proteins involved in cell-cycle progression in *MYCN*-amplified (Kelly, IMR-32) and nonamplified (SH-SY5Y) NB cells following treatment with THZ1 100 nM for 3 and 6 hr.

See also Figure S2.

the vast majority of tumor cells in the THZ1-treated animals demonstrated necrosis, reduced proliferative activity and increased apoptosis. To ensure target engagement in the tumor cells, we used bio-THZ1 to pull down CDK7 in cell lysates from both vehicle- and THZ1-treated animals, noting decreased binding with bio-THZ1 in the latter (Figure S1H). We also confirmed that the lack of toxicity in the animal models did not reflect THZ1 selectivity for human CDK7, as bio-THZ1 formed a complex with murine CDK7 in cell lysates from NIH 3T3 cells treated with THZ1 (Figure S1H). These results demonstrate the feasibility of specifically targeting CDK7 in tumor cells driven by deregulated *MYC* or *MYCN*.

THZ1 Affects Both Transcription and Cell-Cycle Progression in *MYCN*-Amplified Cells

As a transcriptional kinase, CDK7 exerts its effects through regulation of RNA Pol II-mediated transcriptional initiation and pause establishment, while also affecting elongation through its CAK activity on other transcriptional CDKs (Glover-Cutter et al., 2009; Larochelle et al., 2012; Palancade and Bensaude, 2003). We observed a dose-dependent decrease in the initiation-associated serine 5 (S5) and serine 7 (S7) and the elongation-associated serine 2 (S2) Pol II phosphorylation in *MYCN*-amplified but not nonamplified cells treated with THZ1 (Figures 2A and S2A). Pol II CTD phosphorylation was also downregulated in tumor cells from animals treated with THZ1 (Figure 2B). Downregulation of CDK7 phosphorylation was seen in *MYCN*-amplified cells (Figure S2B), consistent with the finding that CDK7 is regulated by phosphorylation within its own activation (T) loop (Larochelle et al., 2012). Phosphorylation of CDK9 was also decreased in *MYCN*-amplified cells (Figure S2C), reinforcing the effect of THZ1 on transcription elongation. Total protein levels of CDK9 were also decreased in these cells but not nonamplified cells, suggesting that THZ1-induced CDK7 inhibition might also target the transcription of CDK9 (Figure S2C).

The decrease in Pol II phosphorylation after THZ1 treatment in *MYCN*-amplified cells coincided with the loss of the short-lived antiapoptotic protein MCL1 (Figure 2C). Similar effects on Pol II CTD phosphorylation and MCL1 levels were observed in Raji, Daudi, and H262-BTIII cells, all of which depend on *MYC* or *MYCN* overexpression and are sensitive to THZ1 (Figure S2D). Importantly, the effects of THZ1, including Pol II CTD phosphorylation and the induction of apoptosis, could be rescued by a mutation in the covalent binding site of CDK7 ($CDK7^{C312S}$) (Figure S2E), indicating on-target effects of THZ1 on CDK7.

CDK7 also stimulates cell-cycle progression by activating CDK1 and CDK2 through its T-loop phosphorylation function (Larochelle et al., 2007). We observed a time-dependent

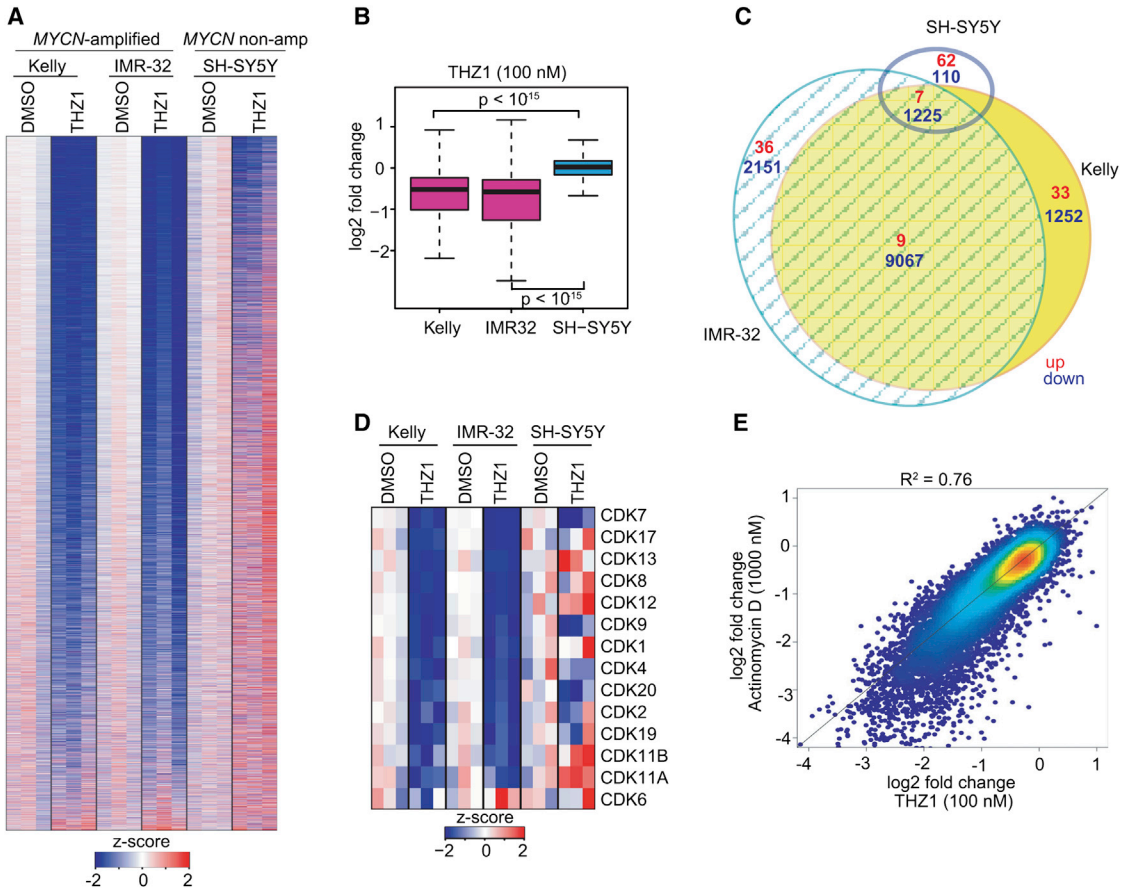

Figure 3. THZ1 Causes Massive Downregulation of Actively Transcribed Genes in *MYCN*-Overexpressing NB Cells

(A) Heatmap of gene expression values in *MYCN*-amplified and nonamplified cells treated with THZ1 (100 nM for 6 hr) versus DMSO. Rows show *Z* scores calculated for each cell type.

(B) Quartile box plots of log2 fold changes in gene expression in *MYCN*-amplified and nonamplified cells treated with DMSO or THZ1 at the same dose and duration as in (A). Box plot whiskers extend to 1.5 times the interquartile range (n = 18,665 expressed genes, $p < 10^{-15}$ for Kelly versus SH-SY5Y and IMR-32 versus SH-SY5Y, two-sided Mann-Whitney U test).

(C) Venn diagram depicting the overlap between sets of differentially expressed transcripts (THZ1 versus DMSO) in *MYCN*-amplified (Kelly, IMR-32), and nonamplified (SH-SY5Y) cells treated with THZ1 as in (A). Red represents upregulated transcripts. Blue represents downregulated transcripts.

(D) Heatmap of gene expression values of transcriptional and cell-cycle CDKs in *MYCN*-amplified and nonamplified cells treated with THZ1 as in (A) versus DMSO. Rows show *Z* scores calculated for each cell type.

(E) Correlation between log2 fold changes in gene expression following THZ1 (100 nM) versus DMSO treatment and actinomycin D (1 μM) versus DMSO treatment for 6 hr. in *MYCN*-amplified NB cells. R^2 (coefficient of determination) calculated using a simple linear regression model.

See also Figure S3.

decrease in CDK1 and CDK2 phosphorylation and in other proteins involved in cell-cycle regulation (pRB and E2F), that was more striking in *MYCN*-amplified cells (Figures 2D and S2F). However, the Pol II inhibitor triptolide appeared to show selectivity for *MYCN*-overexpressing cells, compared to purvanolol, which primarily targets cell-cycle CDKs (Figure S2G). Thus, although THZ1 causes cytotoxicity through transcriptional as well as cell-cycle inhibition in *MYC*-driven tumor cells, the latter effect is most likely through decreased transcription of cell-cycle CDKs.

CDK7 Inhibition Causes Widespread Transcriptional Shutdown in *MYCN*-Amplified NB Cells

Because THZ1 preferentially downregulates RNA Pol II CTD phosphorylation in *MYCN*-amplified cells (Figures 2A and S2A), we next compared the consequences of CDK7 inhibition on global gene expression in *MYCN*-amplified (Kelly and IMR-32) versus nonamplified (SH-SY5Y) cells following exposure to 100 nM THZ1 for 6 hr. Expression profiling was performed with "spike-in" RNA standards normalized to cell number to enable accurate detection of differences in total RNA levels in cells with or without *MYCN* overexpression (Lovén et al., 2012).

We observed a genome-wide decrease in the mRNA expression levels of most actively transcribed genes in *MYCN*-amplified cell lines compared to DMSO-treated cells (Figure 3A). This widespread downregulation of gene expression was not apparent in *MYCN*-nonamplified SH-SY5Y cells treated with the same dose and duration of THZ1 (Figure 3A). Indeed, the percentage of actively transcribed genes significantly downregulated in

these cells was only 7.5%, contrasting with 63% for Kelly and 68% for IMR-32 *MYCN*-amplified cells (false discovery rate [FDR] <0.05) (Figure 3B). Moreover, Kelly and IMR-32 cells had 55% (n = 10,292) downregulated transcripts in common, while only 12% (n = 1,225) of these were also downregulated in SH-SY5Y cells (out of 18,665 genes) (Figure 3C). The most downregulated genes and gene sets in the *MYCN*-amplified cells were transcriptional and cell-cycle regulators (Figures S3A and S3B); including transcripts of CDKs and their partner cyclins (Figures 3D and S3C). Comparison of expression profiles of *MYCN*-amplified cells exposed to THZ1 with those exposed to the general transcription inhibitor actinomycin D revealed a significant correlation between the two (R^2 = 0.76) (Figure 3E). These results led us to conclude that CDK7 inhibition, through THZ1, preferentially downregulates global transcription in *MYCN*-amplified NB cells, affecting most active genes.

THZ1 Targets Deregulated MYCN in NB Cells

The selectivity of THZ1 for MYC/MYCN-deregulated cells led us to investigate its effects on MYCN expression and function. We observed that *MYCN* mRNA was among the top 15% of significantly downregulated transcripts in NB cell lines most sensitive to THZ1. Moreover, transcripts differentially regulated on exposure to THZ1 showed enrichment for previously published MYCN/MYC target gene sets (Figure S4A). THZ1 treatment resulted in a dose- and time-dependent downregulation of *MYCN* mRNA and protein levels in *MYCN*-amplified cells (Figures 4A and 4B), which were rescued by overexpression of the $CDK7^{C312S}$ mutant (Figure S4B), similar to observations with an ATP analog in colorectal carcinoma cells expressing a *CDK7* mutation (Glover-Cutter et al., 2009). We also observed downregulation of MYCN protein levels in the human NB tumors from mice that responded to THZ1 (Figure 4C). These effects primarily reflected a reduction in *MYCN* transcripts, as comparison of MYCN protein turnover in *MYCN*-amplified cells exposed to either THZ1 or actinomycin D showed largely similar rates of degradation (Figure S4C). Finally, analysis of MYCN occupancy at the promoters of two of its known transcriptional targets, *MDM2* (Slack et al., 2005) and *MCL1* (Labisso et al., 2012), revealed significantly decreased MYCN binding, consistent with the disruption of MYCN function by THZ1 (Figure 4D).

Next, we determined whether genetic depletion of MYCN mimicked the effects of THZ1 in *MYCN*-amplified cells. Abrogation of amplified *MYCN* expression in Kelly cells using shRNA knockdown led to decreased Pol II CTD phosphorylation at S2, S5, and S7 (Figure 4E), similar to our findings with THZ1 treatment. The inhibition of transcription associated with *MYCN* knockdown was coupled with complete loss of MCL1 and subsequent cell death (Figure 4E). We next asked whether ectopic expression of *MYCN* would sensitize cells to THZ1. *MYCN*-nonamplified SH-SY5Y cells were engineered to express the oncogene by lentiviral transduction, resulting in approximately 380-fold increases in *MYCN* mRNA and protein levels (Figure 4F), equivalent to those in *MYCN*-amplified cells (Figure S1D). Ectopic expression of *MYCN* in these cells led to a 5-fold greater sensitivity to THZ1 compared with untransfected or vector control-transfected SH-SY5Y cells (Figure 4G). Together, these results indicate that THZ1 specifically targets deregulated MYCN in NB cells.

Amplified *MYCN* Induces Global Transcriptional Amplification that Is Inhibited by THZ1

Downregulation of *MYCN* alone seemed insufficient to account for the widespread effects of THZ1 on the transcriptional output of cells harboring amplified *MYCN*. We therefore questioned whether deregulated MYCN, like MYC, binds promiscuously to active genes, leading to global transcriptional amplification, and whether THZ1 preferentially disrupts this effect. Indeed, ectopic expression of *MYCN* in SH-SY5Y cells led to increased cell size (Figure S5A) and significantly increased expression of all active transcripts (Figures 5A and S5B). Moreover, THZ1 treatment led to significant downregulation of transcriptional output in these cells (Figure 5B) with induction of apoptosis, although MYCN protein levels were not affected (Figure 5C). Furthermore, shRNA knockdown of *MYCN* in *MYCN*-amplified cells led to a striking downregulation of global gene expression in comparison to their control shRNA-expressing counterparts (Figures 5D and 5E), again underscoring the widespread transcriptional effects of deregulated *MYCN*. To determine the extent to which these effects mirrored those of CDK7 inhibition, we compared the expression profiles of *MYCN*-amplified cells expressing a *MYCN* shRNA with those of THZ1-treated cells, noting significant downregulation of the actively transcribed genes in both types of cells, with a close correlation between the top 500 downregulated transcripts in THZ1-treated cells and those in *MYCN* shRNA-depleted cells (Figures 5F and S5C). Hence, disruption of *MYCN*-induced transcriptional amplification also contributes to the striking effects of THZ1.

Super-Enhancers Account for the Selectivity of THZ1 for *MYCN*-Amplified NB Cells

We observed that the ectopic overexpression of *MYCN* in nonamplified cells led to global transcriptional upregulation and sensitization to the growth inhibitory effects of THZ1, although the latter effect did not approach the levels seen in cells with endogenously amplified *MYCN*. We therefore investigated the possible contribution of super-enhancers (SEs) to the extreme susceptibility of endogenous *MYCN*-amplified cells to THZ1. Using chromatin immunoprecipitation with high-throughput sequencing (ChIP-seq) of histone H3K27 acetylation (H3K27ac), a mark of active enhancers (Hnisz et al., 2013), we first identified enhancer regions in *MYCN*-amplified Kelly and nonamplified SH-SY5Y cells (Figure S6A). In both cell types, a subset of H3K27ac-bound enhancers (Kelly 6.1%, SH-SY5Y, 5.4%) had a significantly higher signal than regular enhancers and were therefore classified as SEs (Lovén et al., 2013; Whyte et al., 2013) (Figure 6A). We also analyzed the occupancy of H3K4 monomethylation, a mark that colocalizes with H3K27ac in strong enhancers, noting a high concordance (94%–99%) with enhancers identified by H3K27ac analysis (Figures 6B and S6B).

The SEs in *MYCN*-amplified cells were either unique or disproportionately loaded with H3K27ac, with the largest SE being associated with the *MYCN* oncogene itself, having an H3K27Ac signal that was at least ten times greater than that of any other SE in either these or *MYCN*-nonamplified cells (Figures 6A and 6B).

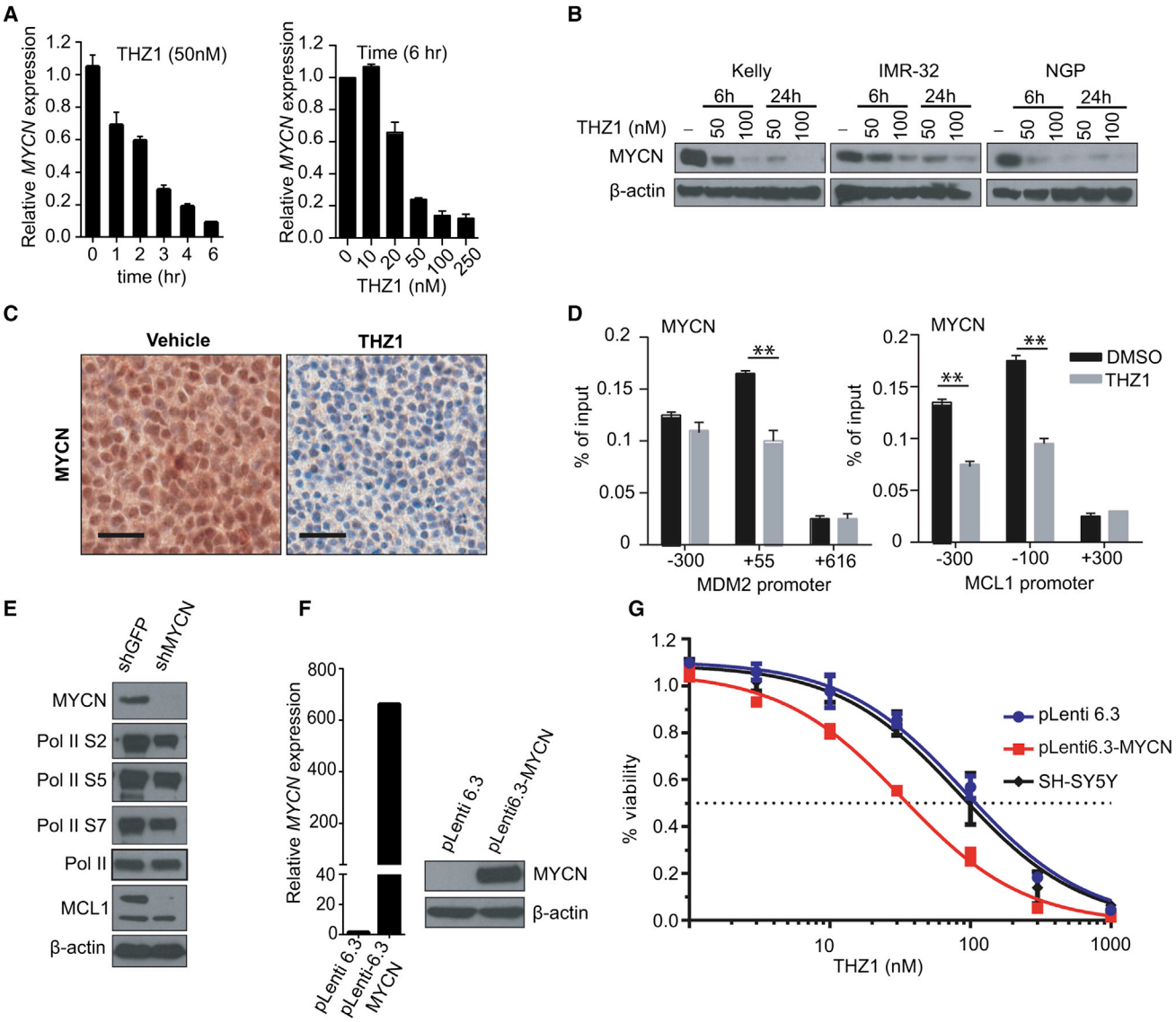

Figure 4. Cytotoxic Effects of THZ1 Are Mediated in Part through Inhibition of MYCN Expression

(A) Quantitative RT-PCR (qRT-PCR) analysis of *MYCN* RNA expression in *MYCN*-amplified Kelly cells treated with THZ1 50 nM for 0–6 hr (left) or 0–250 nM for 6 hr (right). Data normalized to β-actin are presented as mean ± SD of three biological replicates.

(B) Immunoblot analysis of MYCN protein expression in *MYCN*-amplified NB cells treated with the indicated doses of THZ1 for 6 or 24 hr.

(C) IHC analysis of MYCN protein expression in *MYCN*-amplified human NB xenograft models treated with either DMSO or 10 mg/kg i.v. twice daily of THZ1 for 12 days. Scale bars represent 25 μM.

(D) ChIP-qPCR analysis of MYCN binding at the promoters of candidate target genes in *MYCN*-amplified cells following treatment with THZ1, 100 nM for 3 hr. Mean ± SD values for three replicate experiments are shown. **$p < 0.01$ (Student's t test).

(E) Immunoblot analysis of the indicated proteins in *MYCN*-amplified NB cells expressing either an shRNA control (shGFP) or an shRNA directed against *MYCN* (shMYCN). Two different hairpins against *MYCN* [shMYCN(1) and shMYCN(3)] were used with similar results.

(F) qRT-PCR analysis of *MYCN* expression in SH-SY5Y *MYCN*-nonamplified cells engineered to express either a control vector (pLenti 6.3) or *MYCN* (pLenti 6.3-MYCN (left). Immunoblot analysis of MYCN protein expression in these cells (right).

(G) Cell viability analysis of untransfected (SH-SY5Y), control vector-expressing (pLenti 6.3) or MYCN-expressing (pLenti 6.3-MYCN) *MYCN*-nonamplified NB cells treated for 72 hr with increasing doses of THZ1. Results are means ± SD of three replicates.

See also Figure S4.

Because the *MYCN* SE in Kelly cells is contained within the *MYCN* amplicon, we questioned whether its SE status merely reflected the increased number of copies of the amplified gene. To investigate this possibility, we estimated the signal of a single copy of *MYCN* and recalculated its rank within the list of enhancers. A single copy of the *MYCN* enhancer still fell within the group of SEs (ranked 250 out of 746), indicating that increased gene copy number does not account for the high SE

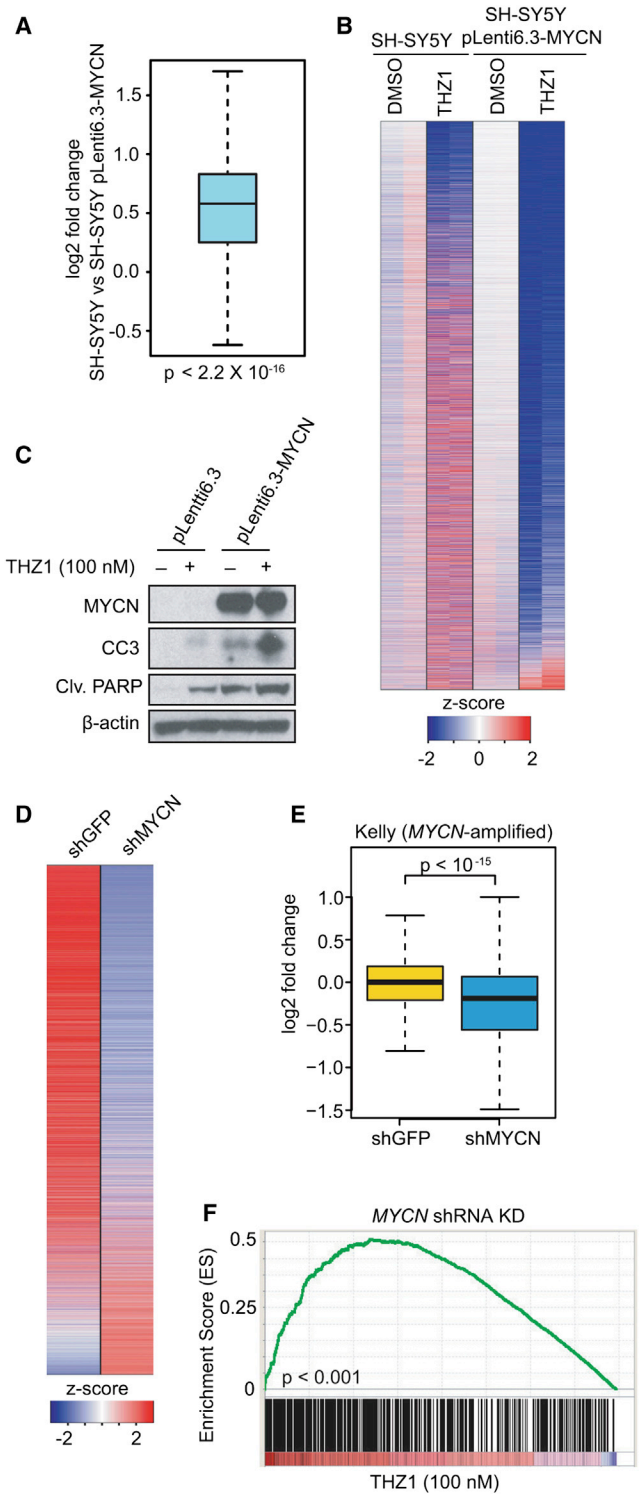

Figure 5. THZ1 Inhibits *MYCN*-Driven Transcriptional Amplification

(A) Box plot depicting the log2 fold changes in actively transcribed genes in *MYCN*-nonamplified SH-SY5Y cells transduced with *MYCN* (pLenti 6.3-MYCN) compared with a control vector (pLenti 6.3). Box plot whiskers extend to 1.5 times the interquartile range (n = 18,665 expressed genes; $p < 2.2 \times 10^{-16}$, two-sided Mann-Whitney U test).

(B) Heatmap of all gene expression values in *MYCN*-nonamplified SH-SY5Y cells versus SH-SY5Y cells overexpressing *MYCN* (pLenti 6.3-MYCN) following either THZ1 (100 nM for 6 hr) or DMSO treatment. Rows show *Z* scores calculated for each vector.

(C) Immunoblot analysis of MYCN, CC3, and cleaved PARP in SH-SY5Y *MYCN*-nonamplified cells engineered to express either a control vector (pLenti 6.3) or *MYCN* (pLenti 6.3-MYCN) following treatment with THZ1.

(D) Heatmap of differentially expressed genes in *MYCN*-amplified NB cells expressing a *MYCN* shRNA versus control shRNA. Rows show *Z* scores calculated for each vector.

(E) Box plots of log2 fold changes in gene expression in *MYCN*-amplified NB cells expressing a *MYCN* shRNA versus a control shRNA. Box plot whiskers extend to 1.5 times the interquartile range (n = 18,665 expressed genes; $p < 10^{-15}$ for shMYCN versus shGFP, two-sided Mann-Whitney U test).

(F) GSEA plot depicting the correlation between the top 500 downregulated genes following THZ1 treatment and the rank-ordered genes that are differentially expressed after *MYCN* knockdown in *MYCN*-amplified NB cells.

See also Figure S5.

signal associated with *MYCN*. The majority of genes associated with the remaining top-ranked SEs were master transcription factors critical to sympathetic neuronal development and cell identity including *PHOX2B* (Pattyn et al., 1999; Stanke et al., 1999), *GATA2* (Tsarovina et al., 2004), *HAND2* (Howard et al., 2000), and *DBH* (Mercer et al., 1991) (Figures 6A and 6C). Another major oncogenic driver in NB, the receptor tyrosine kinase *ALK* (George et al., 2008), was associated with a unique top-ranked SE in *MYCN*-amplified cells (Figures 6A and 6C). In general, the SE domains associated with *MYCN* amplification correlated with pathways involved in the regulation of transcription, while those in nonamplified cells were primarily related to cell adhesion, invasion, metastasis and receptor tyrosine kinase pathways (Figures 6D and S6C). To ensure that the SEs in the cultured cells mirrored those of human NB, we analyzed H3K27ac occupancy in three primary tumors (Figures 6E and S6D). Consistent with our cell line data, the largest SE in *MYCN*-amplified samples NB#1 and NB#2 was associated with *MYCN* (Figures 6E and S6E). SEs associated with *PHOX2B* and *HAND2* were identified in all tumor samples (Figure 6E), in keeping with their lineage-specific role in sympathetic neuronal development.

To determine whether the occurrence of SEs correlates with increased Pol II occupancy, we used ChIP-seq analysis of Pol II and observed that the proximal promoter regions of SE-associated genes had higher levels of Pol II occupancy compared with regular enhancers in both *MYCN*-amplified and nonamplified cells, although the difference was much more striking in the former (Figure 7A). THZ1 treatment led to a striking reduction in Pol II binding at the promoter regions and gene bodies of SE-associated genes in *MYCN*-amplified but not nonamplified cells (Figure 7A). Pol II binding at regular enhancer-associated genes was not appreciably affected by THZ1 in either cell type (Figure 7A). The reduction in Pol II occupancy with THZ1 was observed at the transcription start and end sites of genes associated with the top-ranked SEs, including *MYCN*, suggesting that their expression was severely curtailed in these cells (Figure 7B). Indeed, RNA expression of SE-associated genes was significantly reduced after THZ1 treatment in *MYCN*-amplified cells (Figure 7C) but not of the same genes in *MYCN*-nonamplified cells (Figure 7C). Thus, not only do SEs in *MYCN*-amplified

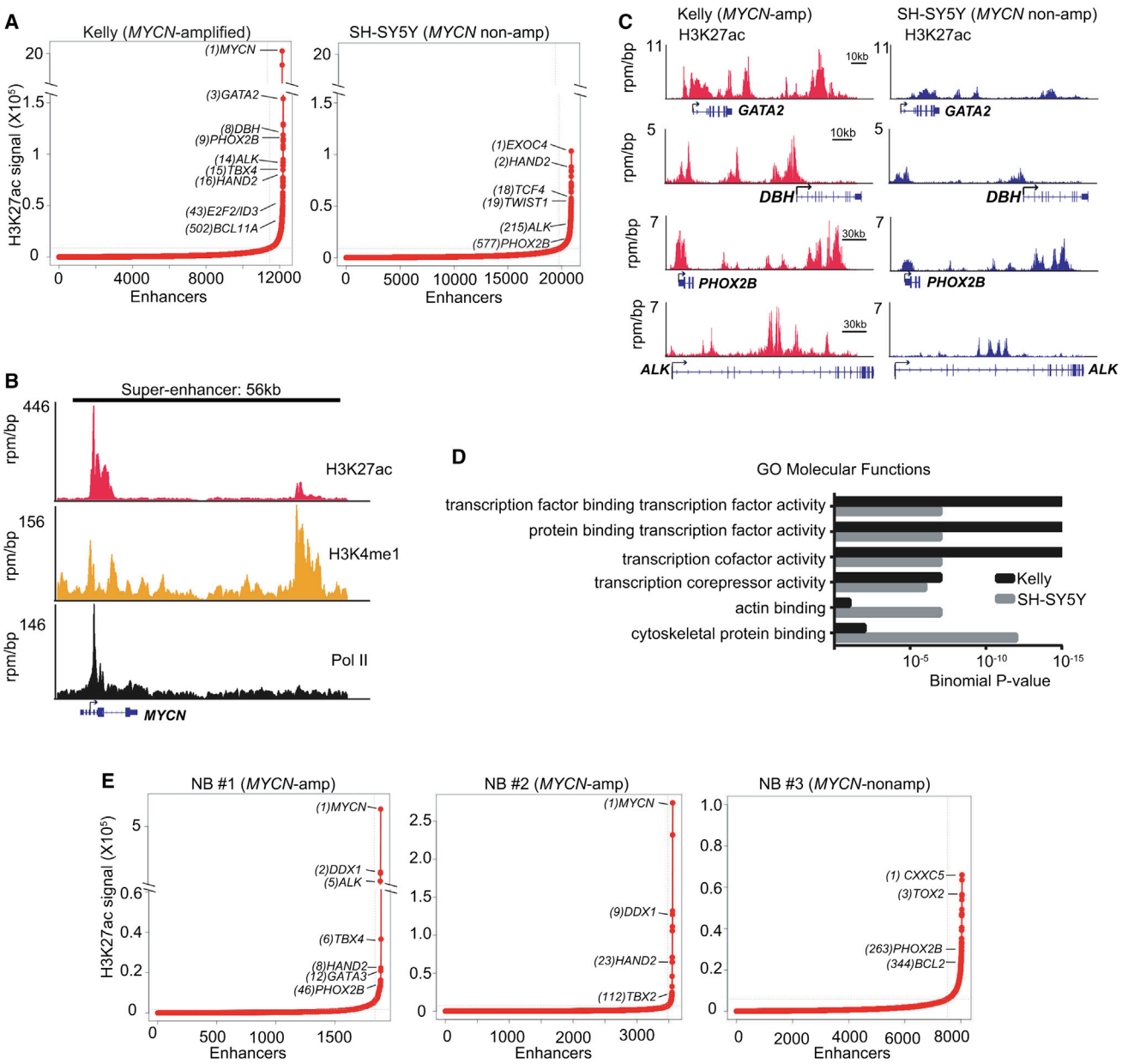

Figure 6. NB Cells Possess Unique Super-Enhancer Landscapes

(A) H3K27ac signal across enhancer regions for all enhancers in *MYCN*-amplified and nonamplified cells. SEs were defined as enhancers surpassing the threshold signal of 8,802 in both cell types. In Kelly and SH-SY5Y cells, 6.1% (746/12,200) and 5.4% (1,136/20,887) of the enhancers comprised 52% and 37%, respectively of all H3K27ac-bound enhancer signal and were classed as SEs.

(B) ChIP-seq profiles for H3K27ac, H3K4me1, and RNA Pol II binding at the *MYCN* SE gene locus in Kelly cells. The x axis shows genomic position and the y axis the signal of histone mark or Pol II binding in units of reads per million per base pair (rpm/bp). The gene model is depicted below and scale bars above the binding profiles.

(C) ChIP-seq profiles for H3K27ac binding at representative SE-associated gene loci in *MYCN*-amplified and nonamplified cells. The x and y axes are as described in (B).

(D) Gene Ontology (GO) molecular functions of SE-associated genes in *MYCN*-amplified (Kelly) and nonamplified (SH-SY5Y) cells identified using GREAT analysis (McLean et al., 2010).

(E) H3K27ac loading across enhancers in *MYCN*-amplified and nonamplified primary NB tumors. SEs were defined as having a threshold signal of 2,427 (NB#1), 5,933 (NB#2), and 5,952 (NB#3). In NB#1 and NB#2, 8.5% (164/1,920) and 3.0% (109/3,561), and in NB#3, 6.4% (522/8,040) of the enhancers were classified as SEs.

See also Figure S6.

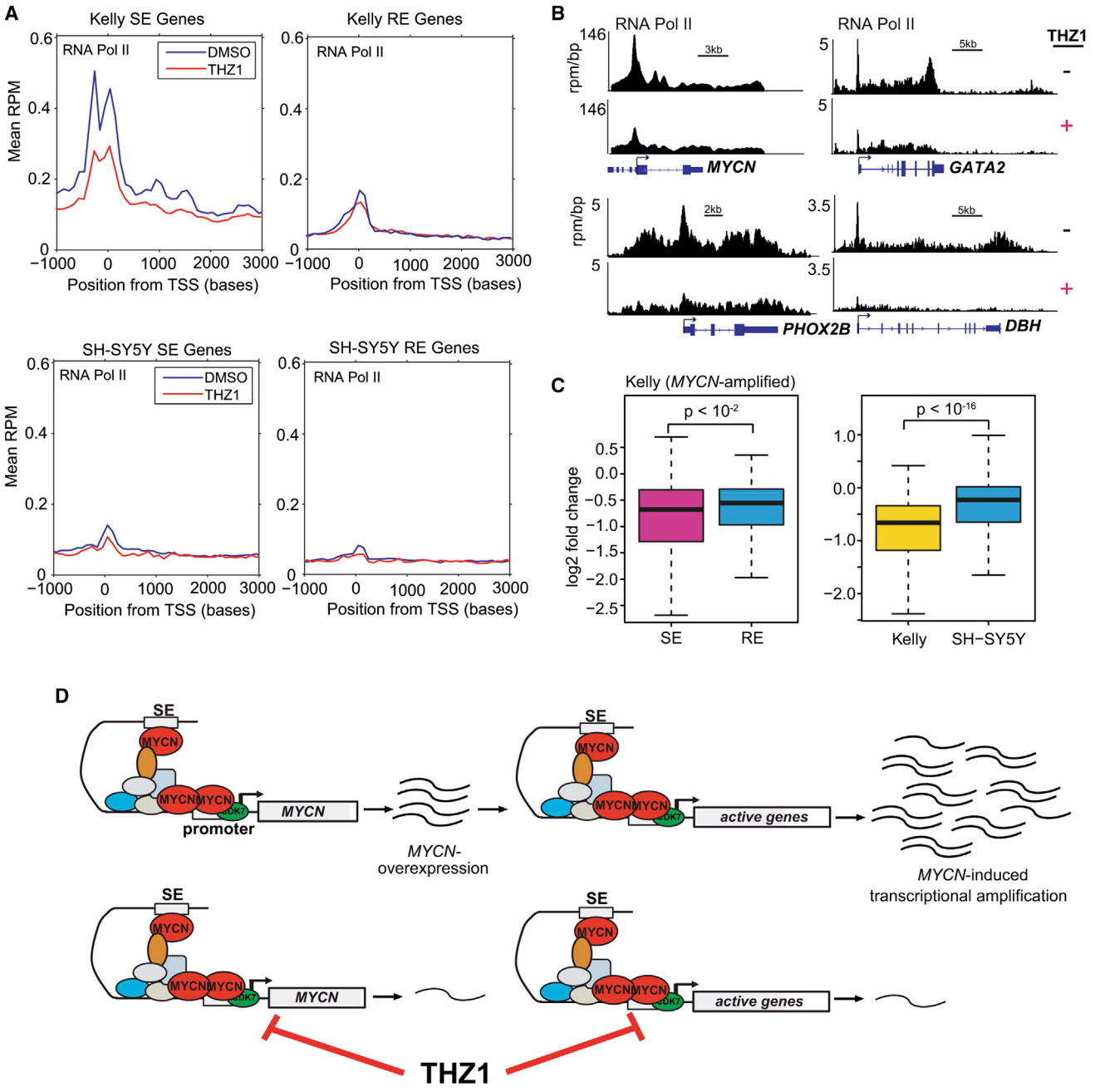

Figure 7. Sensitivity of *MYCN*-Amplified Cells to THZ1 Correlates with *MYCN*-Associated Super-Enhancers

(A) Metagene representation of global Pol II ChIP-seq occupancy at SE- and RE-associated genes in cells with (Kelly) or without (SH-SY5Y) *MYCN* amplification treated with DMSO (blue) or THZ1 (red) (100 nM × 3 hr). TSS, transcription start sites.

(B) Gene tracks of RNA Pol II binding density at representative SE-associated gene loci after DMSO or THZ1 treatment as in (A).

(C) Left: quartile box plots of log2 fold changes in the top 231 genes associated with SEs and regular enhancers (RE) in *MYCN*-amplified cells treated with THZ1 (100 nM × 6 hr) versus DMSO. Box plot whiskers extend to 1.5 times the interquartile range (n = 230 SE; n = 231 RE; $p < 10^{-2}$, two-sided Mann-Whitney U test). Right: quartile box plots of log2 fold changes in gene transcripts associated with the top-ranked SEs unique to *MYCN*-amplified Kelly cells treated with THZ1 as in (A) versus DMSO, compared with the expression changes of the same genes in similarly treated SH-SY5Y nonamplified cells. Box plot whiskers extend to 1.5 times the interquartile range (n = 673; $p < 10^{-16}$, two-sided Mann-Whitney U test).

(D) Proposed mechanism for the action of THZ1 in *MYCN*-amplified NB. Oncogenic *MYCN* is regulated by super-enhancers leading to its high-level expression (left). Overexpressed *MYCN* invades the promoter and enhancer regions of all active genes, including itself, to induce global transcriptional upregulation (right). THZ1 targets the expression of both *MYCN* and *MYCN*-driven transcriptional amplification.

cells cause high-level expression of oncogenic drivers and genes that determine cell identity, but they also provide the basis for the selectivity of THZ1.

DISCUSSION

Here, we demonstrate that the genomically amplified *MYCN* oncogene, by promoting the development of SEs, causes upregulation of the active transcriptional program of NB cells, sensitizing them to inhibition of CDK7, a widely expressed regulator of transcription and cell-cycle transition. This effect suppresses essentially all active transcripts, especially those responsible for the uncontrolled proliferation that characterizes the cancer cell state, leading to potent and selective cytotoxicity while sparing normal cells. The high potency of our CDK7 inhibitor, THZ1, can be explained in part by its unprecedented mode of binding—the formation of a covalent bond with a unique cysteine residue outside the kinase domain—resulting in prolonged and irreversible CDK7 inactivation (Kwiatkowski et al., 2014). This feature contrasts with other transcriptional CDK inhibitors, including flavopiridol, roscovitine and CR-8 **(**Table S1**),** all of which rely on ATP-competitive modes of binding and whose effects on transcription would therefore be expected to be transient. The selectivity of THZ1 for *MYCN*-amplified cells can be attributed to the perturbation of SEs associated with deregulated MYCN and other oncogenic drivers.

Despite risk-based treatment strategies for *MYCN*-amplified NB, responses tend to be brief, with early relapses that are almost uniformly fatal (Matthay et al., 1999). Finding suitable ways to inhibit MYCN, or any MYC family member for that matter, has been notoriously difficult. A recent approach is the modulation of bromodomain and extraterminal (BET) domain coactivator proteins, such as BRD4, which associate with acetylated chromatin and promote transcriptional activation (Delmore et al., 2011; Lovén et al., 2013; Puissant et al., 2013). After successful testing of the BRD4 inhibitor JQ1 in MYC-dependent multiple myeloma models (Delmore et al., 2011), a positive correlation between *MYCN* amplification and sensitivity to JQ1 was demonstrated in the majority of *MYCN*-amplified NB models tested (Puissant et al., 2013). However, others reported growth inhibition of NB using the structurally distinct BRD4 inhibitor I-BET726, irrespective of *MYCN* amplification status or *MYC*/*MYCN* expression levels (Wyce et al., 2013). The intervention we describe has a number of features that would support the clinical development of covalent CDK7 inhibitors for use against *MYCN*-amplified NB and other MYC-driven cancers. These include the ability to achieve potent growth inhibition with relatively low doses of THZ1, the lack of off-target effects, and the absence of discernible toxicity in a mouse model of NB. THZ1 has been demonstrated to cross-react with CDK12/13 (Kwiatkowski et al., 2014); however, shRNA knockdown of these kinases in *MYCN*-amplified cells did not affect MYCN levels (Figure S1B). Furthermore, overexpression of $CDK7^{C312S}$ restored MYCN levels to near amplified levels (Figure S4B). These results would suggest that loss of CDK7 activity dominates the selective effects of THZ1 in *MYCN*-amplified NB cells.

Multiple studies argue that MYC is a global transcriptional amplifier (Lin et al., 2012; Lovén et al., 2012; Nie et al., 2012; Schuhmacher and Eick, 2013), although a recent report has suggested that a portion of this amplification is indirect (Sabò et al., 2014). We believe the transcriptional amplification effects of MYC are direct at the vast majority of active genes and that differences in interpretation of direct versus indirect effects are due to differences in interpretation of ChIP-seq data thresholds. We demonstrate here that deregulated MYCN functions as a transcriptional amplifier of the cell's existing gene expression program rather than a specific target gene set. This effect was not detectable in earlier data sets of *MYCN*-amplified tumor samples because of a limitation of microarray analysis, which in conventional approaches assumes similar levels of total RNA in all the samples (Lovén et al., 2012).

Although in principle, blockade of CDK7 function would be expected to inhibit the expression of any gene poised to undergo transcription, our direct demonstration that manipulation of *MYCN* levels can modulate the sensitivity to THZ1 supports the idea that MYC-induced transcriptional amplification is crucial to THZ1 activity. This transcriptional dependency was illustrated by the massive transcriptional shutdown in *MYCN*-amplified cells with relatively low doses of THZ1 (Figure 3). By contrast, although CDK transcripts were downregulated by THZ1 in *MYCN*-nonamplified cells, this effect did not produce the same profound impact seen in *MYCN*-amplified cells, providing further evidence that aberrant *MYCN* expression and the resultant global amplification of transcription are necessary for cell sensitivity to THZ1. This critical dependency on transcriptional amplification would account for the selective killing of *MYCN*-amplified cells by THZ1 without inducing toxic side effects in mice. The unique SE landscapes of *MYCN*-amplified cells also dictate their response to THZ1. Indeed, genes involved in the oncogenic state—such as *MYCN* and *ALK*, and those that specify sympathetic neuronal cell identity including *PHOX2B* and *HAND2*—were associated with SEs and were far more susceptible to THZ1 than either their counterparts in *MYCN*-nonamplified cells or genes driven by regular enhancers. This selectivity of THZ1 for *MYCN*-amplified cells could stem from its inhibition of the increased Pol II activity at SE-associated genes, leading to downregulation of *MYCN* expression as well as that of the entire transcriptional program of the cell.

Our data suggest that the cytotoxicity induced by THZ1 in *MYCN*-driven NB cells is mediated by inhibition of both *MYCN* expression and *MYCN*-stimulated global transcriptional amplification (Figure 7D). Oncogenic *MYCN* invades the core promoters and enhancer regions of actively transcribed genes, resulting in the formation of SEs at key genes underlying the cancer cell state, including *MYCN*, and ultimately in transcriptional amplification. THZ1, by irreversibly inhibiting CDK7, blocks transcription of *MYCN* (Figure 4) as well as *MYCN*-induced amplification of global gene transcription. The latter conclusion is based on the widespread inhibition of transcription in *MYCN*-amplified cells (Figure 3), the highly significant correlation between the transcripts that were downregulated by THZ1 and those resulting from genetic depletion of *MYCN*, and the fact that ectopic expression of *MYCN* in non-*MYCN*-overexpressing cells sensitizes these cells to widespread transcriptional inhibition by THZ1 (Figures 4 and 5). Together, these two processes effectively deprive tumor cells of the proliferative signals to which

they have become addicted, leading to apoptotic death. Nevertheless, this mechanism is not necessarily specific to deregulated *MYCN* or *MYC*. Rather, we suggest that inhibition of CDK7 or perhaps other transcriptional CDKs would be effective in any context in which tumor cells rely on high-level expression of one or more oncogenic transcription factors for their aberrant growth and survival. However, the net inhibitory effect is likely to be much more profound in cancers that depend on *MYC* (or *MYCN*) as the oncogenic driver.

In conclusion, we use NB and a newly developed transcriptional CDK inhibitor to demonstrate the potency and selectivity of a potential treatment strategy that targets global transcriptional amplification in MYC-driven tumors. Our results suggest that the mechanism by which oncogenic MYC gains control over myriad cellular processes to induce tumor formation also exposes a vulnerability that can be exploited therapeutically. By using THZ1 to disable essential components of the cancer cells' transcriptional machinery, we show that widespread suppression of transcription in MYC-dependent cancers is not only feasible, but also spares normal cells from toxicity.

EXPERIMENTAL PROCEDURES

Cell Lines

Human NB cell lines (from the Children's Oncology Group) and Raji and Daudi cells (provided by D. Sabatini, Massachusetts Institute of Technology) were grown in RPMI-1640, 10% fetal bovine serum (FBS), and 1% penicillin/streptomycin (pen/strep; Invitrogen). H262-BT111 primitive neuroectodermal tumor cells (provided by K. Ligon, Dana-Farber Cancer Institute [DFCI]) were grown in neuronal stem cell (NSC) media with heparin, NSC supplement (Stem Cell Technologies), 1% pen/strep, erythrocyte growth factor (EMD Millipore), and fibroblast growth factor (Life Technologies). NIH 3T3 cells (purchased from ATCC) and B6-MEFs (provided by A. Kung, Columbia University) were grown in DMEM with 10% FBS and 1% pen/strep.

Animal Studies

These experiments were performed with approval from the Institutional Animal Care and Use Committee of the DFCI. Full details are given in Extended Experimental Procedures.

Synthetic RNA Spike-In and Microarray Analysis

RNA samples were prepared as previously described (Lovén et al., 2012). Total RNA was spiked-in with RNA Spike-In Mix (Ambion), treated with DNA-free DNase I (Ambion), analyzed on Agilent 2100 Bioanalyzer (Agilent Technologies) for integrity, and hybridized to Affymetrix GeneChip PrimeView Human Gene Expression arrays (Affymetrix). Data analysis is described in Extended Experimental Procedures.

ChIP-Seq

ChIP was carried out as previously described (Lee et al., 2006) with minor changes described in the Extended Experimental Procedures. The following antibodies were used: RNAPII (Santa Cruz, sc-899), H3K4me1 (Abcam, ab8895), and H3K27ac (Abcam, ab4729).

Data Analysis

All ChIP-seq data were aligned using the short-read aligner Bowtie (version 0.12.7) (Langmead et al., 2009) to build version GRCh37/HG19 of the human genome. To visualize ChIP-seq tracks, reads were extended by 160 bases, converted into tdf files using igvtools (version 2.2.1) and visualized in IGV (Robinson et al., 2011). ChIP-seq peaks were detected using a peak-finding algorithm, MACS version 1.4.2 (Zhang et al., 2008) with the default p value threshold of enrichment of 1×10^{-5} used for all data sets. Active enhancers, ranked according to the magnitude of the H3K27ac signal, were defined as regions of ChIP-seq enrichment for H3K27ac and H3K4me1 outside of promoters. To identify super-enhancers, we employed the ROSE algorithm (https://bitbucket.org/young_computation/rose) (Lovén et al., 2013; Whyte et al., 2013) to rank the enhancers that were identified using MACS in which peaks within 12.5 kb of one another were stitched together and these stitched enhancers were ranked by their difference in H3K27ac signal versus input signal. Further details are given in the Extended Experimental Procedures.

ACCESSION NUMBERS

The data discussed in this publication have been deposited in NCBI's Gene Expression Omnibus and are accessible through GEO series accession number GSE62726.

SUPPLEMENTAL INFORMATION

Supplemental Information includes Extended Experimental Procedures, six figures, and one table and can be found with this article online at http://dx.doi.org/10.1016/j.cell.2014.10.024.

ACKNOWLEDGMENTS

We thank K. Ligon, D. Sabatini., W. Weiss, A. Kung, and the Children's Oncology Group for cell lines and plasmids and P. Baran for the dCA compound. We thank J.R. Gilbert and Takaomi Sanda for insightful discussions. This study was supported by NIH R01CA148688 (R.E.G.), R01CA148688S1 (E.C.), R01CA179483-01 (N.S.G. and T.H.Z.), CA109901, HG002668 (R.A.Y., N.K., B.A.), and R21HG006778 (G.C.Y.); American Cancer Society (RSG-12-247-TBG to R.E.G.); Department of Defense (PR120741A to R.E.G.); and Friends for Life Neuroblastoma Foundation (N.S.G. and R.E.G.). THZ1 has been licensed to Syros Pharmaceuticals for clinical development. N.S.G. and R.A.Y. are scientific founders of Syros Pharmaceuticals.

Received: May 29, 2014
Revised: August 18, 2014
Accepted: September 24, 2014
Published: November 6, 2014

REFERENCES

Arvanitis, C., and Felsher, D.W. (2006). Conditional transgenic models define how MYC initiates and maintains tumorigenesis. Semin. Cancer Biol. *16*, 313–317.

Boon, K., Caron, H.N., van Asperen, R., Valentijn, L., Hermus, M.C., van Sluis, P., Roobeek, I., Weis, I., Voûte, P.A., Schwab, M., and Versteeg, R. (2001). N-myc enhances the expression of a large set of genes functioning in ribosome biogenesis and protein synthesis. EMBO J. *20*, 1383–1393.

Brodeur, G.M., Seeger, R.C., Schwab, M., Varmus, H.E., and Bishop, J.M. (1984). Amplification of N-myc in untreated human neuroblastomas correlates with advanced disease stage. Science *224*, 1121–1124.

Chapuy, B., McKeown, M.R., Lin, C.Y., Monti, S., Roemer, M.G., Qi, J., Rahl, P.B., Sun, H.H., Yeda, K.T., Doench, J.G., et al. (2013). Discovery and characterization of super-enhancer-associated dependencies in diffuse large B cell lymphoma. Cancer Cell *24*, 777–790.

Cohn, S.L., Salwen, H., Quasney, M.W., Ikegaki, N., Cowan, J.M., Herst, C.V., Kennett, R.H., Rosen, S.T., DiGiuseppe, J.A., and Brodeur, G.M. (1990). Prolonged N-myc protein half-life in a neuroblastoma cell line lacking N-myc amplification. Oncogene *5*, 1821–1827.

Delmore, J.E., Issa, G.C., Lemieux, M.E., Rahl, P.B., Shi, J., Jacobs, H.M., Kastritis, E., Gilpatrick, T., Paranal, R.M., Qi, J., et al. (2011). BET bromodomain inhibition as a therapeutic strategy to target c-Myc. Cell *146*, 904–917.

Eilers, M., and Eisenman, R.N. (2008). Myc's broad reach. Genes Dev. *22*, 2755–2766.

Fisher, R.P., and Morgan, D.O. (1994). A novel cyclin associates with MO15/CDK7 to form the CDK-activating kinase. Cell *78*, 713–724.

Garriga, J., and Graña, X. (2004). Cellular control of gene expression by T-type cyclin/CDK9 complexes. Gene *337*, 15–23.

George, R.E., Sanda, T., Hanna, M., Fröhling, S., Luther, W., 2nd, Zhang, J., Ahn, Y., Zhou, W., London, W.B., McGrady, P., et al. (2008). Activating mutations in ALK provide a therapeutic target in neuroblastoma. Nature *455*, 975–978.

Glover-Cutter, K., Larochelle, S., Erickson, B., Zhang, C., Shokat, K., Fisher, R.P., and Bentley, D.L. (2009). TFIIH-associated Cdk7 kinase functions in phosphorylation of C-terminal domain Ser7 residues, promoter-proximal pausing, and termination by RNA polymerase II. Mol. Cell. Biol. *29*, 5455–5464.

Hnisz, D., Abraham, B.J., Lee, T.I., Lau, A., Saint-André, V., Sigova, A.A., Hoke, H.A., and Young, R.A. (2013). Super-enhancers in the control of cell identity and disease. Cell *155*, 934–947.

Howard, M.J., Stanke, M., Schneider, C., Wu, X., and Rohrer, H. (2000). The transcription factor dHAND is a downstream effector of BMPs in sympathetic neuron specification. Development *127*, 4073–4081.

Kohl, N.E., Legouy, E., DePinho, R.A., Nisen, P.D., Smith, R.K., Gee, C.E., and Alt, F.W. (1986). Human N-myc is closely related in organization and nucleotide sequence to c-myc. Nature *319*, 73–77.

Kwiatkowski, N., Zhang, T., Rahl, P.B., Abraham, B.J., Reddy, J., Ficarro, S.B., Dastur, A., Amzallag, A., Ramaswamy, S., Tesar, B., et al. (2014). Targeting transcription regulation in cancer with a covalent CDK7 inhibitor. Nature *511*, 616–620.

Labisso, W.L., Wirth, M., Stojanovic, N., Stauber, R.H., Schnieke, A., Schmid, R.M., Krämer, O.H., Saur, D., and Schneider, G. (2012). MYC directs transcription of MCL1 and eIF4E genes to control sensitivity of gastric cancer cells toward HDAC inhibitors. Cell Cycle *11*, 1593–1602.

Lam, L.T., Pickeral, O.K., Peng, A.C., Rosenwald, A., Hurt, E.M., Giltnane, J.M., Averett, L.M., Zhao, H., Davis, R.E., Sathyamoorthy, M., et al. (2001). Genomic-scale measurement of mRNA turnover and the mechanisms of action of the anti-cancer drug flavopiridol. Genome Biol. *2*, RESEARCH0041.

Langmead, B., Trapnell, C., Pop, M., and Salzberg, S.L. (2009). Ultrafast and memory-efficient alignment of short DNA sequences to the human genome. Genome Biol. *10*, R25.

Lapenna, S., and Giordano, A. (2009). Cell cycle kinases as therapeutic targets for cancer. Nat. Rev. Drug Discov. *8*, 547–566.

Larochelle, S., Merrick, K.A., Terret, M.E., Wohlbold, L., Barboza, N.M., Zhang, C., Shokat, K.M., Jallepalli, P.V., and Fisher, R.P. (2007). Requirements for Cdk7 in the assembly of Cdk1/cyclin B and activation of Cdk2 revealed by chemical genetics in human cells. Mol. Cell *25*, 839–850.

Larochelle, S., Amat, R., Glover-Cutter, K., Sansó, M., Zhang, C., Allen, J.J., Shokat, K.M., Bentley, D.L., and Fisher, R.P. (2012). Cyclin-dependent kinase control of the initiation-to-elongation switch of RNA polymerase II. Nat. Struct. Mol. Biol. *19*, 1108–1115.

Lee, T.I., Johnstone, S.E., and Young, R.A. (2006). Chromatin immunoprecipitation and microarray-based analysis of protein location. Nat. Protoc. *1*, 729–748.

Lin, C.Y., Lovén, J., Rahl, P.B., Paranal, R.M., Burge, C.B., Bradner, J.E., Lee, T.I., and Young, R.A. (2012). Transcriptional amplification in tumor cells with elevated c-Myc. Cell *151*, 56–67.

Lovén, J., Orlando, D.A., Sigova, A.A., Lin, C.Y., Rahl, P.B., Burge, C.B., Levens, D.L., Lee, T.I., and Young, R.A. (2012). Revisiting global gene expression analysis. Cell *151*, 476–482.

Lovén, J., Hoke, H.A., Lin, C.Y., Lau, A., Orlando, D.A., Vakoc, C.R., Bradner, J.E., Lee, T.I., and Young, R.A. (2013). Selective inhibition of tumor oncogenes by disruption of super-enhancers. Cell *153*, 320–334.

Malynn, B.A., de Alboran, I.M., O'Hagan, R.C., Bronson, R., Davidson, L., DePinho, R.A., and Alt, F.W. (2000). N-myc can functionally replace c-myc in murine development, cellular growth, and differentiation. Genes Dev. *14*, 1390–1399.

Matthay, K.K., Villablanca, J.G., Seeger, R.C., Stram, D.O., Harris, R.E., Ramsay, N.K., Swift, P., Shimada, H., Black, C.T., Brodeur, G.M., et al.; Children's Cancer Group (1999). Treatment of high-risk neuroblastoma with intensive chemotherapy, radiotherapy, autologous bone marrow transplantation, and 13-cis-retinoic acid. N. Engl. J. Med. *341*, 1165–1173.

McLean, C.Y., Bristor, D., Hiller, M., Clarke, S.L., Schaar, B.T., Lowe, C.B., Wenger, A.M., and Bejerano, G. (2010). GREAT improves functional interpretation of cis-regulatory regions. Nat. Biotechnol. *28*, 495–501.

Mercer, E.H., Hoyle, G.W., Kapur, R.P., Brinster, R.L., and Palmiter, R.D. (1991). The dopamine beta-hydroxylase gene promoter directs expression of E. coli lacZ to sympathetic and other neurons in adult transgenic mice. Neuron *7*, 703–716.

Nie, Z., Hu, G., Wei, G., Cui, K., Yamane, A., Resch, W., Wang, R., Green, D.R., Tessarollo, L., Casellas, R., et al. (2012). c-Myc is a universal amplifier of expressed genes in lymphocytes and embryonic stem cells. Cell *151*, 68–79.

Nishikura, K., Erikson, J., ar-Rushdi, A., Huebner, K., and Croce, C.M. (1985). The translocated c-myc oncogene of Raji Burkitt lymphoma cells is not expressed in human lymphoblastoid cells. Proc. Natl. Acad. Sci. USA *82*, 2900–2904.

Palancade, B., and Bensaude, O. (2003). Investigating RNA polymerase II carboxyl-terminal domain (CTD) phosphorylation. FEBS *270*, 3859–3870.

Pattyn, A., Morin, X., Cremer, H., Goridis, C., and Brunet, J.F. (1999). The homeobox gene Phox2b is essential for the development of autonomic neural crest derivatives. Nature *399*, 366–370.

Puissant, A., Frumm, S.M., Alexe, G., Bassil, C.F., Qi, J., Chanthery, Y.H., Nekritz, E.A., Zeid, R., Gustafson, W.C., Greninger, P., et al. (2013). Targeting MYCN in neuroblastoma by BET bromodomain inhibition. Cancer Discov. *3*, 308–323.

Robinson, J.T., Thorvaldsdóttir, H., Winckler, W., Guttman, M., Lander, E.S., Getz, G., and Mesirov, J.P. (2011). Integrative genomics viewer. Nat. Biotechnol. *29*, 24–26.

Rossignol, M., Kolb-Cheynel, I., and Egly, J.M. (1997). Substrate specificity of the cdk-activating kinase (CAK) is altered upon association with TFIIH. EMBO J. *16*, 1628–1637.

Sabò, A., Kress, T.R., Pelizzola, M., de Pretis, S., Gorski, M.M., Tesi, A., Morelli, M.J., Bora, P., Doni, M., Verrecchia, A., et al. (2014). Selective transcriptional regulation by Myc in cellular growth control and lymphomagenesis. Nature *511*, 488–492.

Schuhmacher, M., and Eick, D. (2013). Dose-dependent regulation of target gene expression and cell proliferation by c-Myc levels. Transcription *4*, 192–197.

Schwab, M., Alitalo, K., Klempnauer, K.H., Varmus, H.E., Bishop, J.M., Gilbert, F., Brodeur, G., Goldstein, M., and Trent, J. (1983). Amplified DNA with limited homology to myc cellular oncogene is shared by human neuroblastoma cell lines and a neuroblastoma tumour. Nature *305*, 245–248.

Seeger, R.C., Brodeur, G.M., Sather, H., Dalton, A., Siegel, S.E., Wong, K.Y., and Hammond, D. (1985). Association of multiple copies of the N-myc oncogene with rapid progression of neuroblastomas. N. Engl. J. Med. *313*, 1111–1116.

Serizawa, H., Mäkelä, T.P., Conaway, J.W., Conaway, R.C., Weinberg, R.A., and Young, R.A. (1995). Association of Cdk-activating kinase subunits with transcription factor TFIIH. Nature *374*, 280–282.

Slack, A., Chen, Z., Tonelli, R., Pule, M., Hunt, L., Pession, A., and Shohet, J.M. (2005). The p53 regulatory gene MDM2 is a direct transcriptional target of MYCN in neuroblastoma. Proc. Natl. Acad. Sci. USA *102*, 731–736.

Soucek, L., Whitfield, J., Martins, C.P., Finch, A.J., Murphy, D.J., Sodir, N.M., Karnezis, A.N., Swigart, L.B., Nasi, S., and Evan, G.I. (2008). Modelling Myc inhibition as a cancer therapy. Nature *455*, 679–683.

Stanke, M., Junghans, D., Geissen, M., Goridis, C., Ernsberger, U., and Rohrer, H. (1999). The Phox2 homeodomain proteins are sufficient to promote the development of sympathetic neurons. Development *126*, 4087–4094.

Toyoshima, M., Howie, H.L., Imakura, M., Walsh, R.M., Annis, J.E., Chang, A.N., Frazier, J., Chau, B.N., Loboda, A., Linsley, P.S., et al. (2012). Functional

genomics identifies therapeutic targets for MYC-driven cancer. Proc. Natl. Acad. Sci. USA *109*, 9545–9550.

Tsarovina, K., Pattyn, A., Stubbusch, J., Müller, F., van der Wees, J., Schneider, C., Brunet, J.F., and Rohrer, H. (2004). Essential role of Gata transcription factors in sympathetic neuron development. Development *131*, 4775–4786.

Veronese, M.L., Ohta, M., Finan, J., Nowell, P.C., and Croce, C.M. (1995). Detection of myc translocations in lymphoma cells by fluorescence in situ hybridization with yeast artificial chromosomes. Blood *85*, 2132–2138.

Wasylishen, A.R., and Penn, L.Z. (2010). Myc: the beauty and the beast. Genes Cancer *1*, 532–541.

Whyte, W.A., Orlando, D.A., Hnisz, D., Abraham, B.J., Lin, C.Y., Kagey, M.H., Rahl, P.B., Lee, T.I., and Young, R.A. (2013). Master transcription factors and mediator establish super-enhancers at key cell identity genes. Cell *153*, 307–319.

Wyce, A., Ganji, G., Smitheman, K.N., Chung, C.W., Korenchuk, S., Bai, Y., Barbash, O., Le, B., Craggs, P.D., McCabe, M.T., et al. (2013). BET inhibition silences expression of MYCN and BCL2 and induces cytotoxicity in neuroblastoma tumor models. PLoS ONE *8*, e72967.

Zhang, Y., Liu, T., Meyer, C.A., Eeckhoute, J., Johnson, D.S., Bernstein, B.E., Nusbaum, C., Myers, R.M., Brown, M., Li, W., and Liu, X.S. (2008). Model-based analysis of ChIP-Seq (MACS). Genome Biol. *9*, R137.

OPEN

Oncogene (2015), 1–11

www.nature.com/onc

ORIGINAL ARTICLE

ALK inhibitor resistance in ALK^{F1174L}-driven neuroblastoma is associated with AXL activation and induction of EMT

DN Debruyne[1], N Bhatnagar[1], B Sharma[1], W Luther[1], NF Moore[1], N-K Cheung[2], NS Gray[3,4] and RE George[1,5]

The crizotinib-resistant *ALK*^{F1174L} mutation arises *de novo* in neuroblastoma (NB) and is acquired in *ALK* translocation-driven cancers, lending impetus to the development of novel anaplastic lymphoma kinase (ALK) inhibitors with different modes of action. The diaminopyrimidine TAE684 and its derivative ceritinib (LDK378), which are structurally distinct from crizotinib, are active against NB cells expressing *ALK*^{F1174L}. Here we demonstrate acquired resistance to TAE684 and LDK378 in ALK^{F1174L}-driven human NB cells that is linked to overexpression and activation of the AXL tyrosine kinase and epithelial-to-mesenchymal transition (EMT). AXL phosphorylation conferred TAE684 resistance to NB cells through upregulated extracellular signal-regulated kinase (ERK) signaling. Inhibition of AXL partly rescued TAE684 resistance, resensitizing these cells to this compound. AXL activation in resistant cells was mediated through increased expression of the active form of its ligand, GAS6, that also served to stabilize the AXL protein. Although ectopic expression of *AXL* and *TWIST2* individually in TAE684-sensitive parental cells led to the elevated expression of mesenchymal markers and invasive capacity, only *AXL* overexpression induced resistance to TAE684 as well. TAE684-resistant cells showed greater sensitivity to HSP90 inhibition than did their parental counterparts, with downregulation of AXL and AXL-mediated ERK signaling. Our studies indicate that aberrant AXL signaling and development of an EMT phenotype underlie resistance of ALK^{F1174L}-driven NB cells to TAE684 and its derivatives. We suggest that the combination of ALK and AXL or HSP90 inhibitors be considered to delay the emergence of such resistance.

Oncogene advance online publication, 30 November 2015; doi:10.1038/onc.2015.434

INTRODUCTION

The predictable emergence of resistance to tyrosine kinase inhibitors (TKIs), leading to disease progression or relapse, has hindered their long-term therapeutic impact.[1] This obstacle is best exemplified by the development of resistance to imatinib in *BCR-ABL*-expressing chronic myeloid leukemia and gefitinib in *EGFR*-mutant non-small-cell lung cancer,[2,3] and is likely to impede efforts to devise effective targeted therapy for many other cancers, including neuroblastoma (NB). This aggressive childhood tumor is characterized by mutations in the anaplastic lymphoma kinase (ALK) receptor tyrosine kinase (RTK) in 10% of cases.[4–7] Many of these point mutations are considered 'drivers' of the malignant process: not only do they induce constitutive, ligand-independent activation of ALK signaling, but also their inhibition leads to tumor cell death and tumor regression.[5,6] The most common somatic mutation in NB, *ALK*^{F1174L}, is highly tumorigenic, both by itself and when coexpressed with the *MYCN* oncogene, a combination that increases the penetrance of the disease and accelerates tumor formation.[8,9] This mutation confers primary resistance to the ALK inhibitor crizotinib in NB[9] and serves as a mechanism of acquired resistance to crizotinib in patients with *ALK*-translocated cancers.[10]

Several structurally unrelated small molecule ALK inhibitors have been developed such as alectinib (CH5424802) that has shown activity against *ALK*^{F1174L}-positive tumors.[11] Similarly, the lead compound TAE684,[12] from which the recently Food and Drug Administration (FDA)-approved inhibitor ceritinib (LDK378, Novartis) is derived,[13] has exhibited potent activity against ALK^{F1174L} in both *ALK* translocation-positive cancers[10] and NB.[5,14] Nonetheless, resistance to these ATP-competitive agents will inevitably develop as a consequence of their wider clinical application. We therefore sought to elucidate the mechanism(s) underlying acquired resistance to ALK inhibitors in ALK^{F1174L}-driven NB as a means to uncover secondary targets that could be exploited to prolong responses in these patients. By generating TAE684 and LDK378 resistance models of *ALK*^{F1174L}-positive human NB cells, we identified overexpression and GAS6-mediated activation of a TAM family RTK, AXL, as the principal resistance-related alteration in these cells. This change was associated with activation of the mitogen-activated protein kinase (MAPK) signaling pathway and the development of an epithelial-to-mesenchymal transition (EMT) phenotype. Importantly, inhibition of AXL with a small molecule inhibitor led to decreased growth and invasiveness of the resistant cells with a concomitant decrease in extracellular signal-regulated kinase (ERK) signaling. We also demonstrate that HSP90 inhibition, through its impact on AXL binding, induces striking cytotoxicity in TAE684-resistant cells. Hence, we suggest that the combination of ALK and AXL or HSP90 inhibition could serve as part of an effective strategy of targeted therapeutics for ALK^{F1174L}-driven NB and other tumors dependent on this aberrant RTK.

RESULTS

TAE684 resistance is associated with the loss of ALK activity but maintenance of downstream signaling

NB cells that express the *ALK*^{F1174L} mutation are relatively resistant to crizotinib but are sensitive to TAE684.[5,9] To elucidate the

[1]Department of Pediatric Hematology/Oncology, Dana-Farber Cancer Institute and Boston Children's Hospital, Boston, MA, USA; [2]Department of Pediatric Oncology, Memorial Sloan-Kettering Cancer Center, New York, NY, USA; [3]Department of Cancer Biology, Dana-Farber Cancer Institute, Boston, MA, USA; [4]Department of Biological Chemistry and Molecular Pharmacology, Harvard Medical School, Boston, MA, USA and [5]Department of Pediatrics, Harvard Medical School, Boston, MA, USA. Correspondence: Dr RE George, Department of Pediatric Oncology, Dana-Farber Cancer Institute, Dana 640E, 450 Brookline Avenue, Boston, MA 02215, USA.
E-mail: rani_george@dfci.harvard.edu
Received 18 February 2015; revised 15 September 2015; accepted 11 October 2015

mechanisms of resistance to ALK^{F1174L} inhibitors, we first established TAE684-resistant cells (SH-SY5Y-TR) through continuous exposure of SH-SY5Y cells to increasing doses of the compound over 8–12 months (Supplementary Figure S1a). Three individual subclones (SH-SY5Y-TR1, SH-SY5Y-TR2 and SH-SY5Y-TR3) were expanded (Figure 1a), and subsequently maintained in ~35 times the half-maximal inhibitory concentration (IC_{50}) of TAE684.

Resistance to targeted therapy can arise from either secondary mutations in the drug target itself or upregulation of compensatory pathways.[1] We therefore first analyzed the phosphorylation status of ALK and its downstream targets in SH-SY5Y-TR-resistant cells. As compared with results in parental cells, ALK phosphorylation was decreased in both the primary resistant pool (Supplementary Figure S1b) and the three subclones (Figure 1b), suggesting that the acquired resistance was not mediated by secondary mutations in *ALK*. This result was confirmed by sequence analysis and genomic PCR showing the absence of mutations other than *F1174L* or gene amplification, respectively (data not shown). The absence of ALK phosphorylation also ruled out upregulation of drug efflux transporters such as the ABC (ATP-binding cassette) superfamily as a potential mechanism of resistance, as ALK would remain phosphorylated if this were to be the case.

The *ALK*^{F1174L} mutation activates the phosphatidylinositol-3-kinase/AKT/mammalian target of rapamycin (PI3K/AKT/mTOR) and MAPK/ERK pathways in NB cells, both of which are downregulated when ALK is inhibited.[5,9] Despite decreased levels of pALK, AKT activation was maintained in the resistant SH-SY5Y-TR pool as well as all three SH-SY5Y-TR subclones (Figure 1b and Supplementary Figure S1b). Importantly, compared with parental cells, ERK phosphorylation was increased in SH-SY5Y-TR cells and its subclones (Figure 1b and Supplementary Figure S1b). The upregulated ERK signaling in the context of suppressed ALK phosphorylation suggested the development of an alternative mechanism of resistance, most likely activation of another tyrosine kinase capable of bypassing TAE684 inhibition.

The AXL receptor tyrosine kinase is upregulated in TAE684-resistant NB cells

To identify upstream RTKs that may contribute to TAE684 resistance, we compared the phosphorylation status of 42 candidates in SH-SY5Y and SH-SY5Y-TR1 cells before and after treatment with TAE684 (Figure 1c). Parental SH-SY5Y cells showed basal activation of several RTKs, most of which were decreased or

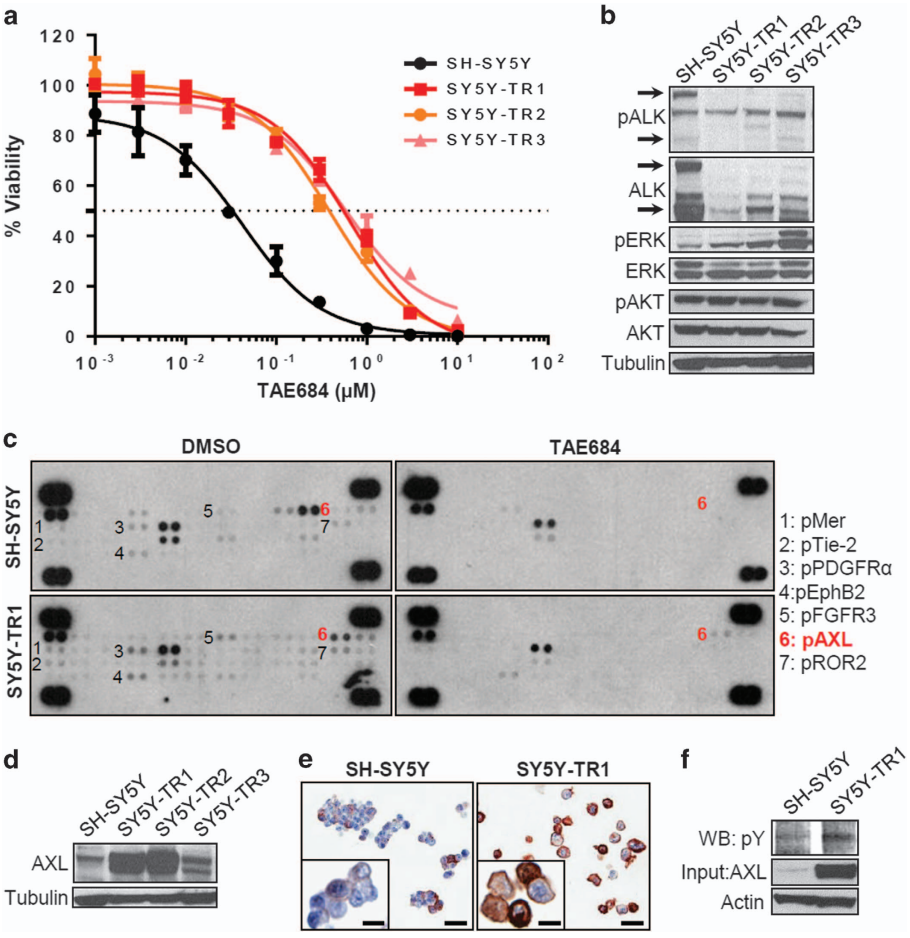

Figure 1. Development of TAE684 resistance is associated with activation of AXL in *ALK*-mutated SH-SY5Y NB cells. (**a**) Dose–response curves for parental SH-SY5Y cells and three TAE684-resistant clones (SY5Y-TR1 to TR3) treated with increasing concentrations of TAE684 for 72 h (half-maximal inhibitory concentration (IC_{50}) = SH-SY5Y, 31 nM; SY5Y-TR1, 521 nM; SY5Y-TR2, 374 nM; SY5Y-TR3, 581 nM). (**b**) Western blot analysis of total and pALK and indicated downstream signaling molecules in TAE684-sensitive and -resistant SH-SY5Y cells. Arrows indicate ALK products of 220 and 140 kDa. (**c**) Phospho-proteomic analysis of RTKs in SH-SY5Y and SY5Y-TR1 cells exposed to either dimethyl sulfoxide (DMSO) or TAE684 (1 μM) for 6 h. Each RTK is shown in duplicate, and the pairs in each corner of the array are positive controls. Significantly regulated RTKs are numbered. (**d**) Western blot analysis of total AXL expression in parental SH-SY5Y and the three SY5Y-TR clones. (**e**) Immunocytochemical analysis of AXL expression in SH-SY5Y and SY5Y-TR1 cells (scale bars, 10 μm, insets, 5 μm). (**f**) Analysis of pAXL in SH-SY5Y and SY5Y-TR1 cells in which AXL was immunoprecipitated using an anti-AXL antibody, followed by western blotting with an anti-phosphotyrosine antibody. Tubulin or actin were used as loading controls in all western blots.

lost upon TAE684 treatment (Figure 1c). Under dimethyl sulfoxide (DMSO) treatment conditions, TAE684-resistant SH-SY5Y-TR1 cells showed enhanced phosphorylation of seven additional RTKs (MER, TIE-2, PDGFRα, EPHB2, FGFR3, AXL and ROR2). Two of these, MER and AXL, belonged to the same TAM receptor tyrosine kinase family whose aberrantly elevated signaling has been linked to cancer progression, metastasis and resistance to therapy.[15] Acute exposure to TAE684 led to complete loss of phosphorylation of all of these candidates except for AXL and EPHB2. Thus, the sustained upregulation of AXL and EPHB2 in the SH-SY5Y-TR1-resistant cells suggested a role for these RTKs in mediating resistance to TAE684.

We selected AXL for further study because of the known role of this transmembrane receptor in mediating drug resistance, especially to TKIs.[16,17] We confirmed that AXL expression was markedly increased in two of the three resistant clones and marginally in the third (Figure 1d). Intense membrane staining of AXL was apparent on immunocytochemical staining of SH-SY5Y-TR1 cells (Figure 1e). Interestingly, parental SH-SY5Y cells also contained a minor subpopulation of *AXL*-expressing cells compared with TAE684-resistant cells (18 of 100 cells vs 94 of 100 resistant cells), suggesting the pre-existence and clonal selection of cells expressing AXL under drug pressure to compensate for the loss of ALK signaling. Finally, the increased protein expression was accompanied by phosphorylation of AXL in SH-SY5Y-TR1 cells (Figure 1f), suggesting activation of the tyrosine kinase. Further evidence to support AXL activation as a key mediator of TAE684 resistance came from experiments with an additional ALK^{F1174L}-driven NB cell line, SK-N-SH. SK-N-SH cells rendered resistant to TAE684 (SK-N-SH-TAE-R) showed upregulation of AXL as well as ERK signaling despite downregulation of phosphorylated ALK (Supplementary Figures S2a and b). Together, these results indicate that TAE684-resistant NB cells express higher levels of alternative RTKs such as AXL to compensate for the loss of ALK phosphorylation.

AXL activation confers resistance to TAE684 in ALK^{F1174L}-driven NB cells

To clarify the role of AXL activation in resistance to TAE684, we first abrogated its expression in SH-SY5Y-TR1 cells using small hairpin RNA (shRNA) knockdown, noting a significant decrease in the growth of AXL-depleted compared with untransfected or control shRNA-expressing cells (Figure 2a). AXL depletion was associated with a decrease in pERK levels at 72 h compared with untransfected or control shRNA-expressing cells at the same time point (Figure 2b). SH-SY5Y-TR1 cells were three times more sensitive to the AXL inhibitor R428[(ref. 18)] than were parental SH-SY5Y cells (Figure 2c). Similar results were seen in the SK-N-SH-TAE-R cells (Supplementary Figure S2c). Importantly, R428 also restored sensitivity to TAE684 in SH-SY5Y-TR1 cells, with a combination of the two agents having an additive effect (Figure 2d). Similar effects were not seen in TAE684-sensitive parental SH-SY5Y cells, possibly reflecting the dependency of the resistant cells on the proliferative and migratory effects of activated AXL. Next, we determined whether overexpression of AXL was sufficient to confer resistance to ALK inhibitors in *ALK*-mutated NB cells. Ectopic expression of *AXL* in TAE684-sensitive SH-SY5Y cells resulted in a twofold decrease in sensitivity to TAE684 (Figures 2e and f). Overexpression of *AXL* also led to an increase in pERK in these cells (Figure 2g). These findings suggest that AXL overexpression contributes to TAE684 resistance in ALK^{F1174L}-driven NB cells and underscores the potential of AXL inhibition as a means to sensitize these resistant cells.

Resistance to the ALK inhibitor LDK378 is also associated with AXL activation

To extend findings with TAE684 to the more clinically relevant ALK inhibitor LDK378 (ceritinib), we first evaluated the sensitivity of both TAE684-resistant SH-SY5Y-TR1 and SK-N-SH-TAE-R cells to LDK378. These experiments showed cross-resistance between the two compounds (Figure 3a), suggesting that AXL activation might serve as a mechanism of resistance to newer ALK inhibitors. To support this hypothesis further, we generated LDK378-resistant SH-SY5Y cells (designated LDK-R-5Y), following the same procedure as used with TAE684 (Figure 3b). Similar to the findings in TAE684-resistant cells, pALK was downregulated in the LDK-R-5Y cells whereas pERK was upregulated (Figure 3c). Moreover, increased expression of AXL at both the mRNA and protein levels, as well as increased phosphorylation of AXL, were observed (Figures 3c–e). LDK-R-5Y cells were more sensitive to AXL inhibition by R428 than were the parental cells (Figure 3f). Thus, activation of AXL and ERK signaling appears to underlie acquired resistance of ALK^{F1174L}-driven NB cells to both TAE684 and LDK378.

TAE684-resistant SH-SY5Y-TR1 cells display functional EMT features

We noted that SH-SY5Y-TR1 cells exhibited striking morphological differences when compared with parental SH-SY5Y cells (Figure 4a). Whereas the parental cells were smaller in size with epithelioid morphology, SH-SY5Y-TR1 cells were elongated, spindle shaped and fibroblast-like, with decreased cell-to-cell contact, consistent with EMT. To determine whether these morphological alterations had an underlying molecular basis, we compared the gene expression profiles of the SH-SY5Y-TR1 cells with those of parental cells (Figure 4b). In addition to upregulation of *AXL* itself, the resistant cells showed significant differential expression of genes with major roles in EMT, with overexpression of the key transcriptional inducers *TWIST2* and *SNAI2*, and the characteristic mesenchymal markers vimentin (*VIM*) and fibronectin (*FN1*) (Figure 4b). Gene set enrichment analysis (GSEA) of the differentially expressed genes indicated significant enrichment of three distinct EMT-related gene signatures (Figure 4c).[19–21] Overexpression of *TWIST2* in the TAE684-resistant cells was confirmed by quantitative reverse transcriptase–PCR (qRT–PCR; Figure 4d). Although E-cadherin (*CDH1*), a key marker of the epithelial cell state, was not significantly altered in the expression signatures (Figure 4b), quantitative PCR analysis demonstrated decreased mRNA levels of this gene as well as increased expression of vimentin in the resistant compared with the parental cells, findings that were also reflected at the protein level (Figure 4e). SH-SY5Y-TR1 cells also displayed significantly increased invasive properties when compared with parental cells on matrigel assays, attesting to their metastatic potential (Figure 4f). Together, these results suggest that acquired resistance to TAE684 by *ALK*-mutated NB cells is associated with functional EMT.

AXL activation leads to EMT features and resistance to TAE684 through different mechanisms

Although AXL activation and EMT induction have both been linked to TKI resistance,[15,22] it is not clear whether EMT induction is an inevitable consequence of AXL activation, or vice versa. We therefore sought to induce EMT features in parental TAE684-sensitive cells and to determine whether this effect would cause increased expression of AXL or, indeed, altered sensitivity to TAE684. Overexpression of FLAG-tagged *TWIST2* (Figure 5a, left), the top EMT-associated gene that was differentially expressed in the resistant cells (Figure 4b), led to significantly elevated vimentin and decreased cadherin levels (Figures 5b and c) in parental SH-SY5Y cells as compared with vector-control transfected cells, as well as increased invasive capacity (Figure 5d). AXL expression, however, was not elevated in SH-SY5Y-TWIST2-expressing cells compared with control cells (Figure 5e). Moreover, these cells remained as sensitive to TAE684 as untransfected or vector control-expressing cells (Figure 5f). In contrast, as shown previously, ectopic expression

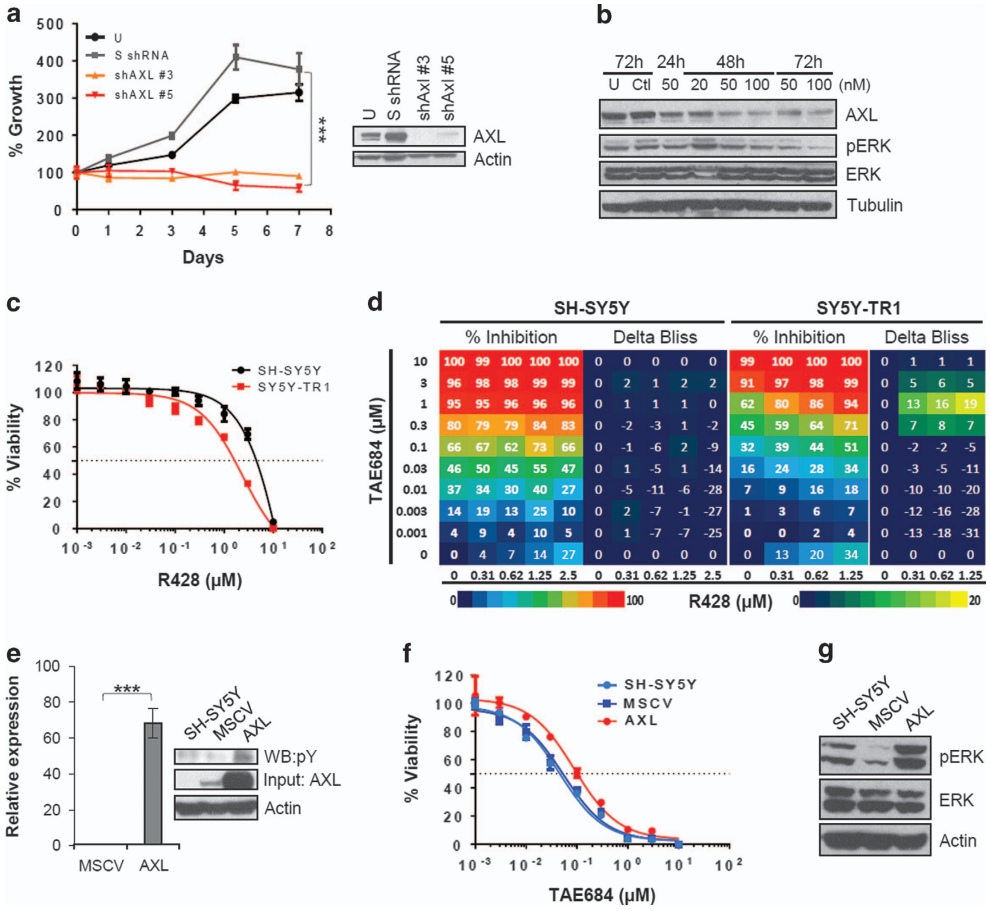

Figure 2. TAE684-resistant cells are dependent on AXL signaling. (**a**) Growth curve (left) of untransfected (U), scrambled (S shRNA) or *AXL* shRNA-expressing SY5Y-TR1 cells. Two different *AXL* shRNAs (3 and 5) were used. The results represent the mean ± s.d. of three separate experiments. ***$P < 0.001$. Western blot analysis (right) of AXL knockdown in the same cells. (**b**) Western blot analysis of AXL and pERK in SY5Y-TR1 cells expressing either a nonspecific (Ctl) or AXL siRNA at the indicated doses for the indicated times. Untransfected SY5Y-TR1 cells (U) were also used as controls. (**c**) Dose–response curves for SH-SY5Y and SY5Y-TR1 cells treated with the AXL small molecule inhibitor, R428, for 3 days (IC_{50}= SH-SY5Y, 4.79 μM; SY5Y-TR1, 1.93 μM). (**d**) Drug matrix illustrating percent inhibition (left) and Delta Bliss (right) for R428 in combination with TAE684 in SH-SY5Y and SY5Y-TR1 cells. Percent inhibition values were derived from the cell viability assay after 3 days of treatment with the two compounds. Considering *A* and *B* to be the fractional growth inhibition (percent inhibition divided by 100) of single drug treatment at a given dose (for example, TAE684 and R428, respectively), a Bliss expectation was calculated using the formula: $(A+B) - A \times B$ for every drug concentration used. The 'Delta Bliss' represents the difference between the Bliss expectation and the observed fractional growth inhibition of the combination of drug *A* and *B* at the same dose. A Delta Bliss of 1 indicates an additive effect, whereas a value < 0 or > 1 indicate antagonistic and synergistic effects of the combination, respectively. Color scales for each specific grid (left = percent inhibition; right= Delta Bliss) are shown. Values represent the mean of two separate experiments. (**e**) qRT–PCR analysis (left) of AXL expression in untransfected (SH-SY5Y) or SH-SY5Y cells stably expressing either AXL (AXL) or vector control (MSCV). ***$P < 0.001$. Western blot analysis (right) of total and pAXL in these cells. AXL was immunoprecipitated using an anti-AXL antibody and western blotting performed with an anti-phosphotyrosine antibody. (**f**) Dose–response curves for cells in (**e**) exposed to TAE684 for 3 days (IC_{50} = SH-SY5Y, 44 nM; SH-SY5Y MSCV, 50 nM; SH-SY5Y AXL, 102 nM). (**g**) Western blot analysis of total and pERK in the same cells as in (**e**).

of *AXL* in parental TAE684-sensitive SH-SY5Y cells caused a twofold reduction in sensitivity to TAE684 (Figures 2e and f), although it did not alter *TWIST2* expression levels (Figure 5e). Overexpression of *AXL* also led to a mesenchymal phenotype characterized by significant modulation of vimentin and cadherin expression (Figures 5b and c) and increased invasiveness (Figure 5d). Finally, simultaneous expression of both proteins in parental SH-SY5Y cells (Figure 5a, right) led to differential expression of vimentin and cadherin (Figures 5b and c), a highly invasive phenotype (Figure 5d) and, importantly, more than threefold decrease in sensitivity to TAE684 (Figure 5f). Together, these observations suggest that, in our model, combined expression of *AXL* and *TWIST2* leads to additive effects on EMT and drug resistance, whereas only AXL activation is associated with resistance to TAE684.

AXL activation is facilitated by elevated levels of the cleaved form of its ligand GAS6

The dependence of TAE684 resistance in NB cells on AXL activation led us to investigate the mechanism of *AXL* upregulation in SH-SY5Y-TR1 cells. Gene amplification was excluded at the outset through quantitative PCR analysis of genomic DNA (Supplementary Figure S3a). Sequencing of the *AXL* promoter and coding regions likewise failed to identify mutations within SH-SY5Y-TR1 cells that could account for elevated AXL expression (data not shown). Methylation-specific PCR and bisulfite sequencing failed to reveal differential CpG hypomethylation as a mechanism of *AXL* overexpression, as previously reported[23] (data not shown). We also assessed the contribution of miR-34a and miR-199a/b, the two acknowledged modulators of AXL expression,[24] noting a decrease in miR-199b levels in the TAE684-resistant cells relative to the sensitive

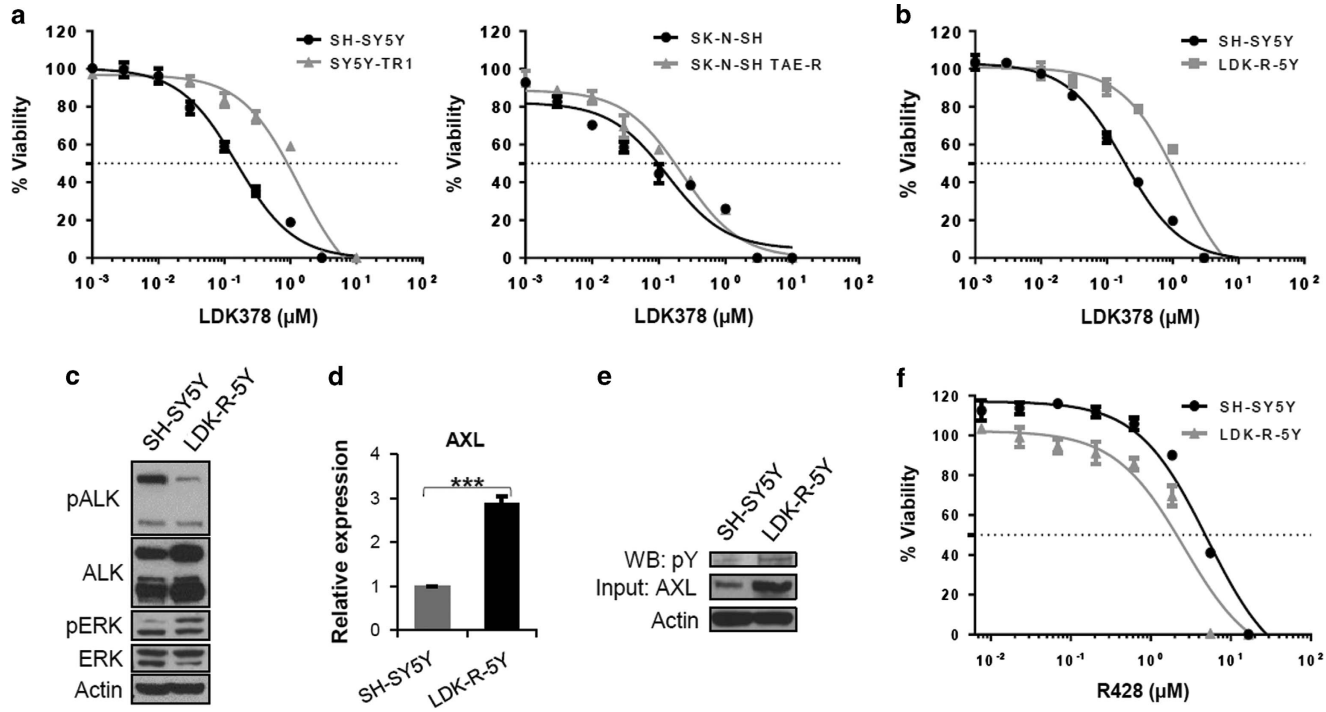

Figure 3. Resistance to LDK378 in ALK^{F1174L}-driven SH-SY5Y cells is also associated with AXL upregulation. (**a**) Dose–response curves for parental SH-SY5Y and TAE684-resistant SY5Y-TR1 cells (left) treated with LDK378 for 3 days (IC_{50} = SH-SY5Y, 150 nM; SY5Y-TR1, 1101 nM), and parental SK-N-SH and TAE684-resistant SK-N-SH-TAE-R cells (right) treated with LDK378 for 3 days (IC_{50} = SK-N-SH, 69.4 nM; SK-N-SH TAE, 149.7 nM). (**b**) Dose–response curves for parental and LDK378-resistant SH-SY5Y (LDK-R-5Y) cells treated with LDK378 for 3 days (IC_{50} = SH-SY5Y, 184 nM; LDK Res 5Y, 1049 nM). (**c**) Western blot analysis of total and pALK and ERK in parental and LDK-R-5Y cells. (**d**) qRT–PCR analysis of AXL in SH-SY5Y and LDK-R-5Y cells. $^{***}P < 0.001$. (**e**) Analysis of pAXL in parental and LDK-R-5Y cells in which AXL was immunoprecipitated using an anti-AXL antibody, followed by western blotting with an anti-phosphotyrosine antibody. (**f**) Dose–response curves for parental and LDK-R-5Y cells treated with R428 for 3 days (R428: IC_{50}= SH-SY5Y, 4420 nM; LDK-R-5Y, 2260 nM).

ones (Supplementary Figure S3b). Forced expression of miR-199b in SH-SY5Y-TR1 cells, however, failed to induce downregulation of *AXL* at either the mRNA (Supplementary Figure S3c) or protein (Supplementary Figure S3d) level. Notably, no effect on pERK levels (Supplementary Figure S3d) was seen, suggesting that aberrant microRNA regulation was not a major determinant of the increased *AXL* expression seen in the TAE684-resistant NB cells.

AXL receptor dimerization and activation through autophosphorylation has been reported to occur through binding of its physiological ligand GAS6 that triggers a cascade of intracellular signaling events that culminate in cell proliferation and survival.[25] *GAS6* is normally expressed in two forms: the full-length 75 kDa protein and a slightly larger protein, GAS6-SV (86 kDa), because of alternative splicing.[26] This modification leads to the insertion of a 43-amino-acid sequence that contains a consensus cleavage site, whose proteolytic cleavage results in a soluble 50 kDa product that is ultimately responsible for AXL receptor activation.[26] We observed a marked increase in GAS6 protein levels in TAE684-resistant SH-SY5Y-TR1 cells compared with parental cells, as well as significantly higher mRNA levels of the GAS6 splice variant, GAS6-SV (Figure 6a). Importantly, the same findings, in conjunction with *AXL* upregulation, were observed in SH-SY5Y cells that were made resistant to LDK378 (Figure 6b). Moreover, analysis of conditioned media from SH-SY5Y-TR1 cells revealed an abundance of the cleaved active 50 kDa GAS6 fragment (Figure 6c). Hence, the presence of increased levels of GAS6, as well as that of its active secreted form in TAE684-resistant cells, suggested that AXL activation in these cells resulted from upregulation of its ligand. To test this hypothesis, we depleted *GAS6* in SH-SY5Y-TR1 cells through shRNA knockdown, noting a resultant significant decrease in AXL levels and, more importantly, concomitant attenuation of ERK activation (Figure 6d). Moreover, conditioned media from SH-SY5Y-TR1 cells led to increased levels of GAS6 and activated AXL proteins, as well as upregulated ERK signaling in TAE684-sensitive parental SH-SY5Y cells (Figure 6e). These cells became less sensitive to TAE684 while showing increased sensitivity to R428 (Figure 6f). We also noted that *AXL* mRNA levels in both parental and *AXL*-overexpressing SH-SY5Y cells did not increase after treatment with human recombinant GAS6 (rGAS6), arguing against a positive feedback loop on AXL production (Supplementary Figure S4a). Rather, cells that were pretreated with rGAS6 showed higher AXL protein levels in the presence of the protein synthesis inhibitor cycloheximide, suggesting that GAS6 upregulation led to AXL protein stabilization (Supplementary Figure S4b). Together, these results suggest that AXL activation in SHSY5Y-TR1 cells is facilitated by increased production of soluble GAS6 via aberrant expression of cleavable GAS6-SV.

TAE684-resistant AXL-activated SH-SY5Y cells are sensitive to HSP90 inhibition

It has been shown that ALK inhibitor-resistant non-small-cell lung cancer cell lines are susceptible to heat-shock protein 90 (HSP90) inhibitors.[27] Moreover, AXL is an acknowledged substrate of HSP90,[28] prompting us to investigate the consequences of HSP90 inhibition in the context of NB cell resistance to TAE684. We therefore tested the effects of the HSP90 inhibitors geldanamycin (17-AAG) and its semisynthetic derivative, retaspimycin hydrochloride (IPI-504),[27] on TAE684-resistant NB cells. SH-SY5Y-TR1 cells showed a tenfold increase in sensitivity to HSP90 inhibition (Figure 7a). To identify the HSP90 targets whose inhibition led to such a striking response in TAE684-resistant cells, we determined the phosphorylation status of several RTKs in SH-SY5Y-TR1

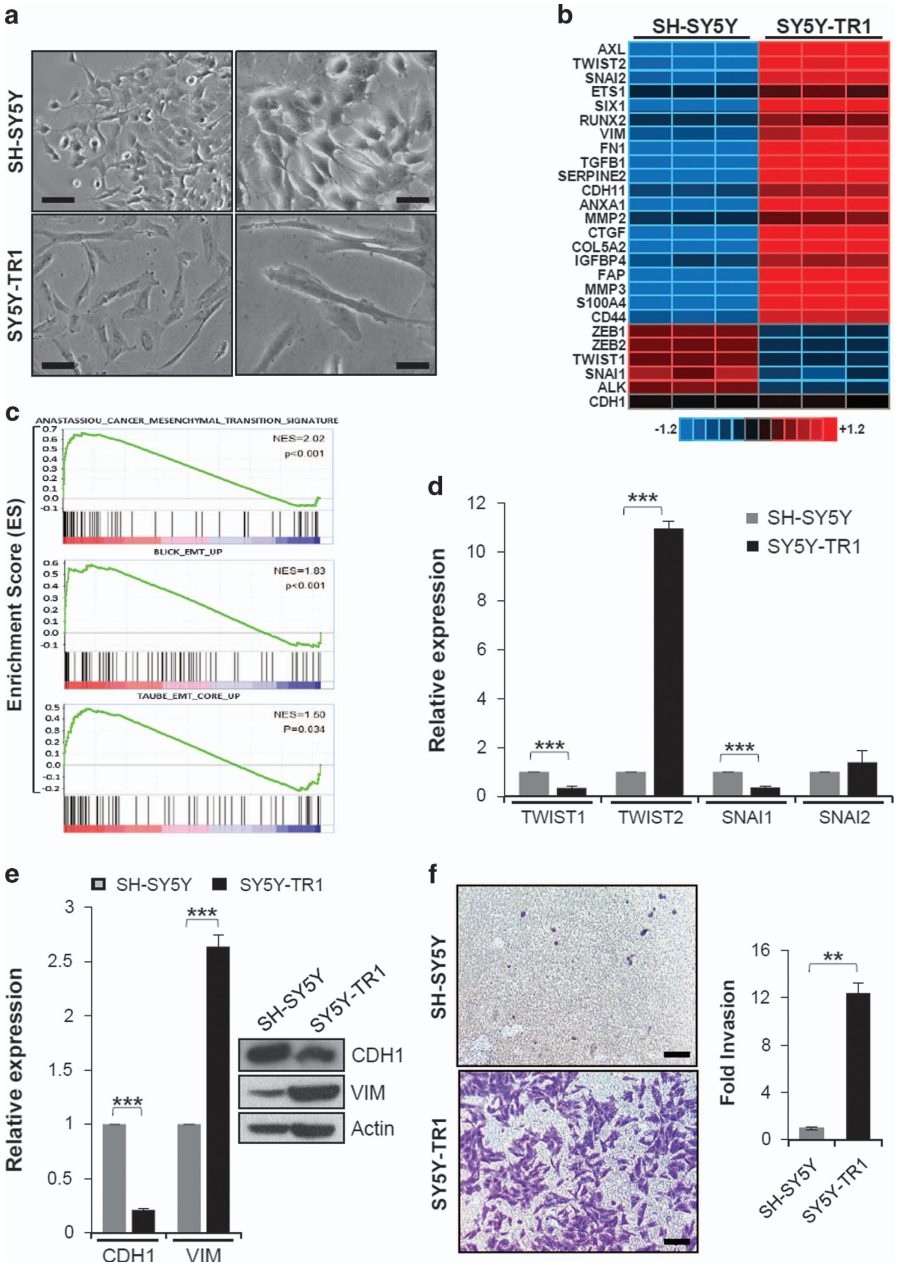

Figure 4. TAE684-resistant SH-SY5Y cells exhibit features of EMT. (**a**) Phase contrast micrographs of SH-SY5Y and SY5Y-TR1 cells (scale bars, 50 μm, inserts, 25 μm). (**b**) Representative heatmap showing differential expression of key EMT-related genes, as well as ALK and AXL, in TAE684-sensitive SH-SY5Y and -resistant SY5Y-TR1 cells. Fold change ⩾2.0; corrected $P < 0.05$). (**c**) GSEA of three previously published EMT gene signatures in SY5Y-TR1 cells as compared with SH-SY5Y cells. NES, normalized enrichment score. (**d**) qRT–PCR analysis of the indicated genes in SH-SY5Y and SY5Y-TR1 cells. ***$P < 0.001$. (**e**) mRNA and protein levels of E-cadherin (CDH1) and vimentin (VIM) in SH-SY5Y and SY5Y-TR1 cells, as analyzed by qRT–PCR (left) and western blotting (right). ***$P < 0.001$. (**f**) Invasion potential (left) of SH-SY5Y and SY5Y-TR1 cells as analyzed by matrigel assay (scale bar, 50 μm). Quantification of invasion potential (right) of the same cells. **$P < 0.01$.

cells after treatment with IPI-504 (Figure 7b). Compared with DMSO-treated SH-SY5Y-TR1 cells, those treated with IPI-504 exhibited a loss of pAXL. EPHB2 phosphorylation was again seen to be increased in SH-SY5Y-TR1 cells (Figure 1c), but this effect was unchanged with IPI-504 treatment, suggesting that this RTK most likely was not involved in TAE684-mediated resistance.

The above results led us to ask whether the decreased phosphorylation of AXL upon HSP90 inhibition was coupled with degradation and loss of total AXL in SH-SY5Y-TR1 cells. Treatment with IPI-504 led to a time-dependent reduction of total AXL levels in SH-SY5Y-TR1 cells (Figure 7c). Importantly, the reduction in AXL levels on exposure to HSP90 inhibitor was accompanied by a concomitant decrease in pERK levels, again indicating that activated AXL signals at least partially through the MAPK pathway in TAE684-resistant cells (Figure 7c). HSP90 functions as a molecular chaperone that stabilizes AXL through direct binding.[28] To establish whether the interaction between AXL and HSP90 in SH-SY5Y-TR1 cells was compromised by IPI-504, we coimmunoprecipitated HSP90 in resistant and parental cells before and after treatment with IPI-504 and analyzed AXL expression by western blotting with an anti-AXL antibody. Although no AXL protein bound to HSP90 in SH-SY5Y cells, binding to HSP90 was observed in SH-SY5Y-TR1 cells, and this was markedly decreased following treatment with IPI-504 (Figure 7d).

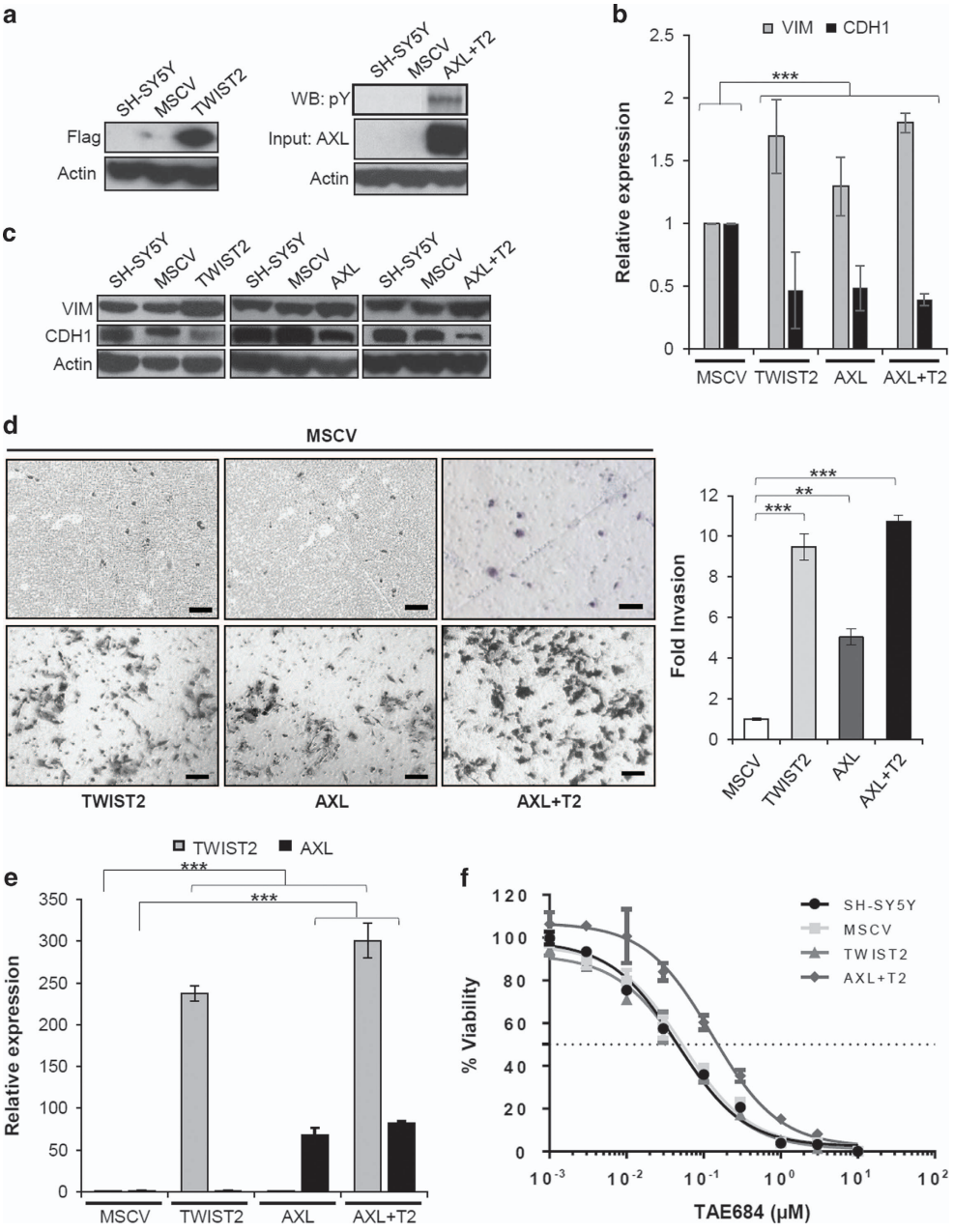

Figure 5. AXL overexpression in SH-SY5Y cells is sufficient to confer both mesenchymal features and TAE684 resistance. (**a**) Western blot analysis (left) of TWIST2 expression in SH-SY5Y cells overexpressing either a vector control (MSCV) or TWIST2 (TWIST2). Western blot analysis (right) of AXL expression and phosphorylation in cells engineered to express both AXL and TWIST2 together (AXL+T2). AXL was immunoprecipitated with an anti-AXL antibody, followed by western blotting with an anti-phosphotyrosine antibody. (**b**) qRT–PCR analysis of cadherin (CDH1) and vimentin (VIM) in SH-SY5Y cells expressing either TWIST2 or AXL singly or in combination. $^{***}P < 0.001$. (**c**) Western blot analysis of CDH1 and VIM expression in the same cells as in (**a**). (**d**) Photomicrographs (left) showing invasion capacities, together with quantification (right) of the same cells as in (**b**) (scale bar, 50 μm). $^{**}P < 0.01$, $^{***}P < 0.001$. (**e**) qRT–PCR analysis of expression levels of TWIST2 and AXL in the same cells. $^{***}P < 0.001$. (**f**) Dose–response curves for the same cells as in (**a**) exposed to TAE684 for 3 days (IC_{50}= SH-SY5Y, 44 nM; SH-SY5Y MSCV, 50 nM; SH-SY5Y TWIST2, 42 nM; SH-SY5Y AXL+T2, 155 nM).

Therefore, HSP90 inhibition in SH-SY5Y-TR1 cells leads to substantial reduction of AXL activity through diminished binding. Together, these results support the hypothesis that activated AXL mediates resistance to ALK inhibition in ALK^{F1174L}-driven NB cells and suggests a therapeutic strategy to overcome such resistance.

DISCUSSION

Resistance to tyrosine kinase inhibitors of ALK has been described in multiple tumor types and can arise through different mechanisms.[1] Here we show that in ALK^{F1174L}-driven NB cells, the development of resistance to TAE684 and its clinically available derivative, LDK378, is associated with *AXL* overexpression and activation, as well as increased ERK signaling. The resistant cells exhibit increased sensitivity to an AXL inhibitor in comparison with TAE684-sensitive parental cells, with concomitant down-regulation of ERK signaling. Aberrantly expressed AXL appears to be activated through increased levels of its ligand, GAS6, that also stabilizes the kinase. Resistance to TAE684 was associated with induction of an EMT phenotype. Finally, TAE684-resistant cells

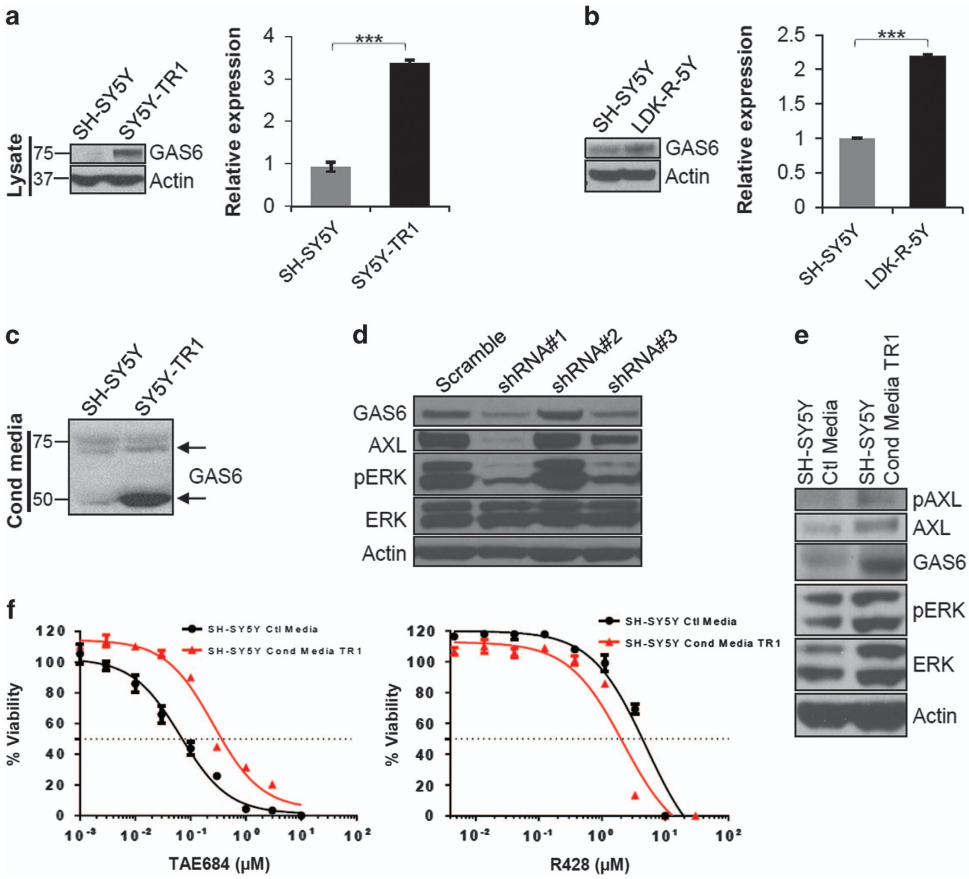

Figure 6. The AXL ligand, GAS6, is highly expressed in TAE684- and LDK378-resistant cells and leads to AXL activation. (**a**) Western blot analysis of GAS6 levels in cell lysates from parental SH-SY5Y and TAE684-resistant SY5Y-TR1 cells (left). qRT–PCR analysis of the GAS6-SV variant in the same cells (right). ***$P < 0.001$. (**b**) Western blot (left) and qRT–PCR analysis (right) of the GAS6-SV variant in the parental and LDK378-resistant SH-SY5Y cells. ***$P < 0.001$. (**c**) Western blot analysis of the 50 kDa cleaved GAS6 product in conditioned media from SH-SY5Y and SY5Y-TR1 cells. Arrows indicate both full-length and cleaved GAS6 forms. (**d**) Western blot analysis of the indicated proteins in SY5Y-TR1 cells expressing either GAS6 shRNAs or a control shRNA (scramble). Three different shRNAs (1, 2 and 3) were used. (**e**) Western blot analysis of total and pAXL and ERK levels, as well as GAS6 protein in SH-SY5Y cultivated for 3 days in conditioned media from control SH-SY5Y or TAE684-resistant SY5Y-TR1 cells. (**f**) Dose–response curves for parental SH-SY5Y cultivated for 3 days in conditioned (Cond) media from control SH-SY5Y or TAE684-resistant SY5Y-TR1 cells and then treated with TAE684 or R428 for 3 days (TAE684: IC_{50}=SH-SY5Y Ctl Media, 66 nM; SH-SY5Y Cond Media TR1, 385 nM; R428: IC_{50}= SH-SY5Y Ctl Media, 4085 nM; SH-SY5Y Cond Media TR1, 1836 nM).

were significantly more sensitive to HSP90 inhibition, at least partly through its impact on AXL binding. Our findings not only identify a molecular mechanism of resistance to ALK inhibition in ALK^{F1174L}-driven NB, but also suggest that effective AXL or HSP90 inhibitors, combined with a TAE684-derived ALK inhibitor, could provide a useful strategy to overcome this complication.

AXL is an RTK in the TAM kinase family whose members function as homeostatic regulators in adult tissues and play prominent roles in the nervous system.[15] When AXL is activated by its ligand GAS6,[25] it also contributes to key physiological processes such as cell survival, proliferation and migration[29] mainly through the MAPK and PI3K signaling pathways.[30,31] *AXL* overexpression has been reported in various cancers and its role in regulating the actin cytoskeleton links this kinase to tumor invasiveness and metastasis, as shown in glioblastoma[32] and breast cancer.[33,34] Moreover, *AXL* overexpression has been implicated in resistance to both standard and targeted anti-cancer agents (mainly epidermal growth factor receptor (EGFR) inhibitors) in various cancers, with or without accompanying EMT features.[16,17,35–37]

To our knowledge, this report provides the first evidence of AXL overexpression and activation as an acquired mechanism of resistance to ALK inhibition in NB. We would stress that the findings presented here are restricted to human NB cells in which the ALK^{F1174L} mutation is the principal if not the sole driver of tumorigenesis. This model accounts for ~2% of all NB cases at diagnosis[38] but does not necessarily apply to cases in which ALK^{F1174L} coexists with other major genetic aberrations such as *MYCN* amplification. It will be important, therefore, to assess the significance of *AXL* overexpression and activation in cases of ALK-inhibitor resistance where the pathogenic role of *ALK* mutations is less dominant. Interestingly, in a study by Duijkers *et al.*,[39] *AXL* overexpression was observed in established human NB cell lines that had not been exposed to targeted therapy, and its genetic depletion led to decreased cell migration and invasion, but not proliferation or downstream signaling.[39] The decreased growth kinetics and downregulated pERK after AXL depletion in the TAE684-resistant cells likely reflect their relatively higher dependence on increased AXL activity.

Whether AXL inhibition alone is sufficient to reverse resistance to TKIs remains unclear. Genetic and pharmacological inhibition of AXL has been shown to restore sensitivity to erlotinib in *EGFR*-mutant lung cancer models with acquired erlotinib resistance, AXL activation and mesenchymal transition.[17] However, in other studies, a functional role for AXL in both erlotinib-resistant *EGFR*-positive or crizotinib-resistant *EML4-ALK*-positive lung cancer cells with *AXL* overexpression and an EMT phenotype has been excluded.[40,41] Our results demonstrate that AXL inhibition by itself

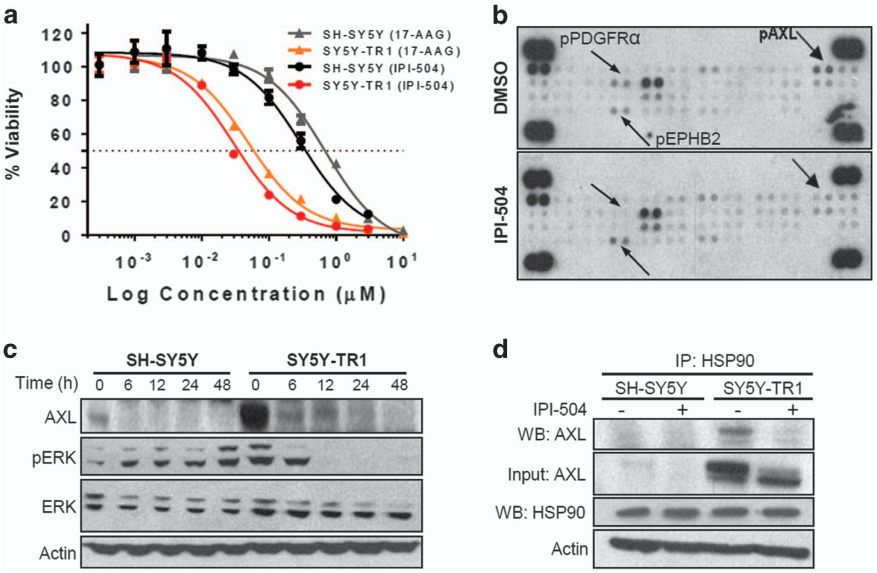

Figure 7. TAE684-resistant SY5Y-TR1 cells are sensitive to HSP90 inhibition. (**a**) Dose–response curves for parental SH-SY5Y and TAE684-resistant SY5Y-TR1 cells treated with the HSP90 inhibitors 17-AAG and IPI-504 for 3 days (IC_{50}=17-AAG, 650 nM (SH-SY5Y), 61 nM (SY5Y-TR1); IPI-504, 352 nM (SH-SY5Y), 35 nM (SY5Y-TR1)). (**b**) pRTK array analysis of SY5Y-TR1 cells treated with either DMSO or IPI-504 (1 μM) for 6 h. (**c**) Western blot analysis of AXL, total and pERK levels in SH-SY5Y and SY5Y-TR1 cells after treatment with 1 μM IPI-504 for the indicated times. (**d**) Western blot analysis of AXL and HSP90 expression levels in SH-SY5Y and SY5Y-TR1 cells treated with or without 1 μM IPI-504 for 6 h and from which AXL was coimmunoprecipitated with an anti-HSP90 antibody.

only partly rescues TAE684 resistance, although it resensitizes these cells to TAE684, similar to results seen in head and neck cancer cells with acquired erlotinib resistance.[35] Thus, although AXL expression may contribute significantly to acquired resistance to TAE684, additional molecular mechanisms appear to be required for full development of the resistance phenotype.

Furthermore, the frequent association of *AXL* upregulation with an EMT phenotype in acquired TKI resistance[17,35] raises the intriguing question of whether AXL truly causes resistance or is merely a biomarker of EMT. In an analysis of multiple human cancer cell lines, in which elevated AXL was associated with a mesenchymal phenotype, EMT-associated drug resistance was found to be independent of AXL function.[41] However, our results indicate that both the acquisition of EMT features and AXL activation are required to confer resistance to TAE684, although the relative contributions of these changes remain to be assessed. Overexpression of *TWIST2*, despite inducing an EMT phenotype, did not alter either AXL expression or sensitivity to TAE684 in parental SH-SY5Y cells, whereas overexpression of *AXL*, although not affecting TWIST2 expression levels, led to an EMT phenotype and modest resistance to TAE684. *TWIST2*, when combined with *AXL* overexpression, led to a greater decrease in TAE684 sensitivity compared with ectopic expression of *AXL* alone. These findings suggest that the activation of AXL is independent of TWIST2 upregulation in TAE684-resistant cells, but can act cooperatively to enhance the resistant phenotype in response to ALK inhibition. Of note, our results may be confounded by the fact that the gene expression patterns of ectopic overexpression of a single EMT-associated gene could differ from a phenotype that develops over time.

The mechanism of AXL activation appears to involve autocrine regulation through its ligand, GAS6. We observed increased levels of cleaved GAS6 protein in the supernatant of TAE684-resistant cells as compared with the parental cells, suggesting that the active form of the ligand is secreted in order to sustain AXL activation and stabilization. Similarly, in mesenchymal non-small-cell lung cancer cell lines with EMT features, resistance to erlotinib and upregulation of AXL was associated with markedly increased levels of GAS6.[16,17] Therefore, cleaved soluble GAS6 could be exploited as a biomarker of resistance to ALK inhibition. Indeed, if validated in human samples from ALK inhibitor-treated patients, the ability to specifically track cleaved GAS6 levels over time in the serum of patients would be a less invasive way to detect the early development of resistance.

We observed that TAE684-resistant cells were highly sensitive to HSP90 inhibition, partly due to depletion of AXL, leading to decreased downstream signaling. AXL was recently identified as an HSP90 substrate and was shown to be degraded in the intracellular compartment by geldanamycin.[42] The increased vulnerability of these cells may reflect the presence of other proteins, including other RTKs that contribute to cell proliferation and survival, and by extension of the resistance phenotype, that are simultaneously disrupted with HSP90 inhibition. Our findings extend the currently emerging paradigm for the design of HSP90 inhibition-based strategies, either alone or in combination with selective ALK targeting, in the management of ALK-driven resistant cancers.

In ALK inhibitor-resistant cells, the ERK pathway appeared to be a major signaling mechanism through which activated AXL contributed to resistance. Whereas the PI3K/AKT/mTOR pathway is primarily involved in ALK downstream signaling in parental SH-SY5Y cells,[5] pERK was upregulated in TAE684- and LDK378-resistant SH-SY5Y cells. Moreover, any alteration in AXL or GAS6 levels was closely correlated with changes in ERK signaling in the resistant cells: genetic and pharmacological depletion of AXL led to decreased ERK phosphorylation, as did shRNA knockdown of *GAS6*, and HSP90 inhibitor-induced depletion of AXL. Although activated AXL could utilize multiple downstream signaling pathways, our observations highlight the ERK pathway as an essential signaling node required to maintain cell survival in the face of targeted treatment. Indeed, two recent publications support the central role of ERK signaling in treatment resistance; first, MAPK pathway mutations are often frequently found in relapsed NBs after chemotherapy,[43] and, second, several RTK ligands can confer resistance to kinase inhibitors (including TAE684) by reactivation of ERK in oncogene-addicted cancer cell lines.[44] It is therefore reasonable to suggest that ERK inhibition with small molecules would be an effective strategy in therapy-resistant tumors or even to prevent the emergence of resistance through this mechanism.

Given the number of tumors that develop resistance to TKIs with upregulation of *AXL*, we propose that this mechanism is common to any tumor targeted with these agents, and that it should be considered in patients who develop such resistance. Especially in NB, where clinical trials of ALK inhibitors alone or in combination with standard chemotherapy agents are planned, it would be reasonable to assume that numerous instances of resistance will involve activation of AXL, and potentially the development of EMT. Indeed, AXL or GAS6 expression could be used as biomarkers of resistance in tumors that have not yet acquired the EMT phenotype. As EMT is driven by transcription factors that are currently undruggable, AXL activation represents an attractive target for inhibition in tumors resistant to ALK or other RTK inhibitors. As an alternative to an effective AXL inhibitor, depletion of this RTK could also be readily achieved by HSP90 inhibition.

MATERIALS AND METHODS

Cell lines and reagents

The human NB cell line SK-N-SH and its derivative SH-SY5Y were purchased from the American Type Culture Collection (Manassas, VA, USA) and their authenticity confirmed by genotyping. Cells were also confirmed to be mycoplasma negative. Parental and resistant cells were grown in RPMI media supplemented with 10% fetal bovine serum and 1% penicillin/streptomycin. TAE684 and R428 were synthesized in-house in Dr Nathanael Gray's laboratory (Boston, MA, USA). 17-AAG, CHX and LDK378 were purchased from Selleck Chemicals (Houston, TX, USA), and IPI-504 was purchased from APExBIO (Houston, TX, USA). Recombinant human GAS6 (rGAS6) was purchased from R&D Systems (885-GS-050; Minneapolis, MN, USA).

Cell viability assay

Viability experiments were performed using the CellTiter-Glo Luminescent Cell Viability Assay (G7573; Promega, Madison, WI, USA) according to the manufacturer's instructions. All dose–response assays were performed in triplicate in 96-well plates and repeated at least three times. The results, representing the mean ± s.d. of three separate biological experiments, were plotted as a nonlinear regression curve fit using Graphpad Prism 6 software (La Jolla, CA, USA). The x axis represents the log2 concentration of the indicated compound.

Western blotting and immunoprecipitation

Cell lysates or conditioned media that were concentrated using Amicon Ultra 0.5 10K Centrifugal Filters (EMD Millipore, Billerica, MA, USA) were prepared using standard protocols. The following antibodies were used: AXL (4566), pAXL (5724), ALK (3333), pALK (3341), AKT (4691), pAKT (9271), ERK (4695), pERK (4377), VIM (5741), CDH1 (3195), tubulin (2128) and actin (4967) from Cell Signaling Technology (Danvers, MA, USA); GAS6 (sc-376087), HSP90 (sc-59577) and phosphotyrosine (sc-81529) from Santa Cruz Biotechnology (Santa Cruz, CA, USA); Flag (F3165) from Sigma-Aldrich (Saint Louis, MO, USA); and AXL antibody for immunocytochemistry from R&D Systems (AF154).

Phospho-RTK array analysis

Cell lysate (500 μg) was incubated on a human phospho-RTK membrane array (ARY001B; R&D Systems) according to the manufacturer's instructions. Target proteins were captured with their respective antibodies. After washing, the proteins were incubated with a phosphotyrosine antibody conjugated to horseradish peroxidase to allow the detection of captured phospho-RTKs.

Invasion assay

A cell suspension containing 5×10^5 cells/ml in serum-free medium was added to the upper chamber of the invasion assembly (ECM550; Chemicon International, Billerica, MA, USA) and 10% fetal bovine serum containing media added to the lower chamber to act as a chemoattractant. After incubation for 48 h, non-migrating cells in the upper chamber were removed with cotton swabs, and cells that migrated to the lower surface of the filters were stained with crystal violet. The results were quantified by counting and averaging three independent fields per condition, and represent the mean ± s.d. of three separate biological experiments.

Lentiviral/retroviral transduction and transient transfection

Lentiviral-based pLKO.1 shRNA constructs (*shAXL*, *shERK* and *shGAS6*) were obtained from the RNAi Consortium of the Broad Institute (Cambridge, MA, USA). The constructs were transfected into 293T cells with helper plasmids for virus production. Cells were then transduced with virus, followed by puromycin selection for at least 3 days. Stable overexpression of the retroviral-based pMSCV vector containing *TWIST2*, *AXL* or both genes was performed similarly. Transient knockdown of *AXL* was performed with specific Silencer Select siRNA (Life Technologies, Carlsbad, CA, USA) according to the manufacturer's instructions. GAS6 siRNA pool was purchased from Dharmacon RNAi Technologies (Lafayette, CO, USA).

Gene expression analysis

Three biological replicates of total RNA were isolated from SH-SY5Y and SY5Y-TR1 cells using the RNeasy Mini kit (Qiagen, Valencia, CA, USA). Total RNA was hybridized to GeneChip Human Genome U133 Plus 2.0 Arrays (Affymetrix, Santa Clara, CA, USA), according to the manufacturer's instructions. The data obtained are accessible through the GEO accession number GSE73292. Data analysis was performed using GenePattern software.[45] GSEA was performed with the GSEA application,[46] using log2 fold change to rank genes.

Immunocytochemistry

1×10^6 cells were formalin fixed and immunocytochemistry performed based on established protocols.[9] AXL antibody (R&D Systems) in a 1:1000 dilution was used to determine AXL expression.

Quantitative RT–PCR

Total RNA was isolated using the RNeasy Mini kit (Qiagen), followed by RT–PCR with the ThermoScript RT–PCR system (Life Technologies). Quantitative PCR was carried out using the QuantiFast SYBR Green PCR kit (Qiagen) in a 96-well plate format, and analyzed on an Applied Biosystems ViiA 7 Real-Time PCR System (Life Technologies). Each sample was run in triplicate and normalized to actin as an internal control. Relative quantification was calculated according to the ΔΔCt relative quantification method. The results represent the mean ± s.d. of three separate biological experiments. Primer sequences are available upon request.

Sequence analysis

The kinase domain of ALK and full-length AXL were amplified from complementary DNA of SH-SY5Y and SY5Y-TR1 cells using the HotStar HiFidelity Polymerase Kit (Qiagen). The PCR products were cloned into the pGEM-T vector (Promega) and confirmed by sequencing. The GAS6 insertion (GAS6-SV) was similarly amplified from the two cell lines, and the gel-purified PCR product confirmed by sequencing.

Statistical analysis

Statistical significance for all comparisons between two groups was determined with the two-sided Student's *t*-test: $^*P < 0.05$, $^{**}P < 0.01$ and $^{***}P < 0.001$. The effect of combining TAE684 and R428 was determined using the Bliss additivity model.[47]

CONFLICT OF INTEREST

The authors declare no conflict of interest.

ACKNOWLEDGEMENTS

This study was supported by NIH/NCI R01 CA148688 (to REG), Friends for Life Neuroblastoma Fellowship (to DND) and a Ruth L Kirschstein NRSA F32CA183566 (to NFM).

REFERENCES

1 Gainor JF, Shaw AT. Emerging paradigms in the development of resistance to tyrosine kinase inhibitors in lung cancer. *J Clin Oncol* 2013; **31**: 3987–3996.
2 Mahon FX, Deininger MW, Schultheis B, Chabrol J, Reiffers J, Goldman JM *et al*. Selection and characterization of BCR-ABL positive cell lines with differential sensitivity to the tyrosine kinase inhibitor STI571: diverse mechanisms of resistance. *Blood* 2000; **96**: 1070–1079.

3 Kobayashi S, Boggon TJ, Dayaram T, Janne PA, Kocher O, Meyerson M *et al.* EGFR mutation and resistance of non-small-cell lung cancer to gefitinib. *N Engl J Med* 2005; **352**: 786–792.
4 Chen Y, Takita J, Choi YL, Kato M, Ohira M, Sanada M *et al.* Oncogenic mutations of ALK kinase in neuroblastoma. *Nature* 2008; **455**: 971–974.
5 George RE, Sanda T, Hanna M, Frohling S, Luther W 2nd, Zhang J *et al.* Activating mutations in ALK provide a therapeutic target in neuroblastoma. *Nature* 2008; **455**: 975–978.
6 Janoueix-Lerosey I, Lequin D, Brugieres L, Ribeiro A, de Pontual L, Combaret V *et al.* Somatic and germline activating mutations of the ALK kinase receptor in neuroblastoma. *Nature* 2008; **455**: 967–970.
7 Mosse YP, Laudenslager M, Longo L, Cole KA, Wood A, Attiyeh EF *et al.* Identification of ALK as a major familial neuroblastoma predisposition gene. *Nature* 2008; **455**: 930–935.
8 De Brouwer S, De Preter K, Kumps C, Zabrocki P, Porcu M, Westerhout EM *et al.* Meta-analysis of neuroblastomas reveals a skewed ALK mutation spectrum in tumors with MYCN amplification. *Clin Cancer Res* 2010; **16**: 4353–4362.
9 Berry T, Luther W, Bhatnagar N, Jamin Y, Poon E, Sanda T *et al.* The ALK(F1174L) mutation potentiates the oncogenic activity of MYCN in neuroblastoma. *Cancer Cell* 2012; **22**: 117–130.
10 Sasaki T, Okuda K, Zheng W, Butrynski J, Capelletti M, Wang L *et al.* The neuroblastoma-associated F1174L ALK mutation causes resistance to an ALK kinase inhibitor in ALK-translocated cancers. *Cancer Res* 2010; **70**: 10038–10043.
11 Sakamoto H, Tsukaguchi T, Hiroshima S, Kodama T, Kobayashi T, Fukami TA *et al.* CH5424802, a selective ALK inhibitor capable of blocking the resistant gatekeeper mutant. *Cancer Cell* 2011; **19**: 679–690.
12 Galkin AV, Melnick JS, Kim S, Hood TL, Li N, Li L *et al.* Identification of NVP-TAE684, a potent, selective, and efficacious inhibitor of NPM-ALK. *Proc Natl Acad Sci USA* 2007; **104**: 270–275.
13 Chen J, Jiang C, Wang S. LDK378: a promising anaplastic lymphoma kinase (ALK) inhibitor. *J Med Chem* 2013; **56**: 5673–5674.
14 Heuckmann JM, Holzel M, Sos ML, Heynck S, Balke-Want H, Koker M *et al.* ALK mutations conferring differential resistance to structurally diverse ALK inhibitors. *Clin Cancer Res* 2011; **17**: 7394–7401.
15 Lemke G. Biology of the TAM receptors. *Cold Spring Harb Perspect Biol* 2013; **5**: a009076.
16 Byers LA, Diao L, Wang J, Saintigny P, Girard L, Peyton M *et al.* An epithelial-mesenchymal transition gene signature predicts resistance to EGFR and PI3K inhibitors and identifies Axl as a therapeutic target for overcoming EGFR inhibitor resistance. *Clin Cancer Res* 2013; **19**: 279–290.
17 Zhang Z, Lee JC, Lin L, Olivas V, Au V, LaFramboise T *et al.* Activation of the AXL kinase causes resistance to EGFR-targeted therapy in lung cancer. *Nat Genet* 2012; **44**: 852–860.
18 Holland SJ, Pan A, Franci C, Hu Y, Chang B, Li W *et al.* R428, a selective small molecule inhibitor of Axl kinase, blocks tumor spread and prolongs survival in models of metastatic breast cancer. *Cancer Res* 2010; **70**: 1544–1554.
19 Anastassiou D, Rumjantseva V, Cheng W, Huang J, Canoll PD, Yamashiro DJ *et al.* Human cancer cells express Slug-based epithelial-mesenchymal transition gene expression signature obtained in vivo. *BMC Cancer* 2011; **11**: 529.
20 Blick T, Hugo H, Widodo E, Waltham M, Pinto C, Mani SA *et al.* Epithelial mesenchymal transition traits in human breast cancer cell lines parallel the CD44 (hi/)CD24 (lo/-) stem cell phenotype in human breast cancer. *J Mammary Gland Biol Neoplasia* 2010; **15**: 235–252.
21 Taube JH, Herschkowitz JI, Komurov K, Zhou AY, Gupta S, Yang J *et al.* Core epithelial-to-mesenchymal transition interactome gene-expression signature is associated with claudin-low and metaplastic breast cancer subtypes. *Proc Natl Acad Sci USA* 2010; **107**: 15449–15454.
22 Sequist LV, Waltman BA, Dias-Santagata D, Digumarthy S, Turke AB, Fidias P *et al.* Genotypic and histological evolution of lung cancers acquiring resistance to EGFR inhibitors. *Sci Transl Med* 2011; **3**: 75ra26.
23 Mudduluru G, Allgayer H. The human receptor tyrosine kinase Axl gene--promoter characterization and regulation of constitutive expression by Sp1, Sp3 and CpG methylation. *Biosci Rep* 2008; **28**: 161–176.
24 Mudduluru G, Ceppi P, Kumarswamy R, Scagliotti GV, Papotti M, Allgayer H. Regulation of Axl receptor tyrosine kinase expression by miR-34a and miR-199a/b in solid cancer. *Oncogene* 2011; **30**: 2888–2899.
25 Mark MR, Chen J, Hammonds RG, Sadick M, Godowsk PJ. Characterization of Gas6, a member of the superfamily of G domain-containing proteins, as a ligand for Rse and Axl. *J Biol Chem* 1996; **271**: 9785–9789.
26 Goruppi S, Yamane H, Marcandalli P, Garcia A, Clogston C, Gostissa M *et al.* The product of a gas6 splice variant allows the release of the domain responsible for Axl tyrosine kinase receptor activation. *FEBS Lett* 1997; **415**: 59–63.
27 Normant E, Paez G, West KA, Lim AR, Slocum KL, Tunkey C *et al.* The Hsp90 inhibitor IPI-504 rapidly lowers EML4-ALK levels and induces tumor regression in ALK-driven NSCLC models. *Oncogene* 2011; **30**: 2581–2586.
28 Wu Z, Moghaddas Gholami A, Kuster B. Systematic identification of the HSP90 candidate regulated proteome. *Mol Cell Proteomics* 2012; **11**: M111 016675.
29 Korshunov VA. Axl-dependent signalling: a clinical update. *Clin Sci (Lond)* 2012; **122**: 361–368.
30 Stenhoff J, Dahlback B, Hafizi S. Vitamin K-dependent Gas6 activates ERK kinase and stimulates growth of cardiac fibroblasts. *Biochem Biophys Res Commun* 2004; **319**: 871–878.
31 Fridell YW, Jin Y, Quilliam LA, Burchert A, McCloskey P, Spizz G *et al.* Differential activation of the Ras/extracellular-signal-regulated protein kinase pathway is responsible for the biological consequences induced by the Axl receptor tyrosine kinase. *Mol Cell Biol* 1996; **16**: 135–145.
32 Vajkoczy P, Knyazev P, Kunkel A, Capelle HH, Behrndt S, von Tengg-Kobligk H *et al.* Dominant-negative inhibition of the Axl receptor tyrosine kinase suppresses brain tumor cell growth and invasion and prolongs survival. *Proc Natl Acad Sci USA* 2006; **103**: 5799–5804.
33 Gjerdrum C, Tiron C, Hoiby T, Stefansson I, Haugen H, Sandal T *et al.* Axl is an essential epithelial-to-mesenchymal transition-induced regulator of breast cancer metastasis and patient survival. *Proc Natl Acad Sci USA* 2010; **107**: 1124–1129.
34 Vuoriluoto K, Haugen H, Kiviluoto S, Mpindi JP, Nevo J, Gjerdrum C *et al.* Vimentin regulates EMT induction by Slug and oncogenic H-Ras and migration by governing Axl expression in breast cancer. *Oncogene* 2011; **30**: 1436–1448.
35 Giles KM, Kalinowski FC, Candy PA, Epis MR, Zhang PM, Redfern AD *et al.* Axl mediates acquired resistance of head and neck cancer cells to the epidermal growth factor receptor inhibitor erlotinib. *Mol Cancer Ther* 2013; **12**: 2541–2558.
36 Hong J, Peng D, Chen Z, Sehdev V, Belkhiri A. ABL regulation by AXL promotes cisplatin resistance in esophageal cancer. *Cancer Res* 2013; **73**: 331–340.
37 Liu L, Greger J, Shi H, Liu Y, Greshock J, Annan R *et al.* Novel mechanism of lapatinib resistance in HER2-positive breast tumor cells: activation of AXL. *Cancer Res* 2009; **69**: 6871–6878.
38 Bresler SC, Weiser DA, Huwe PJ, Park JH, Krytska K, Ryles H *et al.* ALK mutations confer differential oncogenic activation and sensitivity to ALK inhibition therapy in neuroblastoma. *Cancer Cell* 2014; **26**: 682–694.
39 Duijkers FA, Meijerink JP, Pieters R, van Noesel MM. Downregulation of Axl in non-MYCN amplified neuroblastoma cell lines reduces migration. *Gene* 2013; **521**: 62–68.
40 Kim HR, Kim WS, Choi YJ, Choi CM, Rho JK, Lee JC. Epithelial-mesenchymal transition leads to crizotinib resistance in H2228 lung cancer cells with EML4-ALK translocation. *Mol Oncol* 2013; **7**: 1093–1102.
41 Wilson C, Ye X, Pham T, Lin E, Chan S, McNamara E *et al.* AXL inhibition sensitizes mesenchymal cancer cells to antimitotic drugs. *Cancer Res* 2014; **74**: 5878–5890.
42 Krishnamoorthy GP, Guida T, Alfano L, Avilla E, Santoro M, Carlomagno F *et al.* Molecular mechanism of 17-allylamino-17-demethoxygeldanamycin (17-AAG)-induced AXL receptor tyrosine kinase degradation. *J Biol Chem* 2013; **288**: 17481–17494.
43 Eleveld TF, Oldridge DA, Bernard V, Koster J, Daage LC, Diskin SJ *et al.* Relapsed neuroblastomas show frequent RAS-MAPK pathway mutations. *Nat Genet* 2015; **47**: 864–871.
44 Wilson TR, Fridlyand J, Yan Y, Penuel E, Burton L, Chan E *et al.* Widespread potential for growth-factor-driven resistance to anticancer kinase inhibitors. *Nature* 2012; **487**: 505–509.
45 Reich M, Liefeld T, Gould J, Lerner J, Tamayo P, Mesirov JP. GenePattern 2.0. *Nat Genet* 2006; **38**: 500–501.
46 Subramanian A, Tamayo P, Mootha VK, Mukherjee S, Ebert BL, Gillette MA *et al.* Gene set enrichment analysis: a knowledge-based approach for interpreting genome-wide expression profiles. *Proc Natl Acad Sci USA* 2005; **102**: 15545–15550.
47 Greco WR, Bravo G, Parsons JC. The search for synergy: a critical review from a response surface perspective. *Pharmacol Rev* 1995; **47**: 331–385.

Supplementary Information accompanies this paper on the Oncogene website (http://www.nature.com/onc)

Published OnlineFirst September 11, 2015; DOI: 10.1158/1078-0432.CCR-15-1397

CCR Translations

Clinical Cancer Research

Seek and Ye Shall Find: Subclonal Anaplastic Lymphoma Kinase Mutations

Rani E. George

Bellini and colleagues demonstrate the importance of next-generation sequencing to uncover subclonal anaplastic lymphoma kinase (*ALK*) mutations in neuroblastoma. Although the significance of these subclonal aberrations is not yet understood, deep sequencing could identify patients whose tumors may respond to ALK inhibitors. *Clin Cancer Res; 21(21); 4747–9. ©2015 AACR.*

See related article by Bellini et al., p. 4913

In this issue of *Clinical Cancer Research*, Bellini and colleagues (1) demonstrate that targeted deep sequencing of neuroblastoma tumors identifies subclonal mutations in the anaplastic lymphoma kinase (*ALK*) receptor tyrosine kinase that may have gone undetected using conventional Sanger sequencing. Since the original identification of activating somatic mutations in *ALK* in neuroblastoma, multiple sequencing studies have validated this kinase as the main targetable molecular aberration in this disease (2–5). In neuroblastoma, the majority of *ALK* mutations are found in the kinase domain and promote constitutive, ligand-independent activation of the receptor. These alterations are sensitive to small molecule inhibitors of ALK and lead to down-regulation of its activity and that of its downstream targets with consequent growth inhibition of neuroblastoma cells (4). *ALK* is also activated via translocation events in other malignancies, including non–small cell lung cancer, anaplastic large-cell lymphomas, and inflammatory myofibroblastic tumors, where it is thought to contribute to tumorigenesis and progression (6).

In the study by Bellini and colleagues (1), 276 neuroblastoma samples were analyzed by Sanger sequencing, revealing a mutation rate of 4.3% (12 of 276). To confirm the suspicion that conventional Sanger sequencing may not detect subclonal *ALK* mutations because of the limits of detection and background noise inherent in this technology, the authors resequenced these samples using the more sensitive two-step PCR procedure and HiSeq technology (Illumina). Targeted resequencing of exons 23 and 25, which contain the two most frequently observed mutational hotspots, *F1174* and *R1275*, respectively, identified subclonal *ALK* mutations (defined as <20% of the cell population, with up to 50% contamination from normal tissue) in an additional 15 tumors, yielding an overall mutation frequency of approximately 10% (27 of 276). *ALK* mutations at *F1174* were observed in 15 samples, 13 with a mutation leading to the amino acid change *F1174L*, while 2 samples showed *F1174C* and *F1174V* with the mutated allele fractions ranging widely, from 0.5% to 40%. The *R1275* locus was mutated in 12 cases, 11 with the *R1275Q* and one with the *R1275L* mutation; the proportion of cells with the mutated allele ranged from 0.8% to 73%. This wide range of mutated allele fractions was present even when corrected for tumor cell content and chromosome 2p copy-number status.

There was no association between clonal versus subclonal mutations and important clinical prognostic parameters, such as patient age, tumor stage, or outcome (1). Although on univariate analysis there was a worse overall survival in patients whose tumors expressed mutated or amplified *ALK*, especially those with the *F1174* mutation, this was not borne out when other factors were taken into consideration. In multivariate analysis, advanced-stage disease and *MYCN* amplification were the only independent prognostic variables, underscoring the secondary role of mutated *ALK* in determining treatment outcome in this patient cohort.

The authors report a close correlation between mutated *ALK* and amplified *MYCN* with enrichment of *F1174L* in tumors showing *MYCN* amplification (1), attesting to the demonstrated cooperative effect of both alterations in neuroblastoma (7, 8). Although *ALK* mutations were either clonal or subclonal, *MYCN* status was homogeneous throughout the tumor cell population. These observations support the general conclusion that *MYCN* deregulation is the initial event in neuroblastoma tumorigenesis, with *ALK* mutations occurring later in tumor development. An interesting observation was the percentage of clonal and subclonal *ALK* aberrations in the *MYCN*-amplified versus *MYCN*-nonamplified tumors. The majority of *MYCN*-amplified tumors (13 of 15) contained only subclonal populations of *ALK*-mutated cells, while in *MYCN*-nonamplified tumors the majority of *ALK* mutations (10 of 12) were clonal and only 2 of 12 contained subclonal *ALK* (1). This indicates that in most *MYCN*-nonamplified tumors with an *ALK* mutation, the kinase aberration appears to be dominant.

The significance of these subclones is far from clear. They could simply reflect the characteristic genetic heterogeneity of neuroblastoma or they could signal the presence of cell populations with the potential to expand and cause relapse (Fig. 1; ref. 9). The first scenario seems less likely, as almost all of the *ALK* mutations reported in neuroblastoma are activating (6). However, to date,

Department of Pediatric Hematology and Oncology, Dana-Farber Cancer Institute and Boston Children's Hospital, Harvard Medical School, Boston, Massachusetts.

Corresponding Author: Rani E. George, Department of Pediatric Oncology, Dana-Farber Cancer Institute, Dana 640E, 450 Brookline Avenue, Boston, MA 02215. Phone: 617-632-5281; Fax: 617-632-4850; E-mail: rani_george@dfci.harvard.edu

doi: 10.1158/1078-0432.CCR-15-1397

Published OnlineFirst September 11, 2015; DOI: 10.1158/1078-0432.CCR-15-1397

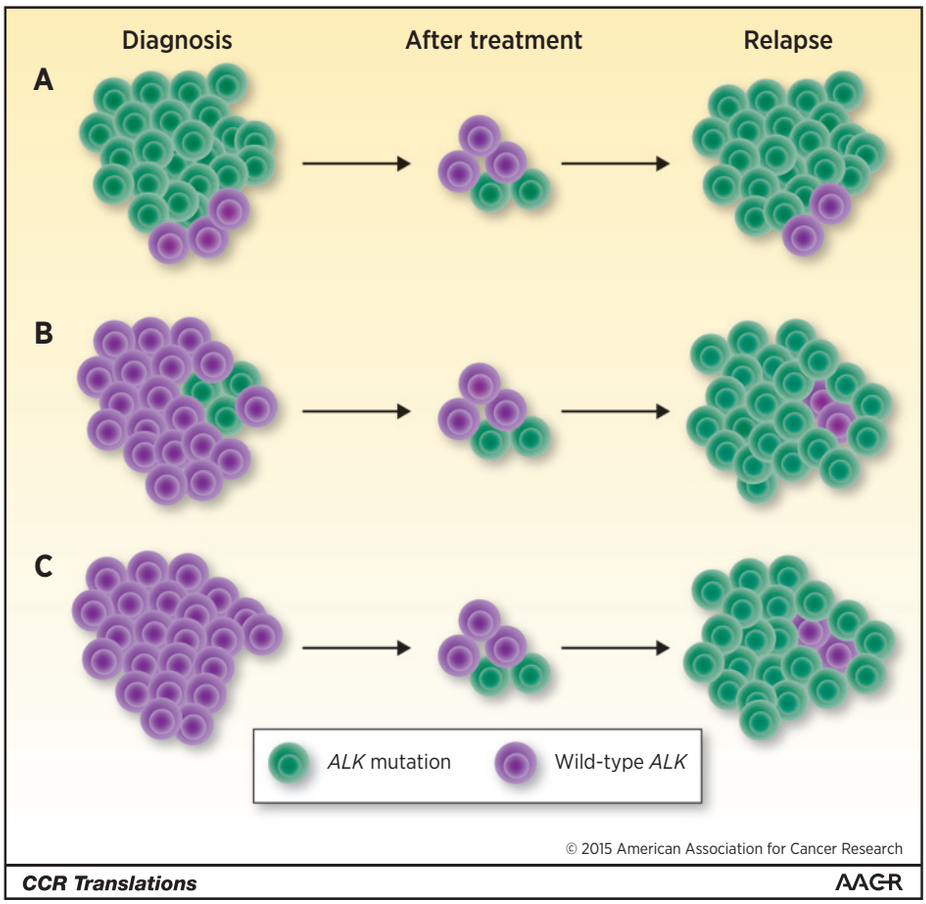

Figure 1.
Possible origins of *ALK* mutations detected at relapse. A, *ALK*-mutated cells can be clonal and form the dominant transformed population. These mutations can be identified through conventional sequencing methods. At relapse, these clonal populations retain their dominance, although the possibility of their replacement by clones bearing new mutations cannot be excluded. B, *ALK*-mutated cells are subclonal at diagnosis and could be either eradicated or evolve and expand at relapse to form the dominant transformed population. These mutations at diagnosis can be missed through conventional sequencing and will need to be searched for through advanced sequencing techniques. C, tumors without *ALK* mutations at diagnosis but in which ALK mutations arise *de novo* after treatment.

there is no experimental evidence that tumors containing malignant subclones have different growth properties or respond differently to *ALK* inhibitors. The numbers of patients used to determine clinical correlations in the Bellini study was relatively small, and repeat tumor biopsies were not available at relapse, eliminating opportunities to track the fate of subclonal *ALK* mutations that were uncovered in the diagnostic samples. Two earlier studies reported a higher frequency of *ALK* mutations at relapse, some of which were present at diagnosis but were below the limits of detection using standard sequencing methods (10, 11). For example, Schleiermacher and colleagues (10) compared 54 paired tumors at diagnosis and relapse and identified 14 *ALK* mutations, 5 of which were not detected at diagnosis. Deep sequencing revealed subclonal *ALK* mutations in 2 of 4 diagnostic samples. Moreover, in a recently published study by Eleveld and colleagues (11), in which whole-genome sequencing of 23 paired diagnostic and relapse samples was performed, 10 cases with *ALK* mutations were identified, of which 3 were not detected in the primary tumor. Ultra-deep sequencing and PCR-based methods identified two of the three being present at low frequency in the primary tumor (11). These examples, as well as the reported establishment of a fully *ALK*-mutated cell line from a primary tumor containing a subclonal *ALK*-mutated population (10), are suggestive of clonal evolution, but need to be validated in larger cohorts and through experimental methods. Therefore, whether the higher frequency of *ALK* mutations seen at relapse reflects those already present at diagnosis or whether they emerged during the development of relapse is a key question that needs to be addressed. It is possible that subclonal *ALK* mutations at diagnosis may not be effectively targeted by standard chemotherapy and therefore continue to evolve, eventually contributing to relapse.

The presence of subclonal *ALK* mutations at diagnosis becomes especially important in cases with *MYCN* amplification, where the majority of *ALK*-mutated cells were subclonal (1). If these patients are to benefit from the administration of an ALK inhibitor at diagnosis, to prevent *ALK*-mutated clones from becoming dominant at relapse, it is critical that subclonal *ALK* mutations are not missed during the initial analysis of the tumor. Sanger sequencing has been used widely in clinical laboratories for the analysis of mutations, but its sensitivity is such that only 20% to 30% of mutated alleles in a wild-type background are detected (12). As more sophisticated technologies become available, such as droplet digital PCR and next-generation sequencing techniques with the potential of detecting mutated allele fractions as low as 0.2%, as previously reported by the authors (10), it should be possible to replace Sanger and other conventional methods for identifying subclonal *ALK* mutations. Most importantly, this enhanced capability will make it possible to accurately track subclonal *ALK* mutations from diagnosis to relapse through repeated tumor sampling to establish their clinical relevance. For instance, if the

findings indicate the persistence and expansion of *ALK*-mutated subclones in a substantial fraction of patients, there would be justification for adding effective new *ALK* inhibitors early in the treatment course or at relapse. Whatever the outcome, the study by Bellini and colleagues (1) has provided the impetus to study more closely the pathogenic role of neuroblastoma subclones bearing *ALK* mutations and hence their potential value as therapeutic targets.

Disclosure of Potential Conflicts of Interest

No potential conflicts of interest were disclosed.

Grant Support

R.E. George was supported by the NIH under award number R01CA148688.

Received August 10, 2015; accepted August 16, 2015; published OnlineFirst September 11, 2015.

References

1. Bellini A, Bernard V, Leroy Q, Rio Frio T, Pierron G, Combaret V, et al. Deep sequencing reveals occurrence of subclonal *ALK* mutations in neuroblastoma at diagnosis. Clin Cancer Res 2015;21:4913–21.
2. Chen Y, Takita J, Choi YL, Kato M, Ohira M, Sanada M, et al. Oncogenic mutations of ALK kinase in neuroblastoma. Nature 2008;455:971–4.
3. Janoueix-Lerosey I, Lequin D, Brugieres L, Ribeiro A, de Pontual L, Combaret V, et al. Somatic and germline activating mutations of the ALK kinase receptor in neuroblastoma. Nature 2008;455:967–70.
4. George RE, Sanda T, Hanna M, Frohling S, Luther W 2nd, Zhang J, et al. Activating mutations in ALK provide a therapeutic target in neuroblastoma. Nature 2008;455:975–8.
5. Mosse YP, Laudenslager M, Longo L, Cole KA, Wood A, Attiyeh EF, et al. Identification of ALK as a major familial neuroblastoma predisposition gene. Nature 2008;455:930–5.
6. Hallberg B, Palmer RH. Mechanistic insight into ALK receptor tyrosine kinase in human cancer biology. Nat Rev Cancer 2013;13:685–700.
7. De Brouwer S, De Preter K, Kumps C, Zabrocki P, Porcu M, Westerhout EM, et al. Meta-analysis of neuroblastomas reveals a skewed ALK mutation spectrum in tumors with MYCN amplification. Clin Cancer Res 2011;16:4353–62.
8. Berry T, Luther W, Bhatnagar N, Jamin Y, Poon E, Sanda T, et al. The ALK (F1174L) mutation potentiates the oncogenic activity of MYCN in neuroblastoma. Cancer Cell 2012;22:117–30.
9. Greaves M, Maley CC. Clonal evolution in cancer. Nature 2012;481:306–13.
10. Schleiermacher G, Javanmardi N, Bernard V, Leroy Q, Cappo J, Rio Frio T, et al. Emergence of new ALK mutations at relapse of neuroblastoma. J Clin Oncol 2014;32:2727–34.
11. Eleveld TF, Oldridge DA, Bernard V, Koster J, Daage LC, Diskin SJ, et al. Relapsed neuroblastomas show frequent RAS-MAPK pathway mutations. Nat Genet 2015;47:864–71.
12. Ihle MA, Fassunke J, Konig K, Grunewald I, Schlaak M, Kreuzberg N, et al. Comparison of high resolution melting analysis, pyrosequencing, next generation sequencing and immunohistochemistry to conventional Sanger sequencing for the detection of p.V600E and non-p.V600E BRAF mutations. BMC Cancer 2014;14:13.